

LIQUID-LIQUID SEPARATION IN DISC-STACK CENTRIFUGES



J.P. VAN DER LINDEN

TR diss
1525

54173
217 0316
TR diss. 1525

LIQUID-LIQUID SEPARATION IN DISC-STACK CENTRIFUGES

PROEFSCHRIFT



Ter verkrijging van de graad van doctor aan de Technische
Universiteit Delft, op gezag van de Rector Magnificus,
Prof. dr. J.M. Dirken ten overstaan van een commissie
aangewezen door het College van Dekanen, te verdedigen
op Donderdag 5 februari 1987 te 14.00 uur

door

JOHANNES PETRUS VAN DER LINDEN

werktuigkundig ingenieur
geboren te 's-Gravenhage

TR diss
1525

Dit proefschrift is goedgekeurd door de
promotor Prof. ir. E.J. de Jong

Stellingen
behorende bij het proefschrift
"Liquid-liquid separation
in disc-stack centrifuges"

1

De algemene opvatting dat het olie-water grensvlak in schotelcentrifuges zich bij voorkeur op de distributiekkanalen moet bevinden dient, uit oogpunt van het risico op extreem niet-uniforme doorstroming van het schotelpakket, herroepen te worden.

2

Het dispergeren van de voeding van een schotelcentrifuge, dat met de acceleratie daarvan gepaard gaat, heeft een niet te verwaarlozen invloed op het scheidingsrendement.

3

De bewering van Schmitz, als zou maldistributie in het schotelpakket geen invloed uitoefenen op het scheidingsrendement van een schotelcentrifuge, is onwaarschijnlijk.

F.J. Schmitz; Milchwissenschaft 12 (1950) p. 418 - 425

4

De wijze waarop Fumoto en Kiyose het door hen in een centrifugaalextractor gemeten weireffect correleren, is onjuist.

H. Fumoto, R. Kiyose; J. Nucl. Sc. Techn. 17 (1980) 9, p. 694 - 699

5

Voor wat betreft de hoogfrequentie permittiviteit van water-in-olie dispersies berust de bewering van Kurkova e.a., als zou de voorspelling van Hanai nauwkeuriger zijn dan die van Wagner, op rekenfouten.

Z.E. Kurkova e.a.; Zhurnal Prikl. Khim. 56 (1983) 5, p. 1034 - 1037

T. Hanai ; Kolloid Zeitschrift 171 (1960) 1, p. 23 - 31

K.W. Wagner ; Arch. Elektrotechn. 2 (1914) 9, p. 371 - 387

6

Als argument voor de toepassing van een capacitieve meetmethode ter bepaling van de waterconcentratie in olie, wordt vaak de aandacht gevestigd op de permittiviteit van water (~ 80), olie (~ 2) en lucht (~ 1). Het op deze wijze insinueren, dat de permittiviteit van een dispersie van twee of drie der bovenvermelde componenten een gewogen gemiddelde is van genoemde waarden, is misleidend.

7

De wettelijke bijdrage "pooling voorheen vrijwillig verzekerden", voortvloeiend uit de "Wet op de toegang tot ziektekostenverzekerden" (WTZ), is in flagrante strijd met het verzekeringsprincipe.

Artikel 246, Wetboek van Koophandel.

8

Het verdient aanbeveling om, in navolging van de verplichte periodieke keuring voor automobielen (APK), ook bestuurders aan een periodieke keuring te onderwerpen.

9

Met het eerste lustrum van de eenmalige uitkering achter de rug, kan gesteld worden dat eenmalig net zo éénmalig is als tijdelijke BTW-verhogingen tijdelijk zijn.

10

De tekst op de kraag van de pedel van de Technische Universiteit Delft is niet up to date.

11

Het verdient aanbeveling om de hondenbelasting te vervangen door een accijns op hondenvoer.

12

In navolging van Newtonse inzichten zou de benaming "centrifuge" plaats moeten maken voor "centripetuge".

13

Objectieve waarnemingen bestaan niet.

Quidquid recipitur per modum recipiendis recipitur.

Thomas van Aquino, 1225 - 1274

Delft, 5 februari 1987

J.P. van der Linden

To Ine, Joop and Stan

CONTENTS

page

Acknowledgements	9
Summary and conclusions	11
Summary and conclusions (Dutch version)	13
List of symbols	15
Introduction	21
1. Scope of present study	27
2. Separation efficiency	35
2.1 Division of chapter 2	37
2.2 Objectives	37
2.3 Background theory	37
2.3.1 Sigma concept	37
2.3.2 Dispersion effect	42
2.3.2.1 Dispersion effect in separators	42
2.3.2.2 Dispersion effect in agitated vessels	43
2.4 Experiments	46
2.4.1 Experimental approach	46
2.4.2 Description of apparatuses	49
2.4.2.1 Centrifuge pilot plant	49
2.4.2.2 Bypass distributor and dummy stack	53
2.4.3 Measurement techniques	54
2.4.3.1 Dispersion experiments	54
2.4.3.2 Separation experiments	55
2.5 Results and observations	57
2.5.1 Dispersion experiments	57
2.5.2 Separation experiments	63
2.6 Conclusions	67

CONTENTS (continued)

	page
3. Hydrodynamics	69
3.1 Division of chapter 3	71
3.2 Objectives	71
3.3 Background theory	71
3.3.1 Hydrostatic pressure gradient	71
3.3.2 Interface position	74
3.3.3 Hydraulic capacity	76
3.3.4 Disc-stack	77
3.3.4.1 Symmetrical flow solution	77
3.3.4.2 Asymmetrical case	80
3.3.4.3 Channel feed	82
3.3.4.4 Stability	83
3.3.5 Weir	87
3.3.6 Hydraulic gradient	97
3.4 Experimental	99
3.4.1 Description of separator	99
3.4.2 Measurement techniques and experiment procedures	103
3.4.2.1 Interface experiments	103
3.4.2.2 Weir head experiments	105
3.4.2.3 Hydraulic capacity experiments	109
3.4.2.4 Endoscope experiments	110
3.5 Results and observations	113
3.5.1 Interface experiments	113
3.5.2 Weir head experiments	123
3.5.3 Hydraulic capacity experiments	134
3.5.4 Endoscope experiments	137
3.6 Prediction of the interface position and hydraulic capacity	139
3.6.1 Approach	139
3.6.2 Interface position	139
3.6.3 Hydraulic capacity	149
3.7 Conclusions	153

CONTENTS (continued)

	page
4. In-line separation-monitoring	155
4.1 Introduction	157
4.2 Objectives	157
4.3 Interface-monitoring, pulse-echo-method	158
4.3.1 Basic principle	158
4.3.2 Description of monitoring system	158
4.3.2.1 Transducer	158
4.3.2.2 Transducer position	159
4.3.2.3 Constructional aspects	160
4.3.2.4 Signal interpretation	162
4.3.3 Experience gained with the interface-monitoring system	163
4.4 Water-content monitoring, capacitance technique	164
4.4.1 Background theory	164
4.4.1.1 Dielectric behaviour of dispersions	164
4.4.1.2 Dual cell principle	167
4.4.1.3 Sensor design	169
4.4.2 Description of apparatuses	171
4.4.3 Experiments	172
4.4.4 Results and observations	172
4.4.5 Experience gained with the capacitance technique	173
4.5 Conclusions	175
References	179

CONTENTS (continued)

	page
Appendix A Physical and chemical properties and measurement procedures	185
Appendix B Hydraulic gradient model for the cylindrical part of the top disc	189
Appendix C Interface calibration formula	193
Appendix D Interface experimental conditions	195
Appendix E Hydraulic capacity experimental conditions	198
Appendix F Short cut model (channel feed)	199
Appendix G Distribution model	203
Curriculum vitae	207

ACKNOWLEDGEMENTS

The assistance given by my promotor Prof. ir. E.J. de Jong, and his enthusiasm, had a very stimulating influence on the progress of the project. Especially the great amount of freedom allowed by him, offered me the opportunity to learn from my own mistakes, which I consider a privilege.

Thanks are due to the mechanical and chemical engineering students who carried out the majority of the reported experiments and considerably contributed to the interpretation of the results.

I would like to thank Alfa-Laval AB for both the financial and technical support and for their permission to carry out this work. I would particularly like to thank Dr. C.G. Carlsson for his helpful advice and constructive criticism during the course of this work.

I would also like to express a word of thanks to all employees of the Laboratory for Process Equipment for their valuable help and assistance in the realization of this work. Further I am indebted to Ir. J.A. Vogel (TPD) for providing reliable transducers, Mr. B. Jäger (Wolf Endoscopie) who made the endoscope system available, Dr. ir. W.Chr. Heerens (TUD) for his assistance, Drs. W.J.P. Vink (TUD) for the pulse-echo-detector and Mr. L.G. Bonsen and his colleagues (Alfa-Laval Industrie B.V.) for providing a hermetic separator.

For the preparation of the text and figures in this work, I would like to express my gratitude to Mrs. M.A. Engelsma for her critical comments on the English text, to Mr. B.N. Sodderland and Mr. J.A. de Vries for the excellent drawings and to Mrs. M.J.J. Tetteroo-La Croix and Mrs. P.W.M. van Hagen for their patience and skill during the endless hours of typing this thesis.

Thanks also to the management of Unilever Research Laboratory for their contribution to this thesis. In particular for the time made available by

Mr. J. van der Meer, whose expert knowledge of the editorial side of this work proved invaluable.

Gratitude is also due to my parents for their unflagging enthusiasm for the project, for the way they always stimulated me and for the possibilities they have offered in many fields, thus enabling me to reach this milestone.

Last but not least, I wish to thank my wife for her sustained encouragement and loving tolerance during the many hours I spent working on this thesis at home.

SUMMARY AND CONCLUSIONS

Separation efficiency of industrial disc-stack centrifuges result from an intensified sedimentation process, and by the manner in which machine/liquid contacting and transport through the centrifuge are established. The theoretical and experimental work, described in this thesis, is intended to elucidate the controlling mechanisms under realistic conditions and to gain an understanding of their interactions. This study has dealt with separation of liquid-liquid systems and in particular a water-in-oil dispersion.

The accelerator of the centrifuge, denominated distributor, into which the feed liquid is discharged, consists of an axial tube provided with radial guiding fins. Initial contact between the feed liquid and the separator occurs at the tips of these guiding fins. This shockwise contact is followed by a transport along the guiding fins towards the surface level, which results in severe stratification. Experimental work, performed with centrifuge internals, designed especially for this purpose, clearly indicates that the above-described phenomenon is the predominating stage in the dispersion process, rather than the wall shear associated with the subsequent axial transport. Not only can this determination be of assistance as far as directed design improvement is concerned, but, moreover, phenomenon-orientated estimations of dispersion characteristics will become possible. The above-mentioned effect reduces separation efficiency in the case of both low feed flow rates and high numbers of revolutions, which is explained, among other things, by the position of the feed liquid interface within the distributor.

Separation experiments performed under realistic conditions affirmed the important effect of the water-oil interface position on the over-all separation result. Whenever this interface would be positioned within the feed point (either the distribution channel or the periphery) the rather undesirable short-cut effect will take place. In this case, only part of the disc-stack will be flown with liquid, hence resulting in a drastic drop in separation efficiency. Moreover, the interface position influences maldistribution which is caused by occurring axial pressure effects. The latter effect explains measured optimum separation efficiency as function of interface position.

Owing to its important effect on separator performance, much attention is paid to the factors determining the interface position. Apart from the densities of both phases and the radii of both outletports, pressure drop is to be included in order to improve the interface formula. This was affirmed by experimental work, performed with an acoustic pulse-echo-method, successfully incorporated within the centrifugal separator.

Connected with the importance of in-line separation-monitoring, the above-mentioned pulse-echo-technique is described in detail, together with a capacitance technique, with the aid of which low water content in oil could be measured. Physical principles, as well as existing limitations, are discussed and verified through experimental work.

From this work it can be concluded that existing theories on dielectric properties of dispersions show adequate agreement with experiments. Presence of air affects the dielectric properties substantially, thus limiting the measuring range.

SUMMARY AND CONCLUSIONS (Dutch version)

Vloeistof-vloeistof scheiding met schotelcentrifuges

De fasenscheiding in industriële schotelcentrifuges komt tot stand door een versterkt sedimentatieproces en is mede afhankelijk van het apparaat/vloeistof contact en transport door de centrifuge. Het theoretische en experimentele werk, beschreven in dit proefschrift, is bedoeld ter verduidelijking van de kontrolerende mechanismen en hun onderlinge interacties onder realistische omstandigheden. Deze studie behandelt de scheiding van vloeistof-vloeistof systemen en in het bijzonder die van een water-in-olie dispersie.

De accelerator van de centrifuge, de zogenaamde distributeur, waaraan de voeding wordt toegevoerd, bestaat uit een axiale buis voorzien van radiale schoepen. Initieel contact tussen de voeding en de separator vindt plaats op de schoeptippen. Dit schoksgewijze contact wordt opgevolgd door transport langs de schoepen naar het vloeistofoppervlak, hetgeen resulteert in een aanzienlijke stratifikatie. Experimenteel werk, uitgevoerd met speciaal voor dit doel ontworpen centrifuge-onderdelen, toont duidelijk aan dat bovenvermeld fenomeen de bepalende stap is in het dispergeringsproces, in plaats van wandschuifspanningen ten gevolge van het daaropvolgende axiale transport. Deze plaatsbepaling kan van dienst zijn bij gerichte ontwerpverbeteringen en bovendien fenomeengerichte schattingen van dispersie karakteristieken mogelijk maken. Bovenvermeld effect reduceert het scheidingsrendement in het geval van lage voedingsdebieten, alsmede hoge toerentallen, hetgeen te verklaren is met, onder andere, het vloeistofniveau in de distributeur.

Scheidingsexperimenten, uitgevoerd onder realistische omstandigheden hebben de belangrijke invloed van het water-olie grensvlak op het scheidingsrendement aangetoond. Indien dit grensvlak dichterbij de centrifuge-as komt te liggen dan het voedingspunt (of de distributiekanaal of de omtrek), vindt een ongewenst kortsluiteffect plaats. In dat geval wordt slechts een gedeelte van de schotelstapel met vloeistof doorstroomd, hetgeen een drastische rendementsdaling tot gevolg heeft. Bovendien beïnvloedt de

grensvlakpositie de mate van maldistributie die door axiale drukeffekten wordt veroorzaakt. Dit laatste verklaart de gemeten optima in het scheidingsrendement als funktie van de grensvlakpositie.

In verband met de belangrijke invloed op het separatie-rendement is veel aandacht besteed aan de invloedsfactoren van het grensvlak. Behalve de dichtheden van de twee fasen en de radii van de uitlaatpoorten moet drukval verdiskonteerd worden om de grensvlakformule te verbeteren. Dit is bevestigd door experimenteel werk, uitgevoerd met een akoestische puls-echo-methode die met succes in de centrifuge is ingebouwd.

In verband met het belang van in-line scheidingskontrolle wordt bovenvermelde puls-echo-methode gedetailleerd beschreven, tezamen met een capacitieve techniek, met behulp waarvan lage watergehaltes in olie gemeten kunnen worden. Zowel de fysische principes, alsmede bestaande beperkingen worden besproken en met experimenteel werk geverifieerd. De konklusie die uit dit werk getrokken kan worden, is dat de bestaande theorieën op het gebied van diëlektrische eigenschappen van dispersies adequate overeenstemming vertonen met de metingen. Aanwezigheid van lucht beïnvloedt de diëlektrische eigenschappen aanmerkelijk, hetgeen het meettrajekt beperkt.

LIST OF SYMBOLS

		dimension
b	width, channel width	m
C	weir constant, constant	-
C _v	weir constant for the velocity	-
C _c	weir constant for the contraction effect	-
C _o	empty cell capacitance	F
C	capacitance	F
CL	length of cylindrical part of top disc	m
d	capacitor plate distance	m
D _{gr}	gravity disc diameter	m
D	agitator diameter	m
d	depth, droplet diameter	m
d _c	critical depth	m
d _o	brink depth	m
d _{max}	maximum droplet diameter	m
d ₁	distance from transducer to trigger surface	m
d ₂	distance from trigger surface to back of mirror	m
D _w	inner diameter of separator bowl	m
E	specific energy	m
E _b	burst ratio	-
Ek _m	Ekman number	-
f	function	-
f _{in}	water fraction in the feed, by weight	kg/kg
f _{out}	water fraction of the oil stream leaving the bowl	kg/kg
F	separator feed	kg/s
F	force	N
g	gravitational acceleration	m/s ²
H	height above the weir	m
h	caulk thickness	m
h	height	m
j	j ² = -1	-
K _{dis}	correction factor for the distributor pressure drop	-
K _{disc}	correction factor to be inserted in disc-stack	

	pressure formula	-
K_{weir}	correction factor to be inserted in weir pressure formula	-
K_{grad}	correction factor to be inserted in gradient pressure formula	-
\hat{k}	unit vector	-
L_e	distance from mirror edge to opposite bowl wall	m
l	meridian co-ordinate	m
L_i	sound path from transducer to interface and back	m
L_t	sound path from transducer to trigger surface and back	m
L	sensor length, bowl length, scale of the energy containing eddies	m
M	tangential velocity profile in between discs	-
M	molecular weight	kg
M	length	m
$M^\circ(\lambda)$	integral of M	-
m	empirical coefficient in pressure equation	-
n	number of revolutions	rpm
N	number of revolutions	1/s
N	meridian velocity profile in between discs	-
$N^\circ(\lambda)$	integral of N	-
N_o	Avogadro's number	1/mole
N_{caulk}	number of caulks per disc	-
N_s	number of disc spaces	-
N_h	number of holes per disc	-
O	oil flow	kg/s
P	hydrostatic pressure	Pa
P	transformed radius	-
p	reduced pressure	Pa
P	weir height	m
Q	volumetric flow rate	m^3/s
q	specific flow	m^2/s
Q_w	separated water	kg/s
q	fraction of the flow going outwards	-
r	distance across which velocity difference is taken	m

r	radius	m
\underline{r}	position vector	m
R_1	inner radius disc-stack, excluding flanges	m
R_2	outer radius disc-stack, excluding flanges	m
R_3	inner radius disc-stack, including flanges	m
R_4	outer radius disc-stack, including flanges	m
R_i	interface radius	m
R_{ch}	channel radius	m
R_e	liquid surface radius in the distributor	m
R_o	oil outlet radius	m
R_w	gravity disc radius	m
Re	Reynolds number	-
Ro	Rossby number	-
S	scalar	-
S	wall shear	N
S	slope	-
S_c	critical slope	-
T	temperature	°C
\underline{u}	fluid particle velocity vector	m/s
U_{out}	flowmeter voltage	V
U	characteristic velocity scale	m/s
v_1	velocity at point 1	m/s
v_2	velocity at point 2	m/s
v_g	stokes sedimentation velocity in the earth's gravitational field	m/s
v_c	critical velocity	m/s
v_ϕ	tangential fluid velocity	m/s
v_δ	surface velocity	m/s
v_1	meridian fluid velocity	m/s
v_{sw}	speed of sound in water	m/s
w	weir length, width	m
W	water flow	kg/s
We	Weber number	-
x	wall distance co-ordinate	m
z	axial co-ordinate, height co-ordinate	m

GREEK

α	resistance factor	Ns/m^5
α	pressure ratio	-
α	polarizability	m^3
β	recovery	kg/kg
β_b	recovery bypass distributor	kg/kg
β_o	recovery original distributor	kg/kg
γ	ρg	N/m^3
γ	entrance angle with disc generatrices	rad
δ	depth, Ekman layer thickness	m
Δ	difference	-
ϵ	dissipated power	W/kg
ϵ_o	permittivity of vacuum	F/m
ϵ	relative dielectric constant	-
ϵ^*	complex relative dielectric constant	-
η	dynamic viscosity	Pa.s
η_κ	length scale of energy dissipating eddies	m
θ	half cone angle/latitude	-
λ	streamparameter	-
λ	wavelength of sound	m
ν	kinematic viscosity	m^2/s
ξ	dimensionless wall distance co-ordinate	-
π	3.1415...	
Π	molar refraction	m^3
ρ	density	kg/m^3
σ	dielectric conductivity	$1/\Omega\text{m}$
σ^*	complex dielectric conductivity	$1/\Omega\text{m}$
σ	interfacial tension	N/m
Σ	Ambler's equivalent area	m^2
τ	time interval, relaxation time	s
τ_w	shear tension	Pa
ϕ	circumferential angle	-
ϕ	volume fraction dispersed phase	-
ψ	fraction of discs loaded with liquid	-
ω	angular velocity	rad/s

INDICES

a	actual
BD	blind disc
c	continuous phase
cap	capacity
ch	distribution channel
col	collecting channel
d	dispersed phase
dis	distributor
F	distributor foot
h	horizontal, hypothetical, high frequency
i	interface
id	inner disc
l	low frequency
n	normal
o	oil
od	outer disc
ref	reference
sym	symmetrical
w	water

INTRODUCTION

Centrifugal separation

Centrifugation is an old technique which is characterized by application of centrifugal instead of gravitational acceleration with intent to increase sedimentation velocities of particles to be separated from a mixture. Within an extremely diversified range of industries centrifugal separators are used for a multitude of operations including recovery of chemicals, solvents and catalysts, clarification of liquids, e.g. beer and wine, classification of pigments and purification. The history and working principles of the disc-stack centrifuge, a specific type of centrifugal separator, and subject of this thesis, are presented below.

History of the disc-stack centrifuge

In June 1878 the Swedish inventor Dr. Gustaf de Laval was granted a patent for a machine that was to revolutionize the dairy industry, and, in due course, other industries as well. With this machine separation of cream from milk by means of settling and skimming became superfluous. Now milk could be skimmed more efficiently and with up to 20% higher capacities. Towards 1890 a German named Clemens von Bechtolsheim inserted discs in the separator bowl. By means of these so-called Alpha discs the separation area, and therefore the capacity, could be improved considerably. Since the separator was also suitable for separating solids from a liquid, it was soon introduced in other industries. Centrifugal separators quickly found new applications during and after the war: first to purify lube oil for turbines and other machines, and after 1920, with the growing engineering industry, to purify cutting oils, hardening oils and many more workshop liquids. During this time, the separator also began to be increasingly used in the process industries for other products. In the near future the centrifugal separator might be used for various separations (e.g. condensate-water) in the offshore industry for reasons of environmental regulations, stipulated by the government, which become stricter every day.

Working principles

Disc-stack centrifuges exist in more designs, which differ in the way the separated phases are discharged. With respect to the liquid phase discharge open and hermetic separators can be distinguished. Open separators discharge the separated liquid(s) through overflow ports. Hermetic separators are provided with rotary seals to avoid foaming and contact with air. Other hermetic designs contain a centripetal pump or "paring ring" with a vaned pump impeller mounted on the stationary feed pipe, in which the kinetic energy of the rotating liquid is largely converted into pressure energy enabling pressurized discharge. With respect to the solid phase discharge, the solids retaining type, and the peripheral discharge separator can be distinguished. In the solids retaining type, the accumulated solids which are deposited against the bowl wall must be removed periodically by hand, which requires stopping and disassembling of the bowl, and removal of the disc-stack. More or less automatic solids discharge is accomplished in the peripheral discharge separator provided with nozzles, which continuously remove solids along with a portion of the liquid phase. In other designs intermittent discharge is realised by a hydraulic mechanism, which opens valves or uncovers a peripheral slit. The use of the latter type is limited to solids having the degree of fluidity or plasticity required to move through the exposed peripheral openings. Within this thesis attention is restricted to liquid- liquid separation for which reason there is chosen for the solids retaining open separator, which will be described below. Besides, the open separator was selected for its accessibility which, in view of the experimental work to be performed, would be advantageous. The solids retaining bowl consists of a cylindrical body and conical hood held together by a threaded lock ring (see figure 1.1). Standard interior fittings comprise the distributor, an axial ribbed tube with a flared lower end carrying the intermediate discs, which matches the slope of the bowl hood to form the heavy phase outlet channel. Secured to the neck of the bowl by a smaller lock ring is the gravity disc, through which the heavy phase overflows into the collecting cover of the bowl hood.

A stationary oil feed pipe, attached to the frame hood, projects down into the neck of the bowl. In the purifier bowl heavy phase is introduced through the feed pipe at the start of the run. By the action of the centrifugal

force a rotating ring is formed at the bowl wall with a vertical cylindrical surface inside the outer edge of the top disc. When the liquid seal has been established in this way, the bowl is fed and separation commences. The feed rises into the disc-stack through aligned holes in the distributor and intermediate discs. The function of the intermediate discs is to divide the separation zone into thin layers, so that the separated phases only have to travel a very short distance to free themselves from each other. The denser phase is thrown radially outward along the undersides of the discs by centrifugal force. The lighter phase, by virtue of its lower density, takes up a position nearest the axis of rotation and is removed. The mutual "border", of both the light and heavy phase is called the interface.

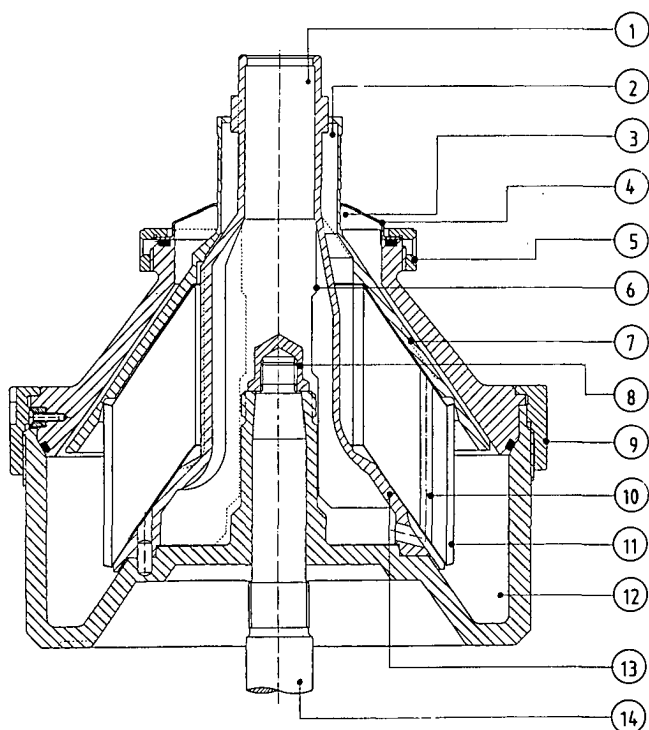


Fig.1.1. Disc-stack centrifuge..

- | | |
|-----------------------|--------------------------|
| 1. feed entrance | 8. top nut |
| 2. light phase outlet | 9. lock ring |
| 3. heavy phase outlet | 10. distribution channel |
| 4. gravity disc | 11. disc-stack |
| 5. lock ring | 12. solids holding space |
| 6. axial rib | 13. distributor. |
| 7. top disc | 14. spindle |

CHAPTER 1

SCOPE OF PRESENT STUDY

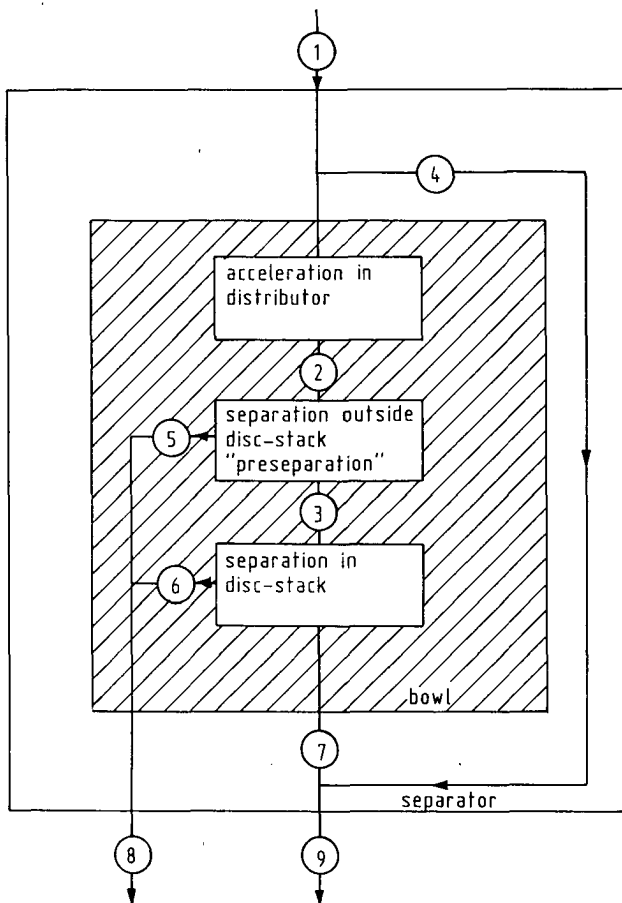


Fig.1.2. Block diagram of the centrifugal separator.

- | | |
|---|-----------------------------|
| 1. feed, dispersion | 5. preseparated heavy phase |
| 2. accelerated feed | 6. separated heavy phase |
| 3. preseparated feed | 7. separated light phase |
| 4. bypass, feed in excess of hydraulic capacity | 8. discharged heavy phase |
| | 9. discharged light phase |

In order to avoid misunderstanding with respect to the different identifications of typical mass flows, figure 1.2 presents the structure of the centrifugal separator used in this study, together with the terminology used in this thesis. Besides, this figure will be referred to, in order to explain some of the experimental results. The feed liquid is partly handled by the bowl up to the amount which can be "swallowed" by the bowl. The remaining part of the feed, by which the hydraulic capacity is exceeded, is discharged together with the separated light phase, which is typical of the open separator applied within this study (see also paragraph 3.4.1 for a detailed description). The physics behind this hydraulic capacity will be paid attention to below. Presence of a pre-separation effect depends upon both the position of the interface and the feed point position. For instance, in a cream separator, which separates butterfat from milk (milk = heavy phase), the interface as well as the distribution channel are positioned near the rotating axis, hence maximizing the skimmed milk residence time with intent to achieve lowest possible fat content in the milk phase. In this and similar cases the separator is designated a concentrator, lacking a pre-separation effect. The opposite situation is found in a lubrication oil separator which separates denser solids (classifier) and or water (purifier) for which the interface and feed positions are located near the outside of the disc-stack, thus providing maximum residence time for the oil phase with intent to minimize water and or solids content in the discharged oil phase. In this situation pre-separation outside the disc-stack is followed by fines removal within the disc-stack. This implies that the disc-stack is not loaded with the entire feed concentration.

Separation efficiency

In an industrial separator, the product particle size distribution and concentration result from particulate processes controlled by both sedimentation force, and by the manner in which both the feed acceleration, distribution and transport through the separator are established. General principles of design and the operating ranges of disc-stack centrifuges have

extensively been described in terms of input-output characteristics under conditions which are often oversimplified and very often very remote from industrial relevance. Centrifugal forces, together with drag and coriolis forces to which a sedimenting particle is subjected in the conical disc space with its rather complex fluid flow field, determine the particle trajectory from which the step to separation efficiency is quickly made. This method was developed by Ambler [1, 2, 3, 4] and is known as the so-called sigma concept, which expresses the separator's performance in terms of equivalent area of a settling tank, which is theoretically capable of doing the same amount of work in a unit gravitational field. More details about this concept can be found in paragraph 2.3.1.

In the course of this study much effort has been put into dispersion characteristics under well-defined conditions: Couette experiments, as well as sedimentation experiments. This work, which unambiguously pointed out the importance of dispersion mechanisms in stirred vessels, was not included in this thesis.

Measurement of drop sizes in the finely distributed dispersions of water in oil, especially encountered in the present study, caused much brain-racking. Photographic analysis, in spite of its reliability, appeared a laborious piece of work, whereas the occurring distributions were typically wide, hence demanding large samples. Commercially available systems, with the Fraunhofer diffraction as basic principle, produced results dependent on the grade of dilution, while the lower end of the distribution (droplet diameters smaller than the wave length of light) substantially contributed to the outreading. Both the assumption that the particles are perfectly opaque and the assumption that the Fraunhofer diffraction approximation holds, are not fully met and may explain the observed phenomenon. Another system was tested, in which particles from a diluted sample were flown through a capillary equipped with a light source and a photo diode. A particle passing the light way would produce a dip in transmitted light intensity being proportional to its projected area. Apart from dispersed phase droplets, suspended solid particles were also measured, resulting in too high base signals.

These aspects, together with financial consequences, associated with the above-mentioned particle analysers, supported the decision to express separator performance in terms of mass-related recovery which could be

measured both by a chemical analysis (Karl Fischer) and by a mass balance method as described in paragraphs 2.4.3.1 and 2.4.3.2. Another important consideration has been that a drop size distribution of both the feed and discharged phases would only provide for additional, but not complete, information.

The present study has deliberately been focused on other phenomena: the effect of both dispersion phenomena and interface position on separation efficiency. It can be presumed that with knowledge of the separator's input characteristics (particle size distribution and volume concentration), combined with the separation characteristic (collecting efficiency as function of particle size), the output characteristics can be calculated. In an industrial separator, however, acceleration, distribution and transport of liquid will, only in a few cases, be established without simultaneous occurrence of population events, which make input-output characteristics based upon population balance concepts doubtful. Especially in the case of mechanically unstable systems, such as flocculated solids or liquid-liquid systems particle disruption/droplet break-up strongly influences separation characteristics.

There is but little literature available on these population events under realistic conditions and especially on these events in industrial scale separators. It is the object of this work to provide knowledge on both the exact causes and locations where these events take place, in order to assist the formulation of design and scale-up strategies, rather than quantification in the form of correlations on dispersion data, which so very often disregard the controlling mechanisms.

In this study the interface position which, apart from being the parameter of interest, provides indirect information on pressure drop in the separator. Pressure drop aspects will be presented in chapter 3, whereas the effect of interface position on efficiency will be explained in chapter 2.

Hydrodynamics

At an early stage of the project attention was paid to the modelling of the interdisc flow with the finite element method applying a software package being developed at the Delft University of Technology. Both the existence of commercially available software packages, capable of solving the full Navier

Stokes equations for 3D-problems, and the consideration that an experimental approach would be more desirable, was the reason that no more effort was put into this subject.

One of the main factors determining the separation efficiency of a centrifugal separator is the interface position.

First, the sigma value or the equivalent separation area (see paragraph 2.3.1) of the separator is strongly influenced by the limiting radius which is in the sigma value to the power 3. Second, from the operational point of view it is necessary to keep the interface position within the outer diameter of the top disc, in order to maintain the liquid seal. In the static situation (no flow), the interface radius is only a function of the density ratio of both phases and the radii of both outlet ports and can easily be calculated with a hydrostatic balance equation. However, in a realistic situation, the interface position deviates from this static position and appears to be a function of operational as well as geometrical parameters.

Apart from the interface position, attention is paid to hydraulic capacity of the separator which is the flow which can be handled just before the distributor, which accelerates and distributes the feed, begins to overflow. This phenomenon is quite typical of an open separator and is not observed when using hermetic separators. The physical meaning of this hydraulic capacity is that the interface between the feed liquid and the air in the open distributor will move to the axis when feed flow is increased, until the moment that the feed liquid interface radius becomes smaller than the internal radius of the distributor.

The positions of both interfaces mentioned above are determined by several effects.

To start with, it must be realized that pressure drop occurs across the disc-stack. The flow problem in between corotating cones is studied by various workers and is influenced by boundary layers which are typical of rotating systems. Within these so-called Ekman layers the coriolis force is balanced by the viscous shear and its thickness is proportional to the square root of the Ekman number (see paragraph 3.3.4).

Besides pressure drop, a weir problem occurs at the location of the outlet ports, where the fluid surface level radius is somewhat smaller than the weir radius, simply in order to provide for a finite discharge velocity

across the fluid layer. This problem has been thoroughly described in literature by the civil engineers for whom fluid height over a dam is an indirect flow measurement technique. In the latter situation typical fluid heights are in the range from a few inches to some feet, whereas the weir head in the light phase outlet of a centrifugal separator amounts to a few millimetres, resulting in extremely different Reynolds numbers (see paragraph 3.3.5).

Finally, liquid gradients can be expected to play a role caused by the existence of viscous friction effects in the open channel upstream the light phase outlet, due to its specific geometry (see paragraph 3.3.6).

The equations governing the oil water interface, as well as the feed liquid interface, will be derived without too many details in paragraphs 3.3.2 and 3.3.3. With respect to the three pressure drop effects outlined above, a short literature review is presented. Further in the experimental study, the interface and hydraulic capacity experiments are presented, and the various pressure effects are quantified as function of geometrical parameters, such as caulk thickness and gravity disc diameter, type of feed: channel or peripheral, operational parameters: rotation speed and flow and physical constants: viscosity and densities.

Choice of test fluids

In this particular experimental study a solid bowl separator was chosen, which is specifically used as a purifier, separating water from mineral or vegetable oil. Mapping out the programme of work belonging to the centrifuge project, typical questions were taken into account, which are reflected in a pre-arranged research programme of an unspecified company active in the field of vegetable oil refining. It is experienced that vegetable oils exposed to higher temperatures quickly oxidize before they ultimately become rancid. Turbine lubrication oil (Shell Turbo T32) was therefore used as a test fluid, because of its excellent stability properties, together with ion-exchanged water as the dispersed phase. More details, with respect to physical properties, can be found in Appendix A.

Joint research programme

Many questions about hydrodynamics, separator efficiency and process monitoring and control, have ultimately led to the initiation of a joint research programme of Alfa Laval Research (Tumba, Sweden) and Delft University of Technology (Laboratory for Process Equipment).

Summary

In correspondence with the three fields of interest: efficiency, hydrodynamics and monitoring techniques, this thesis is subdivided into three main chapters.

Chapter 2 will deal with efficiency and is mainly focused upon dispersion effects in the separator by which the upper limit of the separation efficiency is determined.

Chapter 3 will deal with hydrodynamic aspects which are of importance to the separator: the interface position and hydraulic capacity are both influenced by pressure drop effects.

In chapter 4 attention will be paid to separator monitoring techniques developed within this research programme.

CHAPTER 2

SEPARATION EFFICIENCY

2.1 Division of chapter 2

The theoretical part of this chapter comprises basic equations governing separation efficiency as function of throughput, particle sedimentation data and separator characteristics. Attention is paid to the assumptions from which these equations are derived. The experimental part of this chapter comprises experiments performed with a handicapped separator with intent to locate the dispersion effect. Separation experiments are stated showing the effect of interface position, feed type and caulk type upon separation efficiency in a realistic situation.

2.2 Objectives

In this chapter the dispersion effect, occurring within the separator, will be located. Further, the importance of various geometrical and operational factors will be determined and explained.

2.3 Background theory

2.3.1 Sigma concept

In analysing the performance of a centrifuge, when a high degree of separation is important, the behaviour of the smallest particles in the system is usually the controlling factor. For a variety of centrifuge types Ambler [2, 3] developed the so-called sigma concept. With the sigma concept the particle diameter, d , can be calculated of which 50% will be separated. The sigma value Σ is an index of the size of a centrifuge and is in fact the calculated equivalent area of a settling tank, theoretically capable of doing the same amount of work in a unit gravitational field:

$$Q = 2 v_g \Sigma \quad (2.1)$$

with v_g the Stokes' velocity in the earth's gravitational field:

$$v_g = \frac{\Delta \rho \cdot g \cdot d^2}{18 \cdot \eta} \quad (2.2)$$

and the sigma value for the disc-stack centrifuge (see figure 2.1A):

$$\Sigma = \frac{2 \pi N_s \omega^2 (R_2^3 - R_1^3)}{3 g \tan \theta} \quad (2.3)$$

and for a tubular-bowl centrifuge with bowl length L (see figure 2.1B):

$$\Sigma = \frac{\pi \omega^2 L (R_2^2 - R_1^2)}{g \ln \left(\frac{2 R_2^2}{R_1^2 + R_2^2} \right)} \quad (2.4)$$

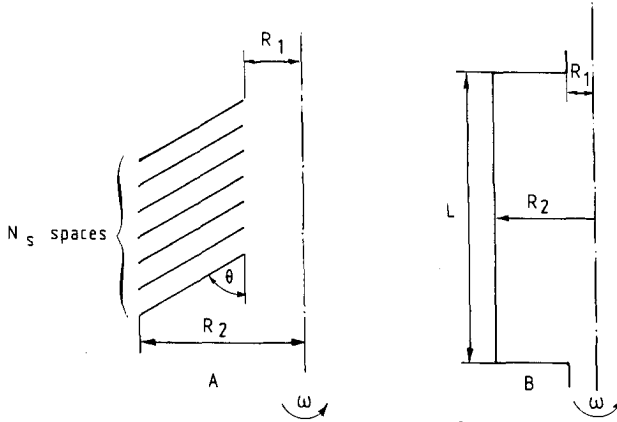


Fig.2.1 Definition of the centrifuge parameters in the case of a
A disc-stack centrifuge
B tubular bowl centrifuge

Developing the sigma concept, Ambler made some assumptions which will be discussed below together with some relevant factors.

1. Sedimentation velocity proportional to radius

First, this assumption contains validity of Stokes' law across the entire disc-stack. For larger particles moving rapidly when their Reynolds number is greater than the order of unity, the viscous resistance becomes negligible compared with the turbulent resistance which is proportional to the square of the velocity of sedimentation. In analysing the performance of

a centrifuge, when a high degree of separation is important, the behaviour of the smallest particles in the system is usually the controlling factor. Viscous resistance may therefore be considered to be of prime importance.

Second, it contains the negligence of the acceleration effect.

A. Brunner in his thesis [7] quantifies this effect for a spherical particle in the gravitational field.

Third, it does not take into account hindered settling which has a negative effect on the effective settling velocity. The effect, caused by mutual interference of the sedimenting particles, can be quantified by inserting a correction factor being a function of volume fraction, Reynolds number and shape such as reported among others by Richardson & Zaki [53]. Besides, corrections must be made for the effects of flow in narrow channels, where the particle may be a considerable proportion of the flow gap, resulting in particle-wall interactions.

2. No particle disruption

Concerning particle disruption an example is given by Ambler [3] who mentions the precipitate of ferric hydrate, the stability of which is influenced to a great degree by the electrolyte concentration of the fluid phase.

In a quiescent field such a precipitate shows a high value of v_g . When introduced into the rotating bowl of a centrifuge the abrupt change in angular velocity substantially changes the diameter of the individual particles. If the retention time in the centrifuge is short, even though the agglomerates do reform in time, there is an apparent shift of Q/Σ to a smaller value for the same degree of clarification as the rotational speed of the centrifuge, and its shearing effect on the feed increases.

Empirical data show that the exponents of the disc radius and angular velocity may vary slightly for various systems. Ambler [1] presents this correction which is not dimensionally correct, but is sometimes used by centrifuge suppliers in predicting performance of disc-stack centrifuges from small scale tests:

$$\Sigma = \frac{2 \pi N_s \omega^{1.5} (R_2^{2.75} - R_1^{2.75})}{3 g \tan \theta} \quad (2.5)$$

This correction considers and places a value on the effect of the initial rotative energy on the size of dispersed particles by reducing the exponent of ω , the angular velocity and/or the increasing lag of the sedimenting particles behind the rotational speed of the rotor with increasing rotor speed. It further considers the difficulty of securing proper distribution through discs as they become larger in size by adjusting the exponent of R. More details on this item are stated in paragraphs 2.3.2 and 2.5.1.

3. Uniform distribution of flow over the disc spaces

This assumption implies that a disc-stack can be considered to be built up as parallel connected settling chambers receiving equal portions of flow.

A. Brunner [8] reports that this assumption is violated in practice. Separating water from fuel oil, a non-evenly distributed solids layer, was observed on the inner bowl wall, increasing in thickness and ash content in the direction of the bowl bottom. Schmitz [56] compared the separation results of a modified cream separator (increased maldistribution accomplished by the insertion of an extended top disc) with the separation results of the original separator, but could not determine a difference. Contrary to Brunner [8], Schmitz [56] is of the opinion that the lower disc spaces, contributing for the greater part to clarification, should be rather trivial, and that separation should not be affected by maldistribution. In his opinion the latter is caused by an improved separation of the upper disc spaces which compensates for the worsened separation performance of the lower disc spaces, being loaded to a greater extent compared with the upper disc spaces. This point of view seems rather dubious: the extreme situation can be compared to a leaky filter.

In practice one sometimes encounters the application of disc-stacks with a somewhat unusual composition. The upper half of the disc-stack contains discs with wider spaces compared with the discs in the lower part. Apart from fouling aspects the maldistribution might in this way be reduced. However, this option has to be "paid" for with a reduction of the total number of disc spaces being N_s in the Σ -equation.

4. Separation criterion

In the derivation the Σ -equation for a disc-stack centrifuge (equation (2.3)) the particle trajectories within the conical disc space form a basis. Complete separation of a particle is assumed to be accomplished when the heavier particle reaches the upper disc. In practice, however, this need not be a guarantee for separation while the particle is subjected to drag forces due to the inwards directed fluid velocity which for the higher λ -values, is an important factor higher than the mean velocity. De Paz [52] points out the significance of this effect which raises R_1 in the Σ -equation dependent upon geometrical data of the disc-stack, physical properties of the liquid and solid contaminant and feed rate. Experimental evidence for this model is presented by Carlsson [12] who finds a reasonable agreement.

5. Effect of caulk type

K.H. Brunner [9] presents experimental data obtained with a single disc separator with a suspension of polyvinyl acetate particles in water. Separation results obtained with 8 long caulks are significantly better than those obtained without caulks. This is explained by a suppression of the circumferential fluid velocity, hence stabilising the interdisc flow (see paragraph 3.3.4.4). Besides, the effects of viscosity and density difference are found to play an important role. Secondary flow increasing on decreasing viscosity affects separation of particles, especially when density difference is low. No difference is observed in between the performance of the free disc space and the disc space with 24 point caulks.

6. Effect of feed type

Apart from the interdisc flow, choice of feed type determines whether cross flow occurs, located at the disc periphery. In the peripherally feeded disc-stack the particles separated will, after sliding down the discs, partially move towards the outer disc space, while the rest of them is being carried along with the feed for the higher discs. Because the subsequent separation is incomplete, it is expected that the overall efficiency decreases on increasing fluid velocity caused by an intensified backmixing. This effect

can be eliminated, for the greater part, by feeding the disc-stack via the distribution channels. Experimental evidence is presented by K.H. Brunner [9].

7. Effect of interface position (purifier)

Ambler [2] states that for the maximum efficiency the position of the holes in the disc-stack, through which the feed is distributed, must correspond to the position of the interface. If this correspondence does not exist, then at least some of the Σ -value of the fraction of the disc-stack, lying between the interface and the feed holes, is not available for purification of the light (if the interface is outside the holes) or of the heavy phase (if the interface is inside the holes). Purifying oil A. Brunner [8] mentions that the interface should be positioned just outside the disc-stack. Svensson & Von Schultz [60] report that it should lie as closely as possible to the disc periphery, whereas Trowbridge [64] claims that it should never be positioned within the stack because of fouling problems.

2.3.2 Dispersion effect

2.3.2.1 Dispersion effect in separators

From the foregoing it became clear that knowledge of the dispersion phenomena within the distributor is of utmost importance in order to gain an understanding of the overall separation characteristics of the centrifuge. In the open literature not much is published about dispersion effects within centrifugal separators. Bell and Brunner [5] studied floc break-up in a decanter centrifuge. Experiments with ultrasonically dispersed PVAC flocs proved that break-up primarily depends on the bowl speed and the feed pipe position. The greatest extent of floc break-up occurred when the feed pipe position corresponded to the most shallow pond depth, i.e., feeding in the conical region of the bowl and at the maximum speed.

In the latter case efficiency shows an optimum with respect to rotating speed. Bell and Brunner suggest that larger pond depths may result in lower values of dissipated power per unit volume and hence less break-up.

Fumoto and Kiyose [24] investigated drop formation in a high speed centrifugal extractor. From their results, the average drop diameter is proportional to the Weber number to the power of -0.58 , when the contact time is long. However, the agitation velocity did not affect the average drop size, when the contact time is short (approximately 10 s). During these experiments the aqueous-organic flow rate ratio was fixed at 1.0. Rotation speeds in between 600 and 2000 rpm were chosen. Datar [13] reports that shear break-up in a centrifugal separator can be reduced by the use of hermetic feed systems and by incorporation of a conical shaped inlet device (figure 2.2) which accelerates the feed to bowl speed, without incurring sudden pressure drops. Apart from shear reduction this conical inlet, which was patented by Alfa-Laval [63], reduces foaming which is a typical problem occurring within cream separators.

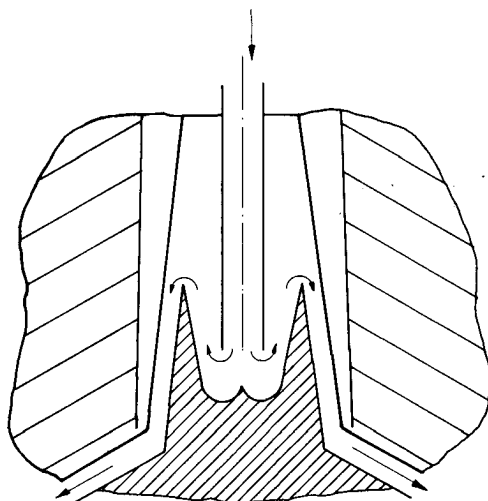


Fig. 2.2 New centrifuge feed geometry designed to reduce effects of shear [63]

2.3.2.2 Dispersion effect in agitated vessels

Turbulence

Drop size distributions depend on turbulence intensity, drop break-up mechanism and the occurrence of coalescence. The complexity of turbulent two-phase dispersed flows demands analysis in statistical terms. The primary

contributions to the study of such flows are given by Kolmogorov [40] and Hinze [35]. These authors, independently, suggested that the maximum size of droplet stable against break-up by turbulence can be estimated by means of dimensional analysis based on the assumption that the rate of energy dissipation in the flow is the key parameter characterizing the structure of turbulence fluctuations. The small-scale velocity fluctuations are determined by the local rate of energy dissipation per unit mass of fluid ϵ and the kinematic viscosity ν . Kolmogorov defines the length scale of the energy dissipating eddies as

$$\eta_K = (\nu^3 / \epsilon)^{1/4} \quad (2.6)$$

For local isotropy to exist, the linear scale L of the energy containing eddies must be large compared to the Kolmogorov microscale η_K . If this condition is met in any small volume of characteristic dimension r ($\ll L$), all velocity correlations must be a function of ϵ and ν only. The mean square of relative velocity $u(r)$ between any two points a distance r apart, is a universal function of ϵ and ν . Furthermore if $L \gg r \gg \eta_K$, $u^2(r)$ is independent of viscosity and a function of ϵ only. In this case, and for very small values of r as well, the form of the universal function can be obtained from dimensional analysis:

$$\overline{u^2(r)} = C_1 (\epsilon r)^{2/3} \quad \text{for } L \gg r \gg \eta_K \quad (2.7)$$

$$\overline{u^2(r)} = C_2 \epsilon r^2 / \nu \quad \text{for } L \gg \eta_K \gg r \quad (2.8)$$

Local isotropy is possible in a stirred vessel equipped with a turbine agitator. The conditions of turbulence in such a mixing vessel can be predicted from a modified Reynolds number ND^2/ν where D is the agitator diameter and N its speed in revolutions per second. Shinnar [58] suggests that fully developed turbulence exists if this modified Reynolds number is above 10^4 .

In case of non-isotropic turbulence it has been shown by Konno et al. [41] that break-up is governed by spatial distribution of average velocities of

flow or by turbulent eddies that have the largest velocity component in the direction of the flow. The $\overline{u^2(d_{\max})}$ may be expressed as follows:

$$\overline{u^2(d_{\max})} = C_3 (N d_{\max})^2 \quad (2.9)$$

Break-up criteria

Break-up of droplets may be caused either by turbulent pressure fluctuations or by viscous shear forces in case droplets are very small ($d \ll \eta_c$). Taylor [62] showed that in theory the drop deformation, due to these viscous forces, is equal to the ratio of viscous to interfacial forces necessary for rupture, E_b :

$$E_b = \frac{(du/dr)_b d_{\max} \eta_c f(\eta_d/\eta_c)}{2 \sigma} \quad (2.10)$$

$(du/dr)_b$ is the shear rate at rupture, d_{\max} the drop diameter at rupture, η_c the viscosity of the continuous phase and σ the interfacial tension. $f(\eta_d/\eta_c)$ is a theoretical function of the viscosity ratio and varies from 1 to 1.2 for viscosity ratios from 0 to infinity.

Many authors measured the reduced shear rate at drop break-up as a function of viscosity ratio. A minimum occurred in the viscosity ratio range of 0.1 to 1, with a rapid increase in reduced shear rate at higher viscosity ratios. An excellent review article including experimental data is given by Grace [27].

In case inertial effects become decisive ($d \gg \eta_c$), drop size relations can be derived based upon the dimensionless Weber number which compares kinetic energy of the oscillating droplet to surface energy:

$$We = \frac{\overline{u^2(d)} \rho_c d}{\sigma} \quad (2.11)$$

Drop size formulae

Combination of velocity functions with break-up criteria results in equations predicting drop sizes in agitated dispersions as a function of mixing parameters and physical constants. Validity of such a drop size

equation can only exist if the conditions are met upon which the velocity function and the break-up criterion are based. If, however, drop sizes in the dispersion and Kolmogorov microscale are of the same order of magnitude, it is not possible to discriminate between the conditions mentioned above ($d \ll \eta_K$ and $d \gg \eta_K$). The drop size equation in the isotropic case with inertial break-up is obtained by combining of (2.7) and (2.11):

$$d_{\max} = C_4 \left(\frac{\sigma}{\rho_c} \right)^{\frac{1}{3}} \epsilon^{-\frac{2}{3}} \quad (2.12)$$

For the non-isotropic case, with inertial break-up, equations (2.9) and (2.11) are combined:

$$d_{\max} = C_5 \sigma^{\frac{1}{2}} \rho_c^{-\frac{1}{3}} N^{-\frac{2}{3}} \quad (2.13)$$

2.4 Experiments

2.4.1 Experimental approach

Dispersion experiments

Preliminary experiments showed that separation of an unmixed feed appeared to be incomplete, which was dedicated to the existence of a dispersion effect. A complication in the study of this dispersion effect has been the coexistence of dispersion and separation which made it impossible to measure these phenomena independently. Because proper sampling of the accelerated and dispersed feed from a rotating system was also impossible, an indirect measurement was considered to be the one and only solution for this problem. The measurement technique which actually has been applied, consisted of a sedimentation analysis performed directly after the dispersion process has taken place. This has been accomplished by handicapping the separation action installed in the disc-stack centrifuge by replacement of the disc-stack by a dummy stack. The latter device consists of a massive piece of brass, being geometrically identical to the exterior of the disc-stack. A description of the dummy stack can be found in paragraph 2.4.2.2.

If it would be possible to introduce an unmixed feed in the distribution channel obtaining a complete separation, it could then be concluded that in the above-mentioned situation the distributor must have been entirely responsible for the dispersion effect. In order to create such an experiment, a special distributor, the so-called bypass distributor (see paragraph 2.4.2.2) was designed. This bypass distributor accelerates water and oil, whereas both phases are physically separated in order to exclude dispersion. By shortening the water discharge pipes, the position from where physical contact between the two phases would occur could be changed. Comparison of the results led to the designation of the exact location which would predominate the ultimate dispersion effect. -

The below-mentioned locations are expected to contribute more or less to the dispersion process.

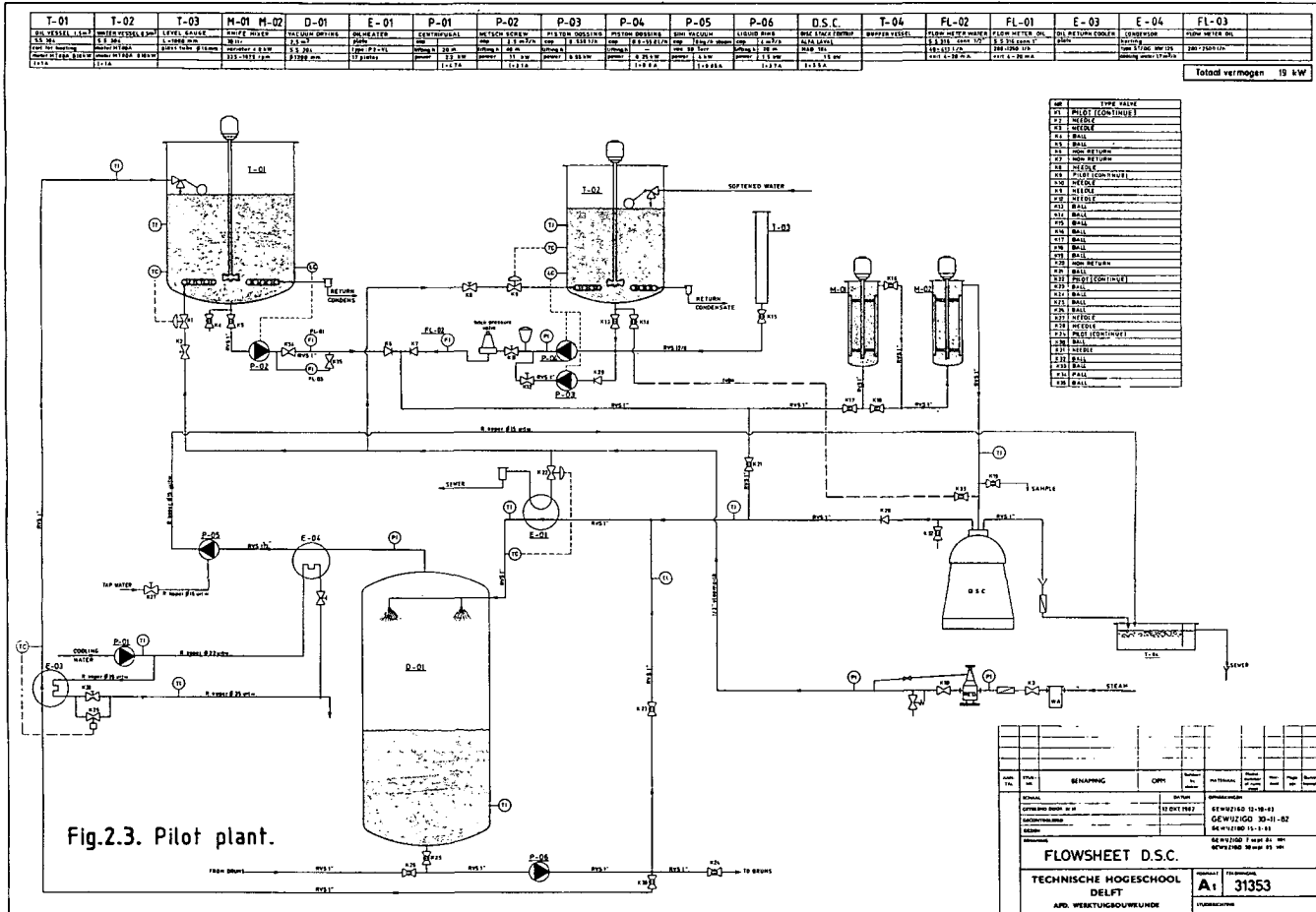
First location where the primary contact between the separator and the feed liquid takes place is the top nut, which, because of its conical shape, deflects the liquid flow, which is discharged through the feed pipe. Due to the restricted contact time hardly any transfer of momentum is expected to take place in the angular direction.

Second location comprises the fin tips in the distributor, where initial intensive contact between the separator and the feed liquid takes place.

Third location is the traject in between the fin tip and the liquid surface in the distributor situated at the pressure side of the guiding fin. Along this traject the feed liquid will be stratified. Prediction of the film thickness seems a formidable task, whereas a free surface is encountered in combination with a free "channel width". The length of the traject is function of R_e only.

Fourth location is the inner wall of the distributor, where axial shear becomes more and more important when the feed liquid surface radius, R_e , is positioned outwards, hence resulting in low liquid depths.

Fifth location is the conical shaped lower end of the distributor, where Ekman layers and hence high shear rates may occur, as far as the flow stability criterion is satisfied.



Separation experiments

Effect of interface position, feed and caulk type

As discussed above, in a centrifugal separator the position of the water-oil interface is believed to play an important role in the separation process. In order to verify the significance of this statement experiments were performed with the centrifuge pilot plant, measuring separation efficiency and interface position simultaneously.

2.4.2 Description of apparatuses

2.4.2.1 Centrifuge pilot plant

The pilot plant, of which the flow sheet is depicted in figure 2.3, basically consists of a dispersion producing section which disperses water in oil from the storage vessels which will be separated partially by the centrifuge. A regeneration section consisting of a flash evaporator removes the unseparated water phase and delivers the water free oil to the storage vessel, hence forming a closed oil loop.

Storage vessels

The oil as well as the water storage vessel are provided with eccentric placed, pitched-bladed agitators and have capacities of 1500 and 500 litres respectively. Temperature is controlled by expansion type thermostatic valves which are situated in the steam supply to the heating coils.

Dosage system

Oil is pumped with an eccentric screw pump with variable speed drive with a capacity in the range from 250-2500 litres per hour. Water is pumped with a piston dosing pump with stroke adjustment, provided with a pressure accumulator before the spring loaded back pressure valve.

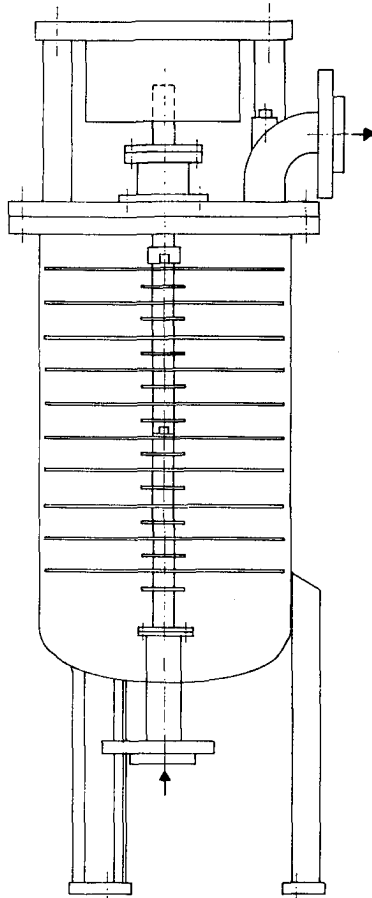


Fig.2.4 Knife mixer.

Dispersion section

Dispersion was produced in two 30 liter knife mixers with variable drive (see figure 2.4). The entrance was situated at the lowest point and the outlet at the highest point, close to the mechanical seal, in order to avoid introduction of air.

One can choose to apply only one mixer or both, or to bypass both knife mixers, hence providing an unmixed feed. Rotation speed can be varied in a range from approximately 350-1400 rpm. Photographic analysis provided drop size information on the produced dispersion. At a rotation speed of 700 rpm $56 \pm 4 \mu\text{m}$ was found for the maximum drop size, for a water fraction of 5.5% by weight. Experiments, not included within this thesis, indicated the validity of equation (2.13), as far as the effect of rotation speed and liquid viscosity were concerned. In spite of reasonable residence times in the knife mixers, different separation results were obtained when applying one instead of two identically adjusted mixers. This was observed most clearly when separation was almost complete, indicating that the time dependent behaviour of the distribution was restricted to the smaller droplets in the distribution.

Regeneration

A 3 m³ flash vessel provided with 4 whirljet nozzles was installed. Vacuum was maintained with a condenser and a vacuum pump. To provide for a steady spray from the nozzles, partial recirculation was realised. The inlet temperature was maintained at 90°C, to provide for an adequate separation result, with the aid of a plate heat exchanger and steam as a heating medium. The recycle stream is cooled down with a second plate heat exchanger before discharge into the storage vessel.

Centrifugal separator

An extensive description of the separator can be found in chapter 3.4.1.

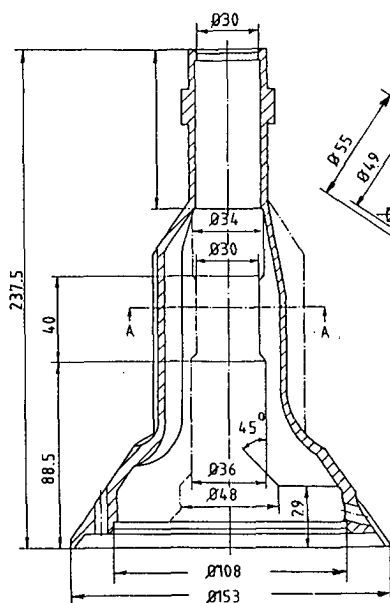


Fig. 2.5 Distributor

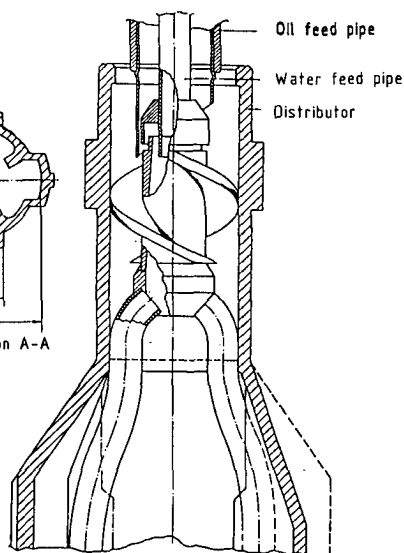


Fig. 2.6a Bypass distributor (Type I)

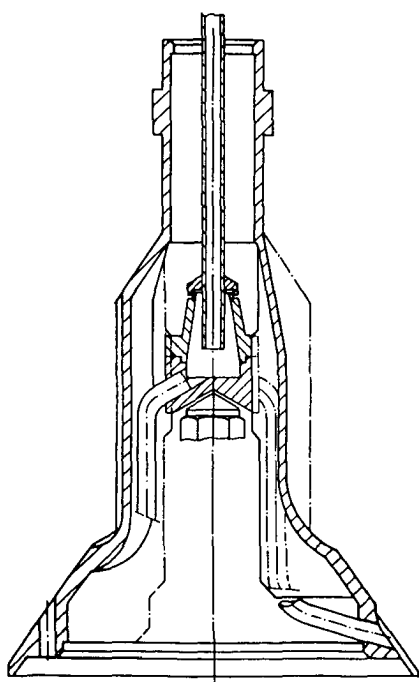


Fig. 2.6b Bypass distributor (Type II)

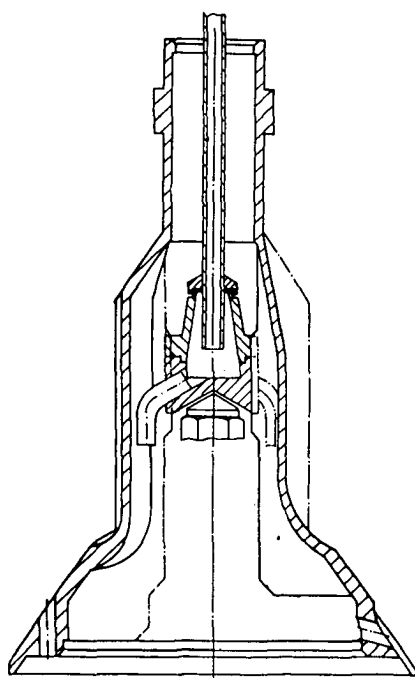


Fig. 2.6c Bypass distributor (Type II short discharge pipes)

2.4.2.2 Bypass distributor and dummy stack

The bypass distributors depicted in figure 2.6 A-C accelerate both oil and water physically separated from one another. This is accomplished by feeding the water via a separate water feed pipe into a slightly conical shaped chamber, to the outside of which two copper pipes are connected which transport the water beyond the location where dispersion is believed to take place. These pipes are connected to two of the six holes in the distributor, whereas the oil flow is established via the remaining four holes. The first design, denominated type I (depicted in figure 2.6A), showed a restricted hydraulic capacity for the oil phase. The second design, type II, was improved by placing the conical shaped chamber directly on the top nut of the spindle, hence eliminating the restriction for the oil flow. The latter type, depicted in figure 2.6B, was changed in such a way that partial bypassing was obtained by shortening the discharge pipes such as shown in figure 2.6C.

The dummy stack, of which the drawing is shown in figure 2.7, is a massive brass body provided with 4 radially directed channels connecting the outer dummy space with the collecting channels of the distributor.

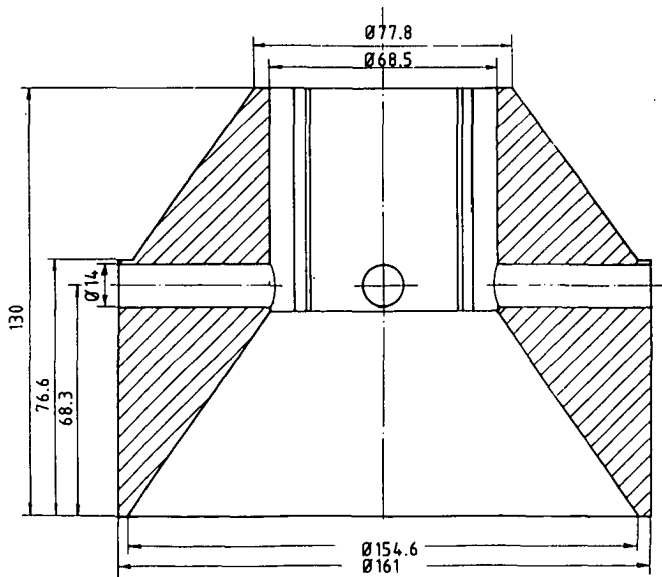


Fig.2.7 Dummy stack with four radial holes.

2.4.3 Measurement techniques

2.4.3.1 Dispersion experiments

Mass balance

Measuring W , the water feed and O , the oil feed and Q_w the discharged water phase mass flow the inlet and outlet dispersed phase fraction can be calculated as well as the separation recovery β :

$$f_{in} = \frac{W}{W + O} \quad (2.14)$$

$$f_{out} = \frac{W - Q_w}{O + W - Q_w} \quad (2.15)$$

$$\beta = 1 - \frac{f_{out}}{f_{in}} \quad (2.16)$$

The accuracy of the result for β mainly depends upon the accuracy of the measurements of the mass flows W and Q_w . In spite of the fact that a stroke adjustable metering pump has been used, it was chosen to measure both W and Q_w with the stopwatch/bucket method. Typical sample times have been in the range of 20 minutes. For the mass measurements a precision balance (Mettler type PN 11 N) was used with a capacity of 10 kg and an accuracy 0.1 g. In all cases the accuracy of β has been better than 0.5%. Additional advantage is that the results found are time averaged.

Experimental procedure

The centrifuge pilot plant was started up and the desired conditions were met within close limits.

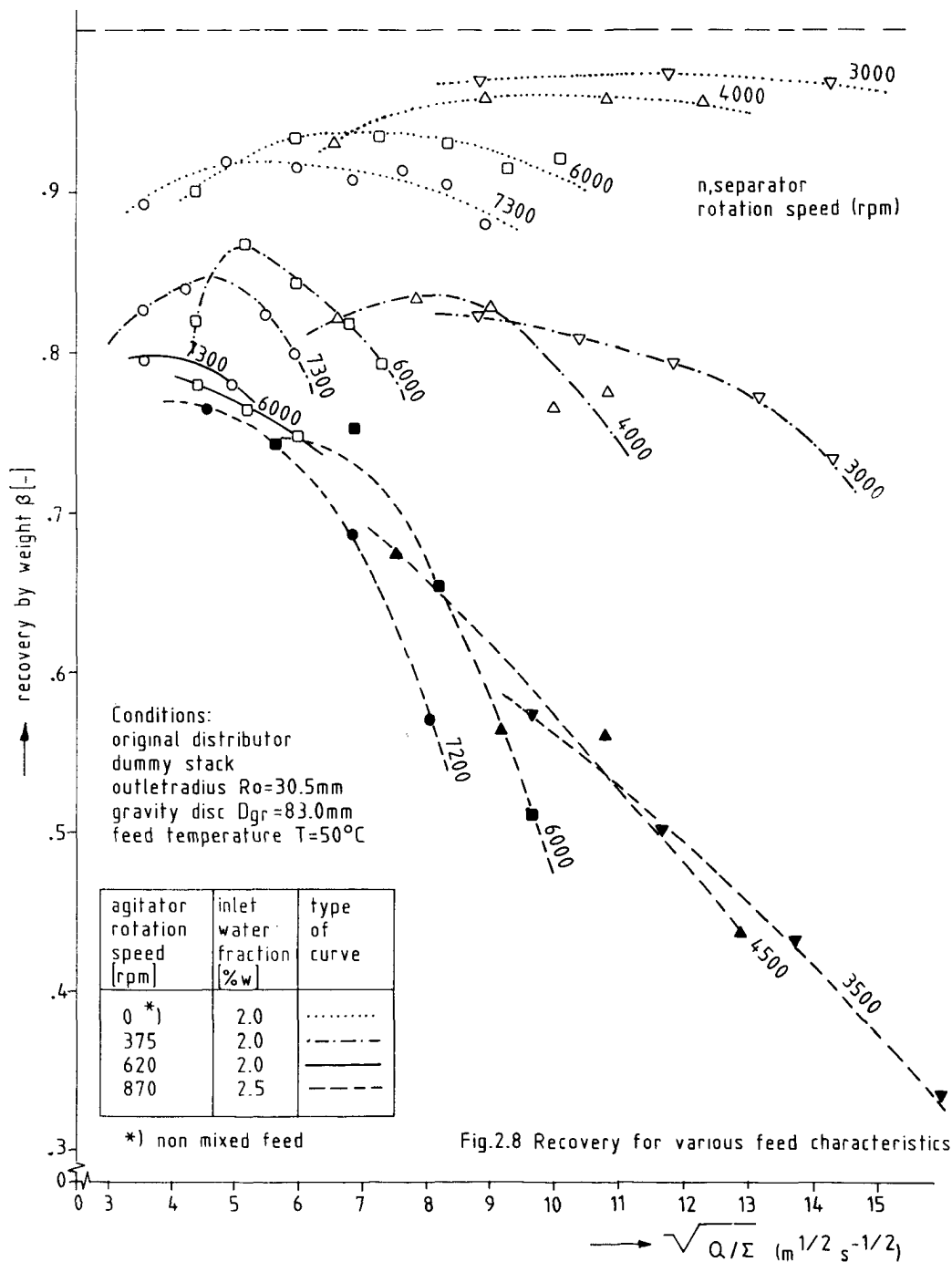
Before measuring efficiencies with this bypass distributor, the hydraulic capacity of both phases was determined in order to be sure that hydraulic capacity would never be exceeded.

With the pulse-echo-method, described in paragraph 4.3, the interface was measured.

2.4.3.2 Separation experiments

For the efficiency two measurement techniques were used: first, the mass balance concept already discussed in paragraph 2.4.3.1 and second, the Karl Fischer analysis. With respect to the latter: a coulometric version was used in which iodine was generated electrolytic within the reaction vessel. The iodine together with a non-specified chemical substance forms a complex which reacts with water. Via conductivity measurement in the reaction vessel the end point determination is automatically made.

With the pulse-echo-method, described in paragraph 4.3, the interface position was measured in the outer disc space ($80.5 < R_i < 98$ mm). Within a restricted area ($R_2 < R_i < R_4$, see paragraph 3.4.1) the measuring area could be extended inward the disc-stack with a few millimetres, due to the disc flanges being flat in that area. Working with both channel feed and peripheral feed, the separator was fed with $1 \text{ m}^3/\text{h}$ water-in-oil dispersion ($T_o = 50^\circ\text{C}$, $f_{in} = 2\%$), produced with one agitator running at 700 rpm. For the separator internals a 1 mm spaced disc-stack was chosen, provided with long caulks in combination with the increased capacity top disc. Three separator rotation speeds were chosen: 3500, 5000 and 7000 rpm. Via the gravity disc diameter, which was decreased bit by bit, the interface position could be varied. The gravity disc diameters used in the experiments were: 70.94, 73.5, 76.0, 78.0, 78.75, 79.5, 80.84, 83.0 and 86 mm. With the quantitative results of the interface model presented in paragraph 3.6 a plot was produced of interface position versus gravity disc diameter for the specific conditions mentioned above, which served as a guide. The plot was verified against experimental data of interface position. The deviation of the measured interface radii compared to the predicted values appeared less than 1 mm for all interface measurements.



2.5 Results and observations

2.5.1 Dispersion experiments

The effects of inlet dispersion

The results of preliminary experiments performed with a handicapped separator (dummy stack) fed with both a non-mixed feed and a real dispersion can be observed in figure 2.8 in which the separation recovery by weight was plotted versus the square root of Q/Σ . The equivalent separation area Σ was calculated with equation (2.4) substituting the interface radius for R_2 and the outer dummy stack radius and height for R_1 and L respectively, according to figure 2.7. Under the assumption of no particle disruption, experimental data points with identical feed characteristics should form a curve, which typical form would depend only on the drop size distribution, as well as the mathematical relationship in between efficiency and dropsize. E.g. in this plot of β vs $\sqrt{(Q/\Sigma)}$ a straight line is expected whenever the cumulative mass would be linear to drop size and the separation efficiency could be represented by a step function of drop size.

As was already mentioned in paragraph 2.3.1 a shift of Q/Σ to smaller values is expected when separator rotation speed increases. As can be observed in figure 2.8 this is not fully the case because clear maxima occur in separation recovery, which position is function of feed characteristics and separator rotation speed.

This phenomenon can be explained by the existence of more break-up mechanisms. Both the existence of stratification along the fins as well as axial shear being a typical function of R_e can explain the trends of figure 2.8.

Bypass distributor (type I)

The hydraulic capacity of the first design bypass distributor appeared to be limited with respect to the oil phase shown in figure 2.9. The capacity with respect to the waterflow appeared to be 125 l/h independent of rotation speed. Within this limited area, six combined experiments were made. For six

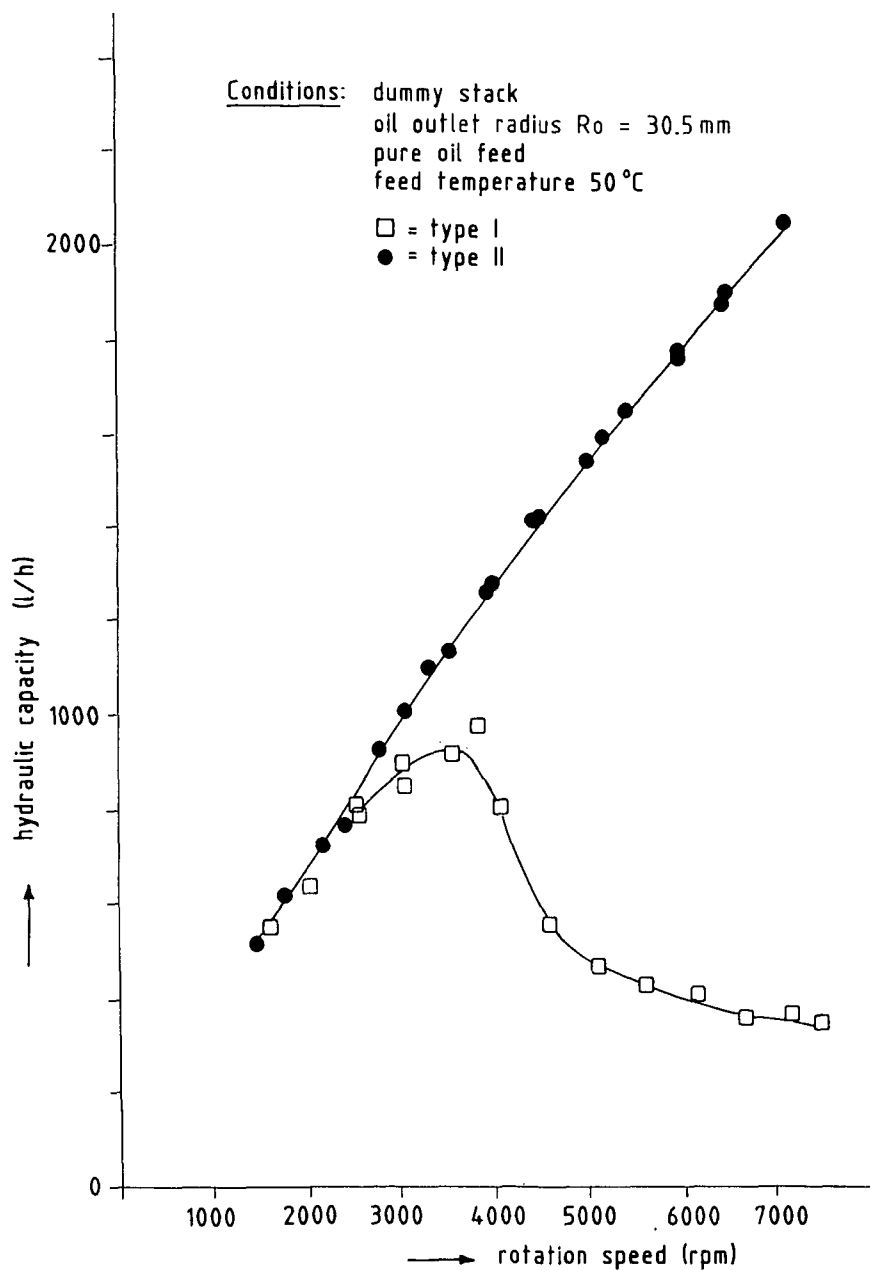


Fig.2.9. Hydraulic capacity of the bypass-distributor.

combinations of rotation speed and feed flow, recovery was measured with both the original and the bypass distributor. The results are presented in table 2.1. Outlet concentration with bypass distributor appears to be roughly half of that in the case of the original distributor.

Table 2.1 Data of the experiments with the type I bypass distributor and the original distributor with dummy stack

rotation speed n [rpm]	feed flow F [kg/h]	recovery original distributor β_o [%w]	recovery type I bypass distributor β_b [%w]	$\frac{1-\beta_b}{1-\beta_o}$ [-]
3030	513	96.25	98.37	0.435
3028	642	97.32	98.71	0.481
3750	641	93.57	97.41	0.403
2500	640	99.10	99.41	0.656
3595	511	94.75	98.22	0.339
6031	274	91.23	95.38	0.527

Conditions: non-mixed feed
inlet water fraction ~ 1.5% (w)
inlet temperature 50 °C
gravity disc diameter 79.5 mm.

Bypass distributor (type II)

Figure 2.10 shows the results for the type II bypass distributor with discharge pipes being connected to two of the six holes in the lower end of the distributor (paragraph 2.4.2.2, figure 2.6 B).

It is observed that even in the case of complete bypass, incomplete separation occurs. Most probably this is caused by a formation of a spray of waterdroplets, which was extensively studied by Schilp [55]. This was also observed during the experiments with the type I bypass distributor (see table 2.1).

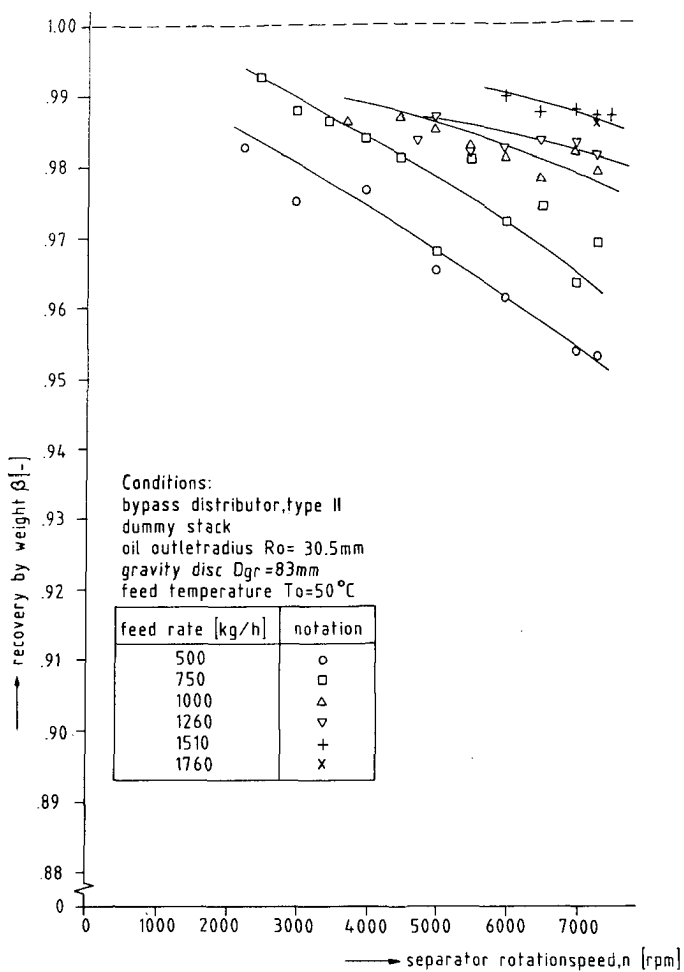


Fig.2.10 Recovery with complete bypass.

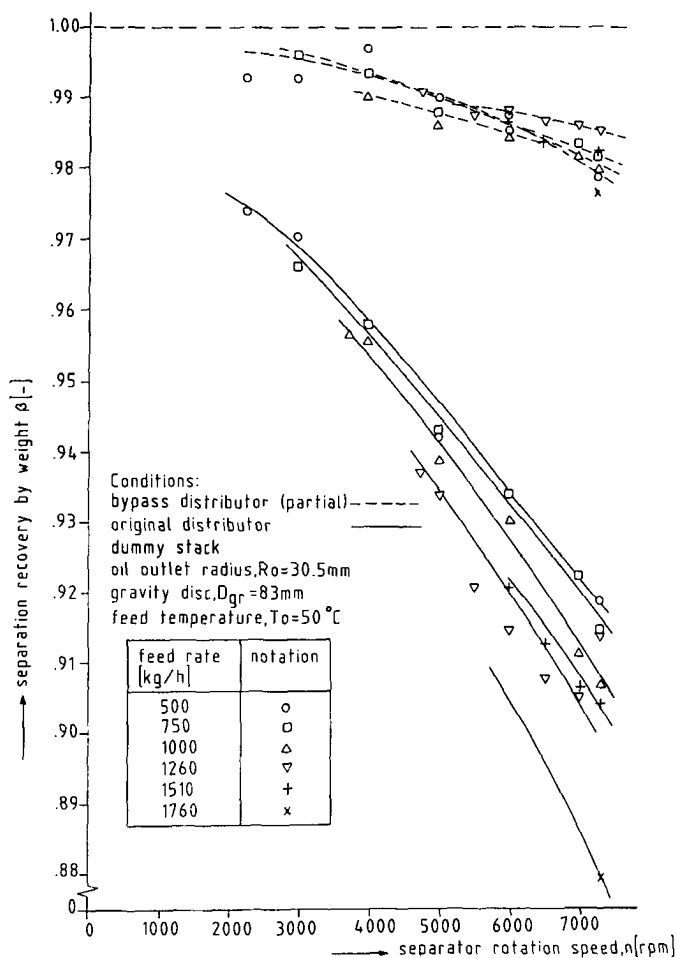


Fig.2.11 Recovery without and with partial bypass.

For feed rates in the range from 500 - 1750 kg/h, and rotation speeds in between 2250 and 7300 rpm, identical experiments were performed. Figure 2.11 shows the results for the original distributor as well as the bypass distributor with short discharge pipes (paragraph 2.4.2.2, figure 2.6 C). Outlet concentration water in oil in the case of the original distributor, appears to be roughly five times as high as compared to the outlet concentration water in oil, in the case of the distributor with short discharge pipes. From this observation it can be concluded that the significance of either location 2 (fin tips), or 3 (stratification) or both, is of prime importance. In order to verify the statement that the feed liquid surface radius will be of any importance, dispersion experiments were performed with the standard distributor and dummy stack and both top discs. In this way a correct comparison could be made, whereas the other parameters would be identical. For instance the interface position was maintained in such a way that it has been a unique function of flow, irrespective of the top disc used. This was verified with the pulse-echo-method, indicating differences within 1 millimetre. Figure 2.12 shows the results, which clearly indicate that the choice of a top disc, which is just able to handle the feed liquid flow, is advantageous with respect to recovery. This also favours the conclusion that hermetic separators will have a typically better performance compared to open separators whereas in hermetic separators the distributor will be completely filled with liquid. The experimental data belonging to the above-mentioned experiments are reported by Van der Donk [15].

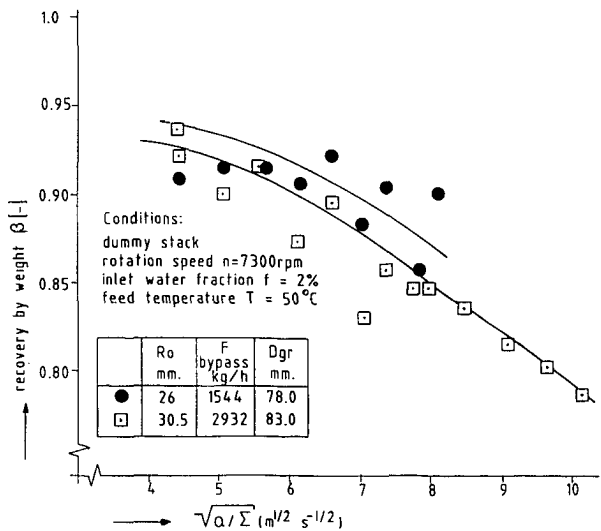


Fig.2.12. Effect of feed liquid surface radius.

2.5.2 Separation experiments

Effect of interface position

The results of the separation experiments have been depicted in figure 2.13 in which recovery β is plotted versus interface radius R_i . Three important radii were indicated with vertical lines: the channel radius, the outer disc radius and the top disc radius. The experiment numbers are printed close to the experimental points. In the plot the experiment trios can be recognised belonging to one and the same gravity disc diameter. Optimum separation results are obtained with the interface positioned just outside the disc-stack (4 - 5 mm from the periphery).

Bearing in mind that the traject $(1 - \beta)$ in figure 2.13 is proportional to the outlet fraction, one can verify that, in the optimum point, outlet fraction is roughly half as big as for the points away from the optimum. Moreover, the importance can be illustrated comparing the $(\partial\beta/\partial n)_{R_i}$ with $(\partial\beta/\partial R_i)_n$. For the channel curves, left of the optimum, $(\partial\beta/\partial R_i)_n$ is estimated to be 0.6 % / mm and $(\partial\beta/\partial n)_{R_i}$ to be 0.2 % / 1000 rpm. In other words 1 mm interface shift can compensate for a decrease in rotation speed with 3000 rpm!

With the distribution model, of which the derivation is presented in Appendix G, a computer simulation was made for the interdisc flows under the circumstances of the separation experiments depicted in figure 2.13. Figure 2.14 shows the numerical results in the form of so-called maldistribution numbers and circulation numbers of which the definitions can be found in the right-hand side upper corner of figure 2.14. The indices o and i refer to the outer and inner discs, and CH and PE to the feed type. The maldistribution number is defined to be the fraction of flow rate, being higher than the uniform flow rate, whereas the circulation number is defined to be the fraction of the total flow rate, which is outwards directed. The latter phenomenon was observed in the lower discs and appeared unique for the channel feeded outer disc-stack. This flow reversal was in most cases restricted to six or seven discs in this particular situation, resulting in a circulation flow along the periphery and through the channel. It amounts to some 7% of the feed flow when the interface is far from the periphery. Only part of the trend shown by figure 2.13, namely in the range of 0 to

10 mm outside the disc-stack, can be explained by maldistribution being a typical function of R_1 according to figure 2.14. The increase in recovery beyond this range, however, remains unexplained. The outcome of this simulation serves a qualitative understanding of the flow profile across the disc height. The outcome of this simulation, however, should experimentally be verified.

Effect of feed type

Apart from data point 31 in figure 2.13 the efficiency measured with channel feed is slightly better compared to peripheral feed which was expected (cross flow).

Another important phenomenon is the drastic drop in efficiency on passing the interface position inwards the feed radius for both channel and peripheral feed. This can be explained by the existence of a short cut effect: the accelerated feed, directly after entering the distribution channel (channel feed) or having passed the periphery (peripheral feed), is distributed over a limited number of discs, hence raising the dynamic pressure drop within the disc-stack compared to the situation where all disc spaces are uniformly loaded. The interface position within the short cut discs will be positioned closer to the axis compared to the "normal" situation, in order to establish a hydrostatic balance between the disc-stack section through which the feed enters and the short cut disc-stack section. This view is most clearly affirmed by the mutual position of the data points in the trios 13/14/15 and 28/29/30 of which, contrary to the rest of the data, the higher rotation speeds score the worst efficiency. In Appendix F the short cut model can be found, together with the qualitative results belonging to one of the above-mentioned trios.

Effect of caulk type

Experiments 52 - 57 were made with point caulks, having identical caulk thickness ($h = 1.0$ mm) as the long caulks disc-stack used within the rest of the experiments. Better efficiencies are found for the point caulks compared to the long caulks which is contrary to the results found by K.H. Brunner [9]. In our opinion this is to be explained by maldistribution, which in the

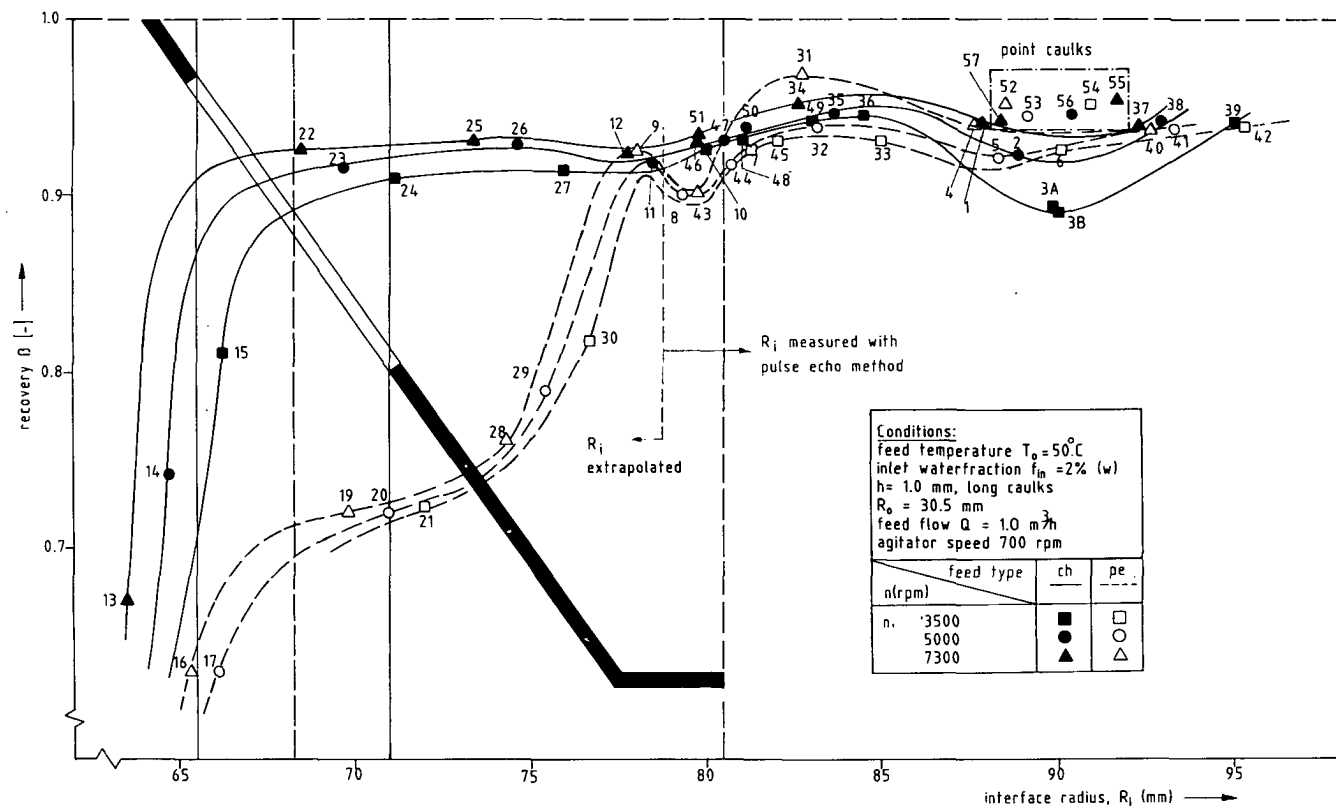


Fig.2.13 Recovery as function of interface radius.

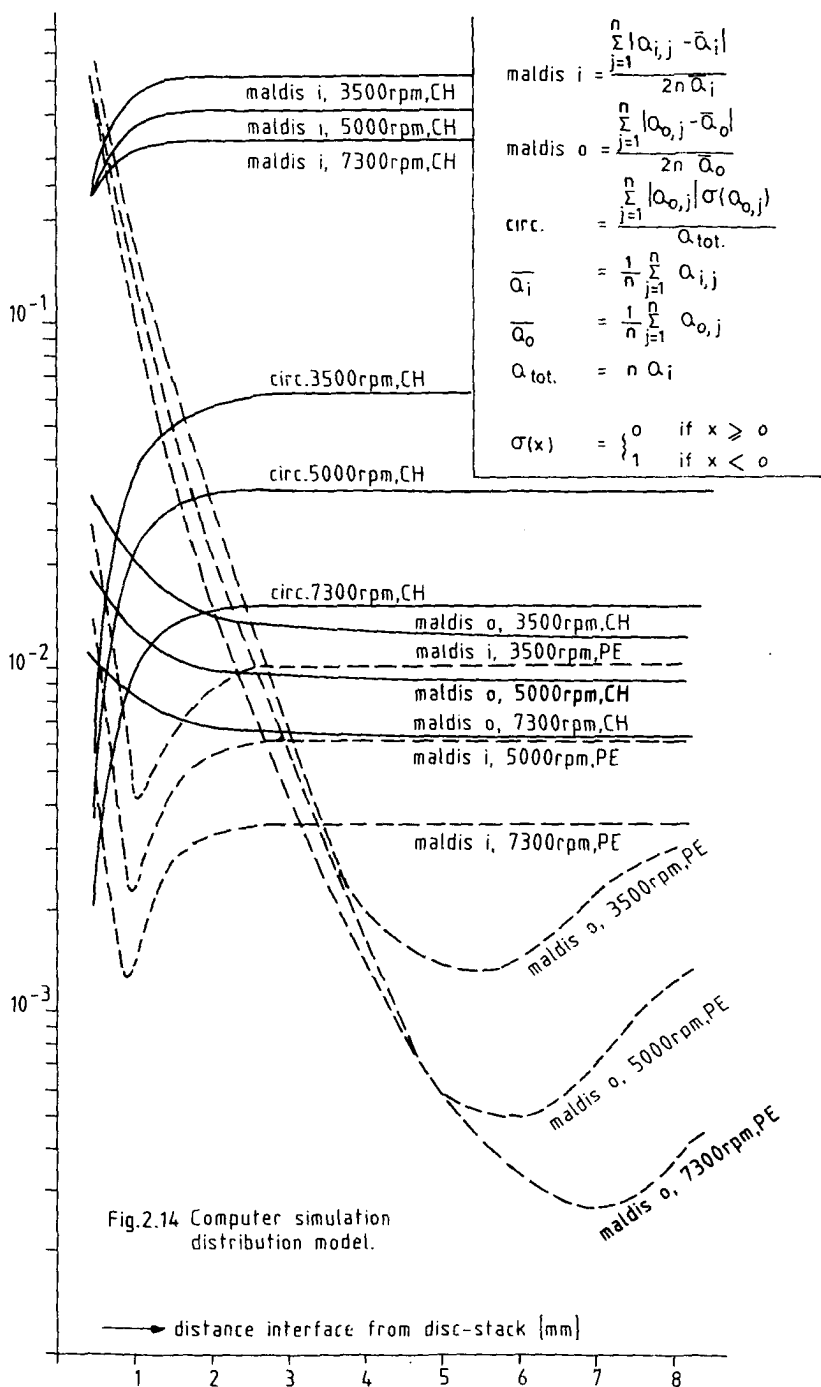


Fig.2.14 Computer simulation distribution model.

point caulk disc-stack is compared less to the long caulks disc-stack. Apparently the difference in maldistribution is significant enough to destroy the better efficiency of point caulks.

Note: Brunner experimentally observed a better efficiency for point caulks using a single disc separator, hence not dealing with maldistribution. The experimental data belonging to the above-mentioned experiments are reported by Van der Donk [17].

2.6 Conclusions

- 1) The dispersion effect in a centrifugal separator is found to be located at the guiding fins in the distributor. Both the initial shock between the feed liquid and the fin tips and the subsequent liquid stratification predominate the ultimate dispersion (paragraph 2.5.1).
- 2) Parameters determining the dispersion characteristics (e.g. in terms of drop sizes) are, in order of relevance, the centrifuge rotation speed and feed flow rate. Except for the effect on stratification itself, the influence of flow is explained by its effect on the position of the feed liquid interface radius in the distributor (paragraphs 2.5.1 and 3.5.4).
- 3) Separator performance, as far as the light phase is concerned, is strongly influenced by the position of the water oil interface. The optimum position, outside the disc-stack close to the periphery, is explained by minimization of maldistribution in the disc-stack (paragraph 2.5.2).
- 4) The water-oil interface in a centrifugal separator should never be positioned inside the feed point (channel or periphery), whereas in this situation separation efficiency sharply decreases which is caused by partial shortcutting of the disc-stack (paragraph 2.5.2).
- 5) The positive attribution of point caulks to separation efficiency of a centrifugal separator is explained by reduction of maldistribution in the disc-stack.

- 6) Liquid-liquid centrifugal separators ought to be provided with direct interface monitoring (paragraph 2.5.2).
- 7) For an experimental study into the influences of various centrifuge internals on separation efficiency, an open separator, not capable of being adjusted while running, is not the obvious type of centrifuge (paragraph 2.5.2).
- 8) On account of the risk of partial shortcutting the disc-stack, the fixed opinion that the interface should coincide with the distribution channels, should be reconsidered (paragraph 2.5.2).

CHAPTER 3

HYDRODYNAMICS

3.1 Division of chapter 3

As explained earlier in chapter 1 three important pressure effects (disc-stack, weir and gradient) can contribute to more reliable equations for the interface position as well as the hydraulic capacity. Without knowledge, however, of the hydrostatic pressure the derived models would only look fancy wherever its basis might be fragile. For this reason attention is paid, in the first place, to the hydrostatic pressure gradient (paragraph 3.3.1). In the next two paragraphs, 3.3.2 and 3.3.3, two interface models are quickly derived which are extended by insertion of the three pressure effects, discussed thereafter in paragraphs 3.3.4 - 3.3.6. In the experimental part various types of experiments are presented: interface experiments, weir head experiments, hydraulic capacity experiments and endoscope experiments.

3.2 Objectives

Providing accurate knowledge on various pressure drops for the sake of a reliable interface equation, as well as, a feed liquid interface equation. The interface radius is, apart from the variable of interest, also an indirect measurement of the pressure drop in both liquid phases.

3.3 Background theory

3.3.1 Hydrostatic pressure gradient

Due to centripetal acceleration in a rotating system, pressure gradient becomes a function of the tangential fluid velocity v_ϕ , radius r and the fluid density ρ . Assuming stationary flow, negligible radial velocity and symmetrical case the radial component of the Navier Stokes equation in a cylindrical, r, ϕ, z co-ordinate system reduces into:

$$\frac{\partial P}{\partial r} = \rho \frac{v_\phi^2}{r} \quad (3.1)$$

In the special case of solid body rotation, where v_ϕ is the product of angular velocity ω and radius r , the result of an integration in between the boundaries $r = R_1$ and $r = R_2$ is:

$$\Delta P_{1,2} = \frac{1}{2} \rho \omega^2 (R_2^2 - R_1^2) \quad (3.2)$$

Schilp [55] discusses various alternatives making use of an empirical power expression for the tangential velocity as function of the radius:

$$v_\phi \cdot r^m = \text{constant} \quad (3.3)$$

The power m is an empirical coefficient with limiting values -1 for solid body rotation and $+1$ for potential flow. In a real fluid system m lies in between -0.5 and $+0.6$ depending upon viscosity, wall effects due to internals and flow [55]. Integrating (3.1) after substitution of (3.3) yields:

$$\Delta P_{1,2} = \rho \frac{v_{\phi, \text{feed}}^2 R_{\text{feed}}^{2m}}{2m} \left[\frac{1}{R_1^{2m}} - \frac{1}{R_2^{2m}} \right] \quad (3.4)$$

In the special case of $m = 0$, equation (3.4) does not hold and the result is then:

$$\Delta P_{1,2} = \rho v_{\phi, \text{feed}}^2 \ln \left(\frac{R_2}{R_1} \right) \quad (3.5)$$

Both equations (3.4) and (3.5) result into lower values for the pressure difference compared to the solid body rotation case (3.2) provided the feed radius is the smaller radius. This is made clear in a quantitative way in figure 3.1 in which the pressure difference, calculated with equations (3.4) and (3.5) relative to the pressure/difference in the case of solid body rotation (equation (3.2)), is plotted against the radius ratio R_2/R_1 for a variety of values of the coefficient m .

For ratios above 1, when the feed radius is the smaller radius, the pressure difference is decreasing rapidly on rising radius ratio and coefficient m ,

due to the fluid's lagging behind the centrifuge. In the case of inward directed flow the spin up effect increases the pressure difference.

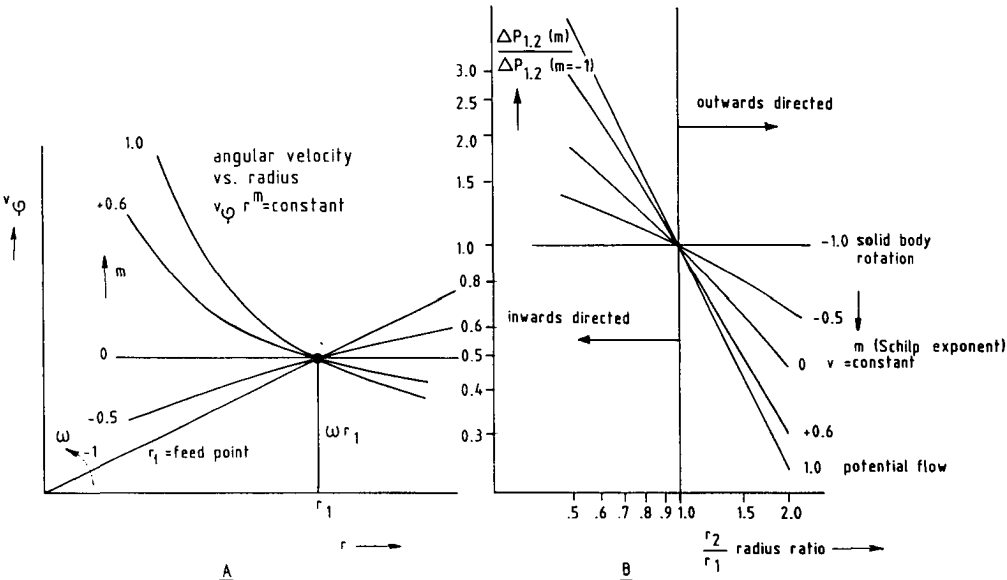


Fig.3.1 A.Tangential velocity as function of radius rand Schilp exponent m.
 B.Static pressure difference between inlet and outlet relative
 to that belonging to solid rotation.

In view of the above shown significant deviation from the frequently applied solid body rotation concept, valid reasons must be produced which can justify the ultimate choice.

During its acceleration the separator feed is forced to corotate due to the presence of guiding fins within the distributor (see paragraph 3.4.1). In the case of channel feed the accelerated feed directly enters the disc-stack and flows inward towards the cylindrical part of the top disc with its three outlet ports. In the case of peripheral feed no slip can occur at a radius smaller than R_4 (paragraph 3.4.1 figure 3.17) due to the specific construction of the distributor's lower end. However, distribution of the accelerated feed over the disc spaces requires axial flow in between the disc-stack and the interface where absence of internals make corotation in this area doubtful. The spin up effect within the disc-stack has been taken into account in the disc-stack pressure drop which significantly exceeds the Hagen-Poiseuille solution, which validity is restricted to the radial flow

situation (more details on this topic can be found in paragraph 3.3.4). The liquid leaving the disc-stack at its inner radius is collected in four axial directed channels in the outside of the distributor (see paragraph 3.4.1, figure 3.16) via which the cylinder is reached. Again corotation is forced by the collecting channels. This illustrates that the velocity magnitude characteristic of the fluid motion in the centrifugal separator can be assumed to be small compared to the basic rotation speed indicating that the solid body rotation concept is bound to be applicable in this situation.

3.3.2 Interface position

In order to obtain optimum separation results and to operate a centrifugal separator, the interface position must be known. For practical purposes the calculated gravity disc serves as a starting point and the optimum interface position is arrived at by trial-and-error adjustment. When the optimum gravity disc has been determined experimentally on a given type of centrifuge, the results may be translated to any other type of centrifuge by calculating an apparent value for the density ratio. Referring to the above-mentioned procedure, Ambler [2] states that, in spite of a questionable mathematical integrity, the results are quite satisfactory. On a variety of locations in the open literature equation (3.6) is presented based upon solid body rotation assuming zero pressure drop:

$$R_i = \sqrt{\frac{\rho_w R_w^2 - \rho_o R_o^2}{\rho_w - \rho_o}} \quad (3.6)$$

Preliminary experiments, however, clearly showed that equation (3.6) underestimates the interface radius (see paragraph 3.5.1). More correctly, one should take into account the pressure drop of the heavy and light-phase liquids in passing through the discharge passages of the centrifuge bowl. Assuming solid body rotation in the separator, a modified equation for the interface position can be derived by introducing pressure drops in both the oil phase, $\Delta p_{o,i}$, as well as in the water phase, Δp_w into the hydrostatic pressure equation:

$$\frac{1}{2} \rho_w \omega^2 (R_i^2 - R_w^2) + \Delta p_w = \frac{1}{2} \rho_o \omega^2 (R_i^2 - R_o^2) + \Delta p_{o,i} \quad (3.7)$$

Writing the interface radius R_i explicitly yields:

$$R_i = \sqrt{\frac{\rho_w R_w^2 - \rho_o R_o^2 + \frac{2}{\omega^2} (\Delta p_{o,i} - \Delta p_w)}{\rho_w - \rho_o}} \quad (3.8)$$

It must be emphasized that R_o is the oil outlet radius of the separator (being 26 mm for the standard top disc and 30.5 mm for the increased capacity top disc, see paragraph 3.4.1), while the actual liquid surface radius is smaller, due to the non-zero liquid height. This effect is accounted for within the pressure drop $\Delta p_{o,i}$. Fumoto and Kiyose [23] observed that the interface position in a centrifugal extractor varied as a result of pressure drop in water and oil phase. From a numeric analysis on photographic observations of the interface radius they learned that pressure drop in the oil phase is proportional to flow rate, and in the water phase to the power of 0.64 of the flow rate. The observed proportionality with respect to the organic flow rate seems doubtful, whereas organic flow rate was varied in a restricted range and spreading in results occurred. The pressure drops at both the organic and anorganic phase weirs, are expressed as unique functions of the Reynolds number which drastically overestimates viscosity effects. The experiments made at constant rotation speed showed a minimum interface radius with respect to the total flowrate at constant phase ratios.

According to Trowbridge [64] loss of head due to liquid pressure drop is small compared with the centrifugal head, and may be ignored for practical purposes. The results presented in paragraph 3.5.1 and subsequent numerical analysis, however, point out the significance of these pressure drops which should actually be compared with the centrifugal head multiplied with the ratio of density difference to oil density $\Delta\rho/\rho_o$ in order to check upon its significance (see also equation 3.8). For instance, deviations of some 10 mm from the static equation have been found in this study, whereas the density difference of the oil used in the experiments is not too small. In other words: deviations would be even higher treating heavier oils.

3.3.3 Hydraulic capacity

For three reasons knowledge of hydraulic capacity is inevitable to understand the working principles of a centrifugal separator.

First, when hydraulic capacity is exceeded the excess of feed is collected and will be discharged together with the purified oil. This implies bypassing of the separator bowl which reduces the overall separation efficiency.

Second, knowing the principles behind hydraulic capacity, the effect of modifications of the separator can be predicted. This knowledge appeared to be quite useful within the centrifuge project, when it was necessary to extend the separator capacity in order to allow wide variations in flow.

Third, knowing the pressure drop which governs hydraulic capacity, knowledge is obtained of the distributor flow and the position of the feed liquid interface with air.

The latter affects the feed dispersion which is a limiting factor for the separation efficiency. In correspondence with paragraph 3.3.2 solid body rotation is assumed and the capacity equation, which is a hydrostatic balance between the incoming feed and separated oil, is written:

$$\frac{1}{2} \rho_o \omega^2 (R_o^2 - R_e^2) = \Delta p_{o, \text{cap}} \quad (3.9)$$

The left-hand side of equation (3.9) is the available pressure due to a difference of inlet and outlet level with corresponding radii of R_e and R_o respectively. The oil density of the feed has been assumed equal to the density of the separated oil. Both a low feed concentration and a pre-separation effect outside the disc-stack allow this assumption to be made. The validity of equation (3.9) is restricted to situations where the interface radius is bigger than the feed radius, a condition which is always fulfilled in practice. It must be emphasized that $\Delta p_{o, \text{cap}}$ in equation (3.9) and $\Delta p_{o, i}$ in equation (3.7) need not be identical: $\Delta p_{o, \text{cap}}$ is expected to be $\Delta p_{o, i}$ to which the pressure effects of the distributor have to be added. In the case of the centrifugal separator used within this study more locations are believed to contribute to the total pressure drop. First, the disc-stack which divides the feed in parallel streams either fed via the channel or via the periphery.

Second, the weirs, nearby the outlet of both phases, where the liquid flows over at a radius smaller than the weir radius itself.

Third, locations where viscosity can play an important role, such as the cylindrical part of the top disc. In the paragraphs to come attention will be focused on the above-mentioned effects in a corresponding sequence.

3.3.4 Disc-stack

3.3.4.1 Symmetrical flow solution

In order to raise separation efficiency, a centrifugal separator is provided with a stack of conical discs. The discs are being spaced by means of caulks which can either be long or short: long caulks or point caulks. In most cases the discs are provided with holes, together forming the distribution channels through which the feed enters the disc-stack. This paragraph will mainly focus on the effects of disc geometry on pressure drop. Existing mathematical models on separation efficiency have been based on the assumption that flow between discs is directed radially inward parallel to the disc surfaces, and is uniformly distributed peripherally. One of the models (Jury & Locke [39]) further postulated that the flow should have a parabolic profile. One might expect such a flow pattern from the disc geometry in a non-rotating system, but it does not hold for rotating ones. In rotating systems, coriolis and incremental centrifugal forces act on fluid particles, tending to impel them at right angles to their local directions of motion. Further, a parabolic velocity profile would violate the Taylor-Proudman theorem (Greenspan [28]) which states that save for flow in exponentially thin boundary layers at the disc surfaces, the bulk interior fluid motion in a rotating system will be two-dimensional viewed on planes perpendicular to the axis of rotation (Willus Fitch [70]). The Navier Stokes equation for the stationary case in a co-ordinate system rotating with constant angular velocity $\underline{\omega} = \omega \hat{\underline{k}}$ ($\hat{\underline{k}}$ is the unit vector) and \underline{r} , \underline{u} , ρ and ν representing the position vector, particle velocity, density and kinematic viscosity is according to Greenspan [28] given by:

$$\underline{u} \cdot \nabla \underline{u} + 2 \omega \hat{\underline{k}} \times \underline{u} = - \frac{1}{\rho} \nabla p - \nu \nabla \times (\nabla \times \underline{u}) \quad (3.10)$$

with p the reduced pressure combining pressure P with the centrifugal acceleration and being defined as follows:

$$p = P - \frac{1}{2} \rho (\underline{u} \times \underline{r}) \cdot (\underline{u} \times \underline{r}) \quad (3.11)$$

With h , the caulk thickness (or disc distance) as the characteristic length scale, $1/\omega$ for the time scale and U for the velocity scale, equation (3.10) is written dimensionless:

$$Ro \underline{u}' \cdot \nabla \underline{u}' + 2 \hat{k} \times \underline{u}' = -\nabla' p' - Ekm \nabla' \times (\nabla' \times \underline{u}') \quad (3.12)$$

The Ekman number, Ekm , is the ratio of viscous forces to coriolis forces ($Ekm = \nu/\omega h^2$) while the Rossby number, Ro , is the ratio of local convective forces to coriolis forces ($Ro = U/\omega h$). The most original work on the disc-stack problem is published by A. Brunner in his thesis [7]. The symmetrical case (no caulks) with peripheral feed and $Ro = 0$ is solved analytically and formulated in a cone co-ordinate system l, x, ϕ with l in the meridian direction (inwards directed), x the wall distance perpendicular to the cone surface ($0 < x < h$) and ϕ the circumferential angle (see figure 3.2 A). For the meridian velocity component A. Brunner [7] derives (see figure 3.2 B):

$$v_l = \frac{dp}{2 \rho \omega \frac{dr}{dr}} N(\xi, \lambda) \quad (3.13)$$

and for the tangential velocity component (see figure 3.2 C):

$$v_\phi = \frac{dp}{2 \rho \omega \frac{dr}{dr}} M(\xi, \lambda) \quad (3.14)$$

with the streamparameter λ which is a direct function of the Ekman number:

$$\lambda = \frac{1}{\sqrt{Ekm}} = h \sqrt{\frac{\omega \sin \theta}{\nu}} \quad (3.15)$$

and the dimensionless wall distance co-ordinate ξ :

$$\xi = x \sqrt{\frac{\omega \sin \theta}{\nu}} \quad (3.16)$$

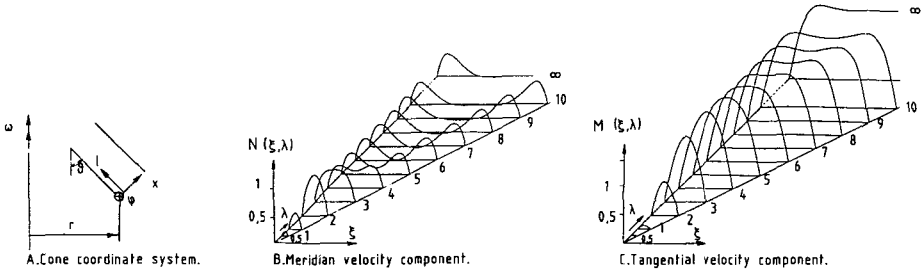


Fig.3.2. Velocity profiles in between corotating conical discs, axisymmetrical solution. Source: A. Brunner [7].

The velocity profiles are expressed as analytical functions of ξ and λ :

$$N(\xi, \lambda) = \frac{\sinh(\xi) \sin(\lambda - \xi) + \sinh(\lambda - \xi) \sin(\xi)}{\cosh(\lambda) + \cos(\lambda)} \quad (3.17)$$

$$M(\xi, \lambda) = 1 - \frac{\cosh(\xi) \cos(\lambda - \xi) + \cosh(\lambda - \xi) \cos(\xi)}{\cosh(\lambda) + \cos(\lambda)} \quad (3.18)$$

Integration of equation (3.17) and (3.18) in between the boundaries $\xi = 0$ and $\xi = \lambda$ yields:

$$\begin{aligned} N^\circ(\lambda) &= \frac{1}{h} \int_0^h N(\xi, \lambda) dh = \frac{1}{\lambda} \int_0^\lambda N(\xi, \lambda) d\xi = \\ &= \frac{1}{\lambda} \frac{\sinh(\lambda) - \sin(\lambda)}{\cosh(\lambda) + \cos(\lambda)} \end{aligned} \quad (3.19)$$

$$\begin{aligned} M^\circ(\lambda) &= \frac{1}{h} \int_0^h M(\xi, \lambda) dh = \frac{1}{\lambda} \int_0^\lambda M(\xi, \lambda) d\xi = \\ &= 1 - \frac{1}{\lambda} \frac{\sinh(\lambda) + \sin(\lambda)}{\cosh(\lambda) + \cos(\lambda)} \end{aligned} \quad (3.20)$$

Integration of the pressure gradient dp/dr in equation (3.13) combined with equation (3.19) in between the boundaries $r = R_1$ (inner disc radius) and $r = R_2$ (outer disc radius) yields the pressure drop in the symmetrical case:

$$\Delta p_{\text{sym}} = \frac{\rho \omega Q \ln R_2/R_1}{\pi h N_s N^\circ(\lambda)} \quad (3.21)$$

It can quite easily be verified that this pressure drop exceeds the radial solution, which can be calculated straight forward when assuming parabolic flow, but also is the limiting case of the above-presented solution for $\lambda \rightarrow 0$:

$$\Delta p_{\text{radial}} = \frac{6 n Q \sin\theta}{N_s \pi h^3} \ln \frac{R_2}{R_1} \quad (3.22)$$

3.3.4.2 Assymmetrical case

Due to the suppression of the geostrophic flow in between the discs, presence of long caulks reduces pressure drop. According to Carlsson [11] this effect can be calculated with a correction factor:

$$\frac{\Delta p_{\text{caulks}}}{\Delta p_{\text{sym}}} = \frac{N^\circ(\lambda)^2}{N^\circ(\lambda)^2 - M^\circ(\lambda)^2} + \frac{\sin\theta \ln(\sqrt{2}+1)}{N_{\text{caulk}} \ln \frac{R_2}{R_1}} \cdot \frac{M^\circ(\lambda)^2}{N^\circ(\lambda)^2 + M^\circ(\lambda)^2} \quad (3.23)$$

provided that:

$$\left(\frac{R_1}{R_2} \right)^{\frac{N_{\text{caulk}}}{2 \sin\theta}} \ll 1$$

The radial solution (3.22) is always the minimum value!

Quite remarkable is that the resulting pressure drop in the non-symmetrical case is not a function of the radius ratio anymore. Substituting $\theta = 35^\circ$, $N_{\text{caulk}} = 6$, $R_1 = 0.03909$ and $R_2 = 0.07728$ a value of 0.495 is found for the correction factor for high values of λ . For $\lambda = 0$ (no rotation) the correction factor has the trivial value of 1. Goldin [26] calculates, the

flow pattern in between the discs in case of peripheral feed and with long caulks. The result, an analytical expression for the fluid velocities, is obtained with the conform mapping technique. Contrary to the expression derived by Carlsson (equation 3.23), Goldin's solution, however, does not fulfil the Navier Stokes equation. It follows from this work that the role of the feed conditions of the liquid is very considerable. The more the fluid entrance angle γ tends to the radial direction, the more rapidly the trajectories of the liquid approach the generatrices of the discs, while the flow becomes radial with a velocity practically identical over the whole width of the gap between the discs. With an increase of the entrance angle γ , there is an increase in the sector of fully established radial flow and, what is most important, the surface of the discs is found to be loaded over more non-uniformly by the flow. In this case most of the liquid flows near the leading caulk, or trailing caulk when the entrance angle is negative. It is evident that the optimum is the ideal case with a radial peripheral feed (see figure 3.3). In practice this situation might be approached by the application of a winged disc-stack, a disc-stack provided with radial baffles situated in the outer disc space.



Profiles of fully established meridian velocities:
a) $\lambda=5$; b) 10; c) 15

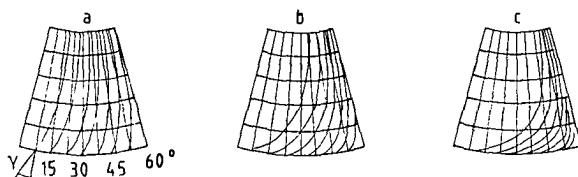


Fig.3.3 Flow lines different inlet conditions of the liquid:
a) $\gamma=30^\circ$; b) 60° ; c) 75° . Source: Gol'din [26]

3.3.4.3 Channel feed

The effect of channel feed is taken into account by Goldin [25], introducing point source solutions on the interdisc flow pattern, making use of a conform mapping technique. With these results the pressure drop from the channel towards the inner radius of the disc-stack can be calculated:

$$\Delta p_{ch} = \frac{\rho \omega Q \sin \theta}{2\pi h N_h N_s N^s(\lambda)} \left[\ln \frac{P_2^{2N_h} + P_{ch}^{2N_h} - 2P_2^{N_h} P_{ch}^{N_h} \cos(N_h \cdot \phi)}{P_1^{2N_h} + P_{ch}^{2N_h} - 2P_1^{N_h} P_{ch}^{N_h} \cos(N_h \cdot \phi)} + \right. \\ \left. - \ln \frac{P_2^{2N_h(1-q)}}{P_1^{2N_h(1-q)}} \right] \quad (3.24)$$

$$\text{with } P = \left(\frac{R}{\sin \theta} \right)^{1/\sin \theta} \quad (3.25)$$

and q the fraction of the flow going outwards, and ϕ the circumferential angle defined $\phi = 0^\circ$ at the channel. The channel feed situation can be compared with the peripheral feed situation evaluating equations (3.21) and (3.24). The ratio of the pressure drops for both feed types appears to be dependent upon geometrical data only, and is a weak function of ϕ , the circumferential angle. For the symmetrical solution two options were considered: first, peripheral feed of the complete disc and second, peripheral feed of a disc with outer diameter identical to the channel diameter of the former. Geometrical data used in the calculations can be found in paragraph 3.4.1. The fraction of the flow going outwards, q , is assumed to be zero.

The results, presented in table 3.1, show that the pressure drop near the channel ($\phi = 0^\circ$) exceeds the pressure drop in between the channels ($\phi = 30^\circ$) with approximately 10%. The effect of feeding at six discrete points, rather than the complete circumference at identical radius, results in roughly identical pressure drop.

Table 3.1 Disc pressure ratios according to equations
(3.21) and (3.24) for the MAB 104 separator

$\frac{\Delta p_{ch}}{\Delta p_{sym}} (\phi = 0^\circ) = 0.863$	$\frac{\Delta p_{ch}}{\Delta p_{sym}} (\phi = 0^\circ) = 1.055$
$\frac{\Delta p_{ch}}{\Delta p_{sym}} (\phi = 30^\circ) = 0.785$	$\frac{\Delta p_{ch}}{\Delta p_{sym}} (\phi = 30^\circ) = 0.960$

3.3.4.4 Stability

The above-mentioned solutions can turn instable. In view of the separation efficiency this phenomenon can be considered to be harmful. In a treatise on this problem, Greenspan [28] refers to the work of Tatro & Mollo - Christensen [61] who performed experiments on Ekman-layer instability; in a cylindrical-shaped vessel velocity profiles were measured using the hot wire anemometer technique. Their results correspond rather well to the analytically derived solution ($Ro = 0$): the geostrophical flow appeared somewhat weaker due to non-linearity. The Rossby and Reynolds numbers were defined for the local measured values in the boundary layer:

$$Ro = \frac{v_\phi}{\omega r} \quad (3.26)$$

$$Re = \frac{\delta v_\phi}{\nu} \quad (3.27)$$

Here v_ϕ is the relative azimuthal component of the interior velocity; δ is the local value of the boundary layer thickness. Results of the work of Tatro & Mollo - Christensen are depicted in figure 3.4.

It appears that the instability labelled type II by Faller [21] always occurs first, and at zero Rossby number the critical Reynolds number is 56 ± 2 . This instability originates in the boundary layer, but at slightly higher Reynolds number the fluctuations persist far into the geostrophical region. At higher Reynolds number another instability appears of shorter wavelength and slower speed, type I reported by Faller, which is confined to the boundary layer.

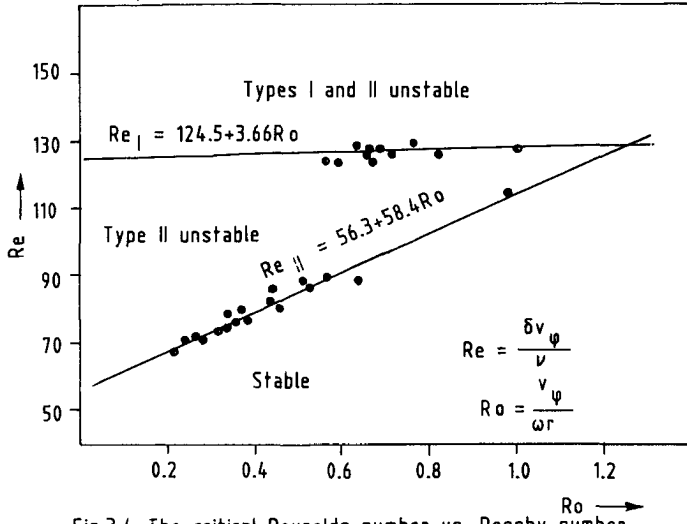


Fig.3.4 The critical Reynolds number vs. Rossby number types I and II instabilities.
Source : Tatro & Mollo-Christensen

With the Reynolds number defined in (3.27) a general criterion for the onset of instability can be derived according to Greenspan [28]. Boundary layer instability may first be expected when:

$$Re = Ro \cdot Ekm^{-\frac{1}{2}} = 56 \quad (3.28)$$

In his thesis K. Brunner [9] presents stability data, obtained with a transparent single disc separator. Making use of a marking fluid, the transition from laminar to turbulent flow was determined for various caulk thicknesses, flow rates rotation speeds and viscosities. Two disc types were applied: first, one without caulks, second, a disc with 8 long caulks. The half cone angle of this disc is 35° , which is identical to that in the MAB 10⁴ separator used in this study. Results of this work can be found in figure 3.5 with Ro' defined as:

$$Ro' = \frac{\bar{v}_1}{\omega R_2} \quad (3.29)$$

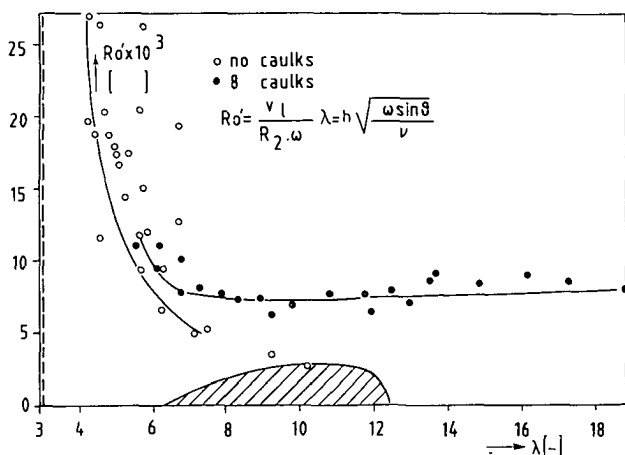


Fig.3.5. Critical Rossby number as function of λ .
(hatched area = industrial separators)
Source: K. Brunner

In order to compare the two studies Brunner's variables were converted to Greenspan's notation for Ro (3.26) and Re (3.27). Using (3.29) and (3.30) the average velocity can be converted from the meridian towards the tangential direction (axisymmetrical case) with the following result:

$$Re = Ro' \frac{\lambda R_2}{h \sin \theta} \frac{M^o(\lambda)}{N^o(\lambda)} \quad (3.30)$$

Figure 3.6 shows Brunner's data. From this plot it can be concluded that the presence of caulks has a stabilizing effect most probably due to suppression of the geostrophical flow. It must be noted that the same conversion factor (equation 3.30) has been used for both the symmetrical case, and the non-symmetrical case. For the latter case this means that the geostrophical flow is overestimated, resulting in higher Reynolds values. It seems, however, that this suppression is a function of caulk thickness. For the lower λ -values ($\lambda < 2\pi$) higher values for Reynolds are observed, which might be explained by the fact that both "Ekmanlayers" within the disc space will interfere more and more at decreasing λ , before they ultimately transform into a parabolic profile.

From figure 3.6 it can be seen that several instability points occur at a Reynolds number which is significantly lower than the above-mentioned value of 56. A minimum value for Reynolds is also reported by Gusev & Bark [29]

who made a study of the stability problem for the steady shear flow between two parallel planes, rotating with the same angular velocity. The critical Reynolds number has a minimum value $Re_c \sim 31$ for $\lambda = 6.2$. Leibovich & Lele [46] made an extensive study on the influence of the horizontal component ω_h of the angular velocity ω on the instability of the Ekman layer. It is shown that the horizontal component of angular velocity destabilizes the Ekman layer. The classical steady Ekman layer is a motion everywhere parallel to a plane; in it, deviation from a state of rigid rotation exists with coriolis accelerations and pressure gradients balanced by viscous forces. The coriolis accelerations that enter are those associated with ω_n , the component of the angular velocity of the reference frame that is normal to the planes of motion. It is found that the critical Reynolds value of 54.2 in the case of $\theta = 90^\circ$ (θ is defined to be the latitude in the geophysical context: $\tan\theta = \omega_n/\omega_h$) is reduced to 30.8 for latitudes of 26.2° and less.

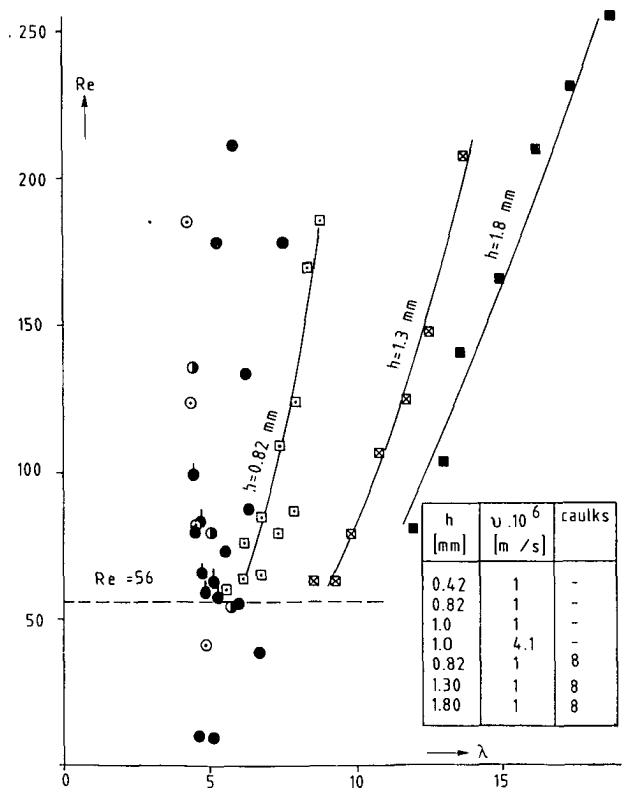


Fig.3.6 Stability of interdisc flow Data:K.Brunner [9]

3.3.5 Weir

In the open literature vast quantities of information on weirs can be found. Especially in the field of civil engineering knowledge on this subject is available in the case of water and high weirs. In order to have an overview on literature, a well-known handbook written by Vennard [65] is quoted. Besides, attention is paid to side effects such as fluid physical properties.

Open-channel flow

Weir flow can -in some cases- be considered to be a special case of open-channel flow. Although open-channel problems practically always involve the flow of water, and although the experimental results used in these problems were obtained by hydraulic tests, modern fluid mechanics indicate the extent in which these results may be applied to the flow of other fluids in open-channels. Open-channel flow may be laminar or turbulent, steady or unsteady, uniform or varied, tranquil or rapid. Because laminar flow of liquids in open channels has few practical applications for the civil engineer, and the problem of unsteady flow is an exceedingly complex one, the discussion will therefore be confined to steady turbulent flow. When the depth of flow continually varies when the forces acting on fluid particles (gravity only) are unbalanced, this type of fluid motion is termed "varied flow". As soon as resistance forces due to fluid viscosity and channel roughness are present, a constant velocity motion is attained, which is characterized by no change of flow cross section and thus no change in the depth of flow: the depth of flow remains constant, hence the term "uniform flow". Varied flow occurs in practice to a far greater extent than uniform flow. In short channels, for example, uniform flow conditions may never be attained because of the long reach of channel necessary for the establishment of uniform flow.

Critical depth

In channel flow a maximum rate of flow occurs at the critical depth since the point of maximum flow for a given specific energy content is the same as that of minimum energy for a given rate of flow. Since critical depth occurs when specific energy is minimal for a given rate of flow, the equations of critical flow may be obtained by differentiating the expression for specific energy and equating the result to zero.

It is convenient, at this point, to deal with flow in a channel of rectangular cross section, whose simple geometrical form will allow the use of simple equations to illustrate the fundamentals. If a uniform velocity distribution is assumed in the rectangular channel of figure 3.7, the unit rate of flow q through a vertical strip of 1 m width will be given by $q = Vd$, which will eliminate the width of channel b from subsequent equations. The expression for the specific energy E is given to be:

$$E = d + \frac{v^2}{2g} \quad (3.31)$$

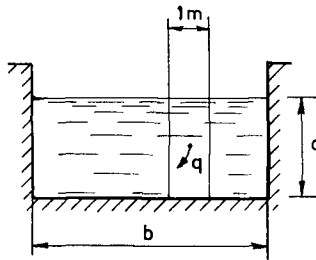


Fig.3.7. Uniform channel flow.

Substitution of the equation for q into (3.31) gives:

$$E = d + \frac{q^2}{2gd^2} \quad (3.32)$$

Plotting this equation assuming q constant introduces some new concepts to open-channel flow. The specific energy curve possesses a point of minimum energy at which the depth is termed the "critical depth". For every specific

energy, E , there are two "alternate" depths at which flow may take place, one greater and one less than the critical depth. If the depth of flow is greater than the critical depth, the flow is said to be "tranquil" and the slopes, which bring about such flows, are designated as "mild" slopes. The flow is said to be "rapid" if depth is less than the critical depth; rapid flows are caused by "steep" slopes (see figure 3.8). In the region of flow near the critical depth, the depth may change for practically constant specific energy. Physically this means that, since many depths may occur for practically the same specific energy content, flow near the critical depth will possess a certain instability (which frequently manifests itself by undulations in the liquid surface).

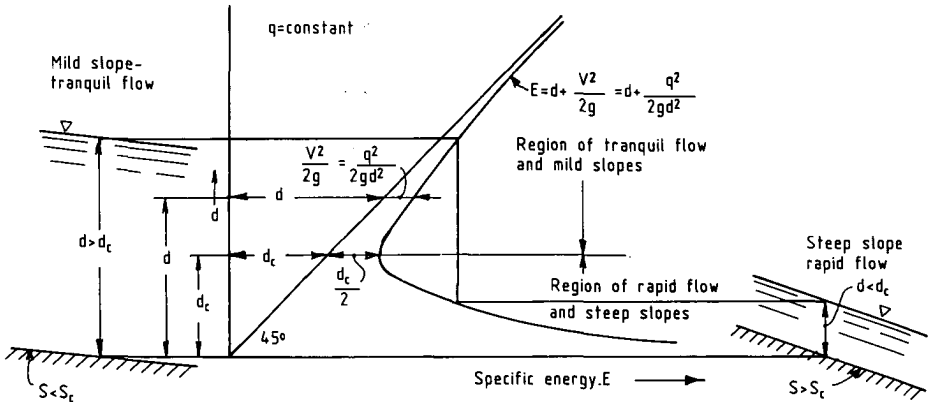


Fig.3.8 The specific energy diagram.
Source: Vennard [65]

Since critical depth occurs when specific energy is minimal for a given rate of flow the equations of critical flow may be obtained by differentiating equation (3.32):

$$\frac{dE}{dd} = 1 - \frac{q^2}{g d_c^3} = 0 \quad (3.33)$$

The critical depth d_c is:

$$d_c = \sqrt[3]{\frac{q^2}{g}} \quad (3.34)$$

The velocity v_c at critical conditions may be obtained as:

$$v_c = \sqrt{g d_c} \quad (3.35)$$

which at the same time is the velocity of propagation of a small wave on the surface of a body of liquid of depth d_c which offers rough means of identifying rapid, tranquil and critical flows. Substituting equation (3.35) into equation (3.31), the specific energy at the critical point is found to be $1.5 d_c$ which is the far upstream depth, provided no energy is lost due to friction.

Position of critical point

Critical depth will occur in open-channel flow when a change in channel slope brings about a change from tranquil to rapid flow or from rapid to tranquil flow. At a free overfall the critical depth will occur a short distance upstream from the brink. According to Rouse [54] this distance is equal to approximately four times the critical depth upstream from the crest for relatively smooth channels. Since in the case of negligible resistance the critical depth was an extremely great distance upstream, it might be reasoned that increasing resistance (hence increasing slope of the surface) would cause the computed critical section to move nearer and nearer to the crest. This explains the necessity of inserting a variable coefficient in the equation relating flow to the depth at an established point of measurement.

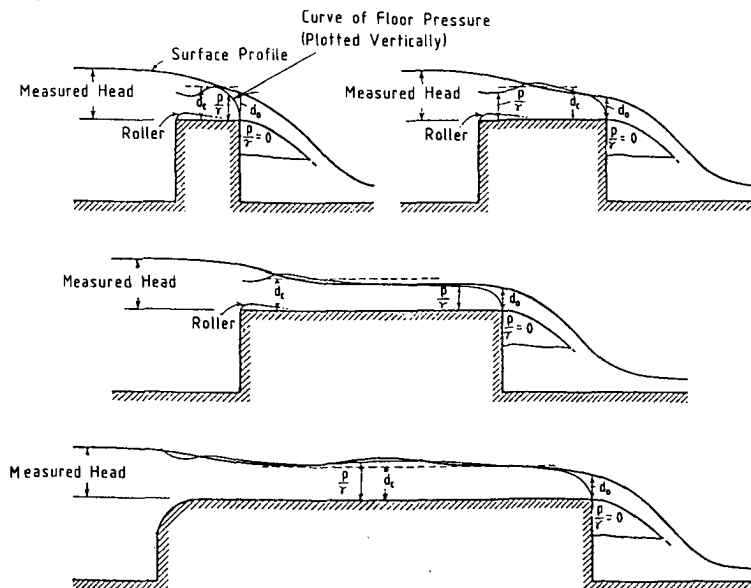


Fig3.9 Typical surface profiles and pressure distributions for broad-crested weir of various proportions .Source:Rouse [54]

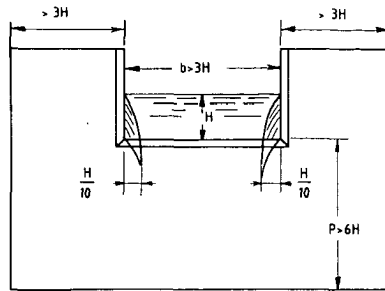


Fig.3.10 Rectangular contracted weir
Source: Vennard [65]

Weirs

A weir may be defined in a general way as "any regular obstruction in open flow over which flow takes place". Weirs for measuring purposes are usually of more simple and reproducible form consisting of smooth, vertical, flat plates with upper edges sharpened. Such weirs, called "sharp-crested" weirs, appear in a variety of forms, the most popular of which is the rectangular weir which has a straight, horizontal crest. When provided with nappe contractions at the ends of the weir rectangular, notches are also called contracted weirs. Obviously, when rectangular weirs extend from wall to wall of an open channel, these contractions are eliminated or suppressed, and for this reason this type of weir is termed a "suppressed" weir. Also for the weir head model the derivation is presented.

The assumptions are 1) uniform upstream velocity distribution, 2) horizontal velocity above the crest, 3) zero pressure in the nappe and 4) no influence of viscosity, turbulence, secondary flows and surface tension. Bernoulli's equation for streamline 1-2 (see fig. 3.11B):

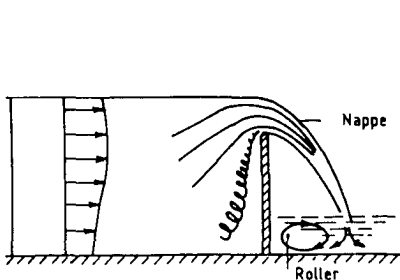


Fig.3.11a Weir flow (actual).

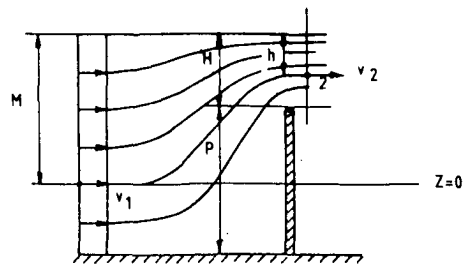


Fig.3.11b Weir flow (simplified).

$$p_1 + \frac{1}{2}\rho v_1^2 + \rho g z_1 = p_2 + \frac{1}{2}\rho v_2^2 + \rho g z_2$$

$$\rho g M + \frac{1}{2}\rho v_1^2 + 0 = 0 + \frac{1}{2}\rho v_2^2 + \rho g(M-h) \quad (3.36)$$

hence:

$$v_2^2 = 2 g \left(h + \frac{v_1^2}{2g} \right) \quad (3.37)$$

Integration of this velocity profile provides the flow Q:

$$Q = b \sqrt{2 g} \int_0^H \left(h + \frac{v_1^2}{2g} \right)^{\frac{1}{2}} dh \quad (3.38)$$

$$Q = \frac{2}{3} b \sqrt{2 g} \left[\left(H + \frac{v_1^2}{2g} \right)^{\frac{3}{2}} - \left(\frac{v_1^2}{2g} \right)^{\frac{3}{2}} \right] \quad (3.39)$$

For small values of v_1 this can be simplified:

$$Q = C \frac{2}{3} b \sqrt{2 g} H^{\frac{3}{2}} \quad (3.40)$$

in which C is an inserted experimental coefficient. Rouse [54] makes some calculations on this coefficient for the special case of a free overfall shown in figure 3.12.

According to Rouse [54] the constant C in equation (3.40) can be seen to be built up as a product of C_c , the coefficient of contraction and C_v which includes in dimensionless terms the velocity of approach

$$C_v = \left[\frac{h + \frac{v_1^2}{2g}}{h} \right]^{\frac{1}{2}} - \left[\frac{\frac{v_1^2}{2g}}{h} \right]^{\frac{1}{2}} \quad (3.41)$$

Assuming now that the free overfall is a sharp-crested weir of zero height, and that the discharge head is the critical depth ($h = d_c$), the discharge coefficient C may be computed from the critical discharge relationship (eq.(3.34)).

$$Q = \sqrt{g} b d_c^{\frac{3}{2}} = C \frac{2}{3} \sqrt{2g} b d_c^{\frac{3}{2}} \quad (3.42)$$

$$C = \frac{3}{2\sqrt{2}} = 1.061 \quad (3.43)$$

C_v may also be computed from the relationship between hydrostatic critical depth and velocity head:

$$C_v = \left[\frac{1 + \frac{1}{2}}{1} \right]^{\frac{1}{2}} - \left[\frac{\frac{1}{2}}{1} \right]^{\frac{1}{2}} = 1.485 \quad (3.44)$$

From these two values, the result for the coefficient of contraction C_c is:

$$C_c = \frac{C}{C_v} = \frac{1.061}{1.485} = 0.715 \quad (3.45)$$

Rouse has experimentally verified that this contraction coefficient is equal to the ratio between crest depth and computed critical depth, regardless of rate of discharge or channel width b .

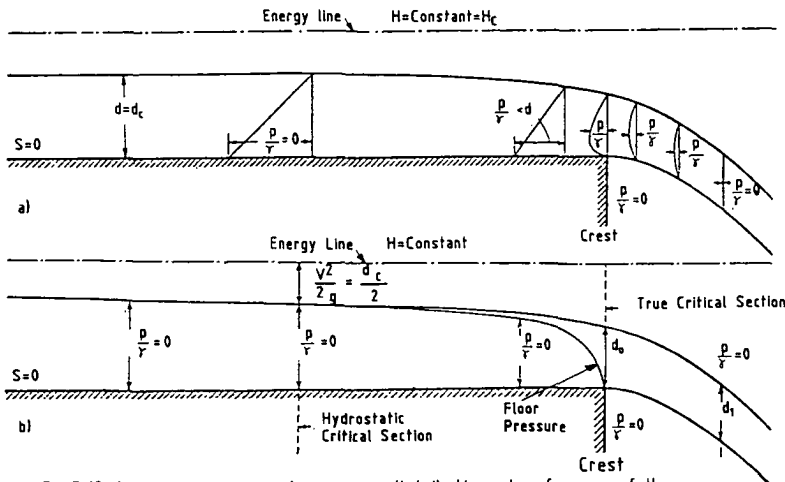


Fig.3.12 Surface profiles and pressure distribution at a free overfall
(a) Assumed case of constant specific energy.
(b) an actual profile pressure distribution in the nappe is similar to that in (a) [54]

Influencing factors

A. Geometrical form

Weir height

For a given head the weir coefficient C increases with decreasing weir height or for a weir of fixed height the coefficient increases with increasing head. Slocum [59], who experimented with viscous fluids, noted an increase in liquid-height gradient with decrease in weir height.

Weir thickness

Both at the upper end of the weir and at the crest region abrupt accelerations occur. If the weir is very broad, it is reasonable to expect the first transition curve to end some distance upstream from the transition of the crest region. A narrow weir, however, may result in a mutual interference of the two transition curves, in which case neither attains its full independent form [54]. See figure 3.9 for typical profiles.

Weir shape

If the upstream end of the weir is a sharp corner, a region of discontinuity can be observed between the flow and the floor of the weir, this region being filled with a roller of water as shown in figure 3.9. Because of the effective height of this roller above the weir floor, the flow reaches its toe at a velocity somewhat above the critical, and the surface thereafter is either highly undular (for very broad weirs) or of the general rising profile typical of such rapid motion, depending upon the ratio between the head, h , and the weir breadth. If the upstream end of the weir is rounded sufficiently, this roller will no longer exist. The surface will remain undular, however, unless the rounding be exceedingly gradual, but the critical depth will not occur until the transition region of the crest is reached according to Rouse [54].

Weir length

The rectangular contracted weir (figure 3.10) may be treated by the method suggested by Francis who found, experimentally, that the end contraction was a unique function of the head on the weir and was equal to one-tenth of the head [65]. He reasoned that the end contractions reduced the effective weir length from b to $(b-2H/10)$, and proposed the equation

$$Q = C \frac{2}{3} (b - \frac{2H}{10}) \sqrt{2g} H^{\frac{3}{2}} \quad (3.46)$$

Frese [21] in an extensive article deals with the effects of the channel geometry. The latter concludes that the weir constant increases on increasing relative weir length. A formula is derived for the weir coefficient which fits closely with experimental results obtained by various workers.

3. Fluid physical properties

Viscosity

Lenz [47] made a study of triangular weir flow using liquids other than water. It was found that the weir coefficient increased with viscosity. Within the range of tests, as a result of increasing viscosity 150 times, the weir coefficient for the same head was increased 3-7% for the 90° notch and 5-11% for the 20° notch. Slocum [59], who worked with viscous fluids, finds that the weir head is roughly proportional to the power 1/3 of the viscosity. The application of his correlation is limited to weirs of 0.1 inch or higher.

Surface tension

Lenz [47] tried to find out the effect of surface tension and found that the weir coefficient increases with surface tension. Surface tension was varied from 1 to 0.41 times that of water, however, it was never

independently varied. In the discussion of the paper it is pointed out that the derived formula is valid in a restricted range of the parameters Re and We .

Temperature

For a head of 0.5 ft water on a 90° weir a change in temperature from 40 to $165^\circ F$ changes the value for C from 0.5860 to 0.5803 which is about 1% [47]. The effect of water temperature is inappreciable compared with other factors present.

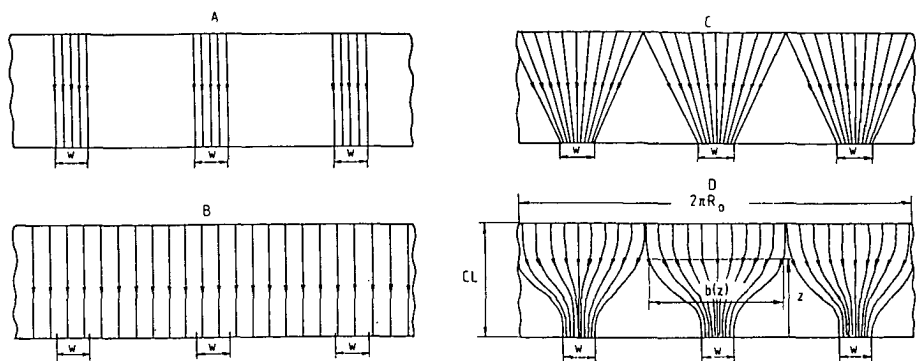
C. Factors with respect to flow

Velocity distribution

Schoder and Turner [57] have experimentally verified the significant effect of the velocity distribution upstream from the weir. The extreme difference in discharge due to altering the velocity distribution, keeping the head constant, amounted to 26 per cent. For precision it is necessary not to deal (as in most formulas) with the head corresponding to the mean velocity of approach, but with the head corresponding to the velocity above the level of the weir crest.

Dynamic similarity

The shape of the flow profile is directly dependent upon the relation between a variable discharge and a constant geometrical form of the hydraulic device. Since the surface profile must then vary in shape, as the discharge changes, geometric similarity between any two discharges is impossible, and hence complete dynamic similarity is quite out of the question. This condition, however, is possible for instance in the case of a ventilated sharp-crested suppressed weir of infinite (that is extremely great) height, sloping at any desired angle within reasonable limits; the free overfall at the end of a long channel is one specific case of such a weir, the weir face then being approximately horizontal [54].



A. Parallel. B. Parallel, full circumference. C. Linear. D. Sine function.

Fig.3.13. Stream profiles at oil outlet.

3.3.6 Hydraulic gradient

So far negligible resistance was assumed when deriving the above-mentioned equations. The fundamental equation for uniform open-channel flow may be derived readily by equating the equal and opposite forces of gravity and resistance in the channel. In the case of steady turbulent flow this leads to the well-known Chezy-equation which relates channel flow to the slope (Vennard [65]). Knowledge of the surface liquid gradient is important when one is interested in the surface level far upstream the edge. In order to get an impression of the hydraulic gradient in the situation described in this study, calculations were made for the cylindrical part of the top disc (see Appendix B). The result of this model is a differential equation for the fluid depth δ as function of the axial co-ordinate z :

$$\frac{d\delta}{dz} = \frac{3vQ}{\omega^2 R_0 b \delta^3 \left(1 - \frac{\delta}{R_0}\right) + \frac{6}{5} \frac{Q^2}{b}} \quad (3.47)$$

In equation (3.47) b is certainly not a constant, but is a function of the axial co-ordinate z . Because it is far from desirable to postulate a certain flow type across the cylinder, four different options for the channel width b are presented and compared afterwards.

Assuming the problem to be one-dimensional, two options can be discerned:

$$b(z) = 3w \quad (3.48)$$

$$b(z) = 2\pi R_o \quad (3.49)$$

The first option assumes no contraction, but a discontinuity at the position where the oil leaves the disc-stack.

The second option assumes no contraction, but a discontinuity near the edge. In order to eliminate the problem of discontinuity, two more options were chosen in which b is a function of the axial z -co-ordinate.

$$b(z) = 3w + \frac{2\pi R_o - 3w}{CL} \cdot z \quad (3.50)$$

$$b(z) = 3w + \frac{1}{2}(2\pi R_o - 3w) (1 - \cos[\frac{z}{\pi CL}]) \quad (3.51)$$

In figure 3.13 the four different options were drawn in a development of the cylinder surface of the top disc.

Boundary condition

Inserting the boundary condition for the fluid depth at the edge ($z_o = 0$), or in other words the brink depth, the fluid depth upstream the edge can be calculated at any place where the differential equation holds.

At the end of the cylindrical part of the top disc ($z = 0.06$ m for the increased capacity top disc; figure 3.15, paragraph 3.4.1) a jump in the surface level with the well-known factor 1.5 is expected, as discussed in paragraph 3.3.5. An alternative for the boundary condition might well be the critical depth which is positioned 3 to 4 times the critical depth from the edge. Ultimately, with the Runge-Kutta method the differential equation can be solved.

3.4 Experimental

3.4.1 Description of separator

Throughout this thesis experimental work was performed with a disc-stack centrifuge Alfa-Laval type MAB 104 B. At some points this commercially available separator was altered. Most important is the variator with which experiments could be performed at rotation speeds in between 2000 and 7300 rpm.

Table 3.2 Available separator internals

part name	characteristic dimensions	figure
top disc (standard)	$R = 26 \text{ mm}$, $CL = 60 \text{ mm}$	3.14
top disc (increased capacity)	$R_o^o = 30.5 \text{ mm}$, $CL=54 \text{ mm}$	3.15
distributor (standard)	$R_e = 15 \text{ mm}$	3.16
4 disc-stacks with 6 long caulks	$h = 0.4, 0.6$ $0.8 \text{ and } 1.0 \text{ mm}$	3.17 3.18B
3 disc-stacks with 12 point caulks	$h = 0.4, 0.6$ $\text{and } 1.0 \text{ mm}$	3.18A
blind disc (without holes, but with 6 long caulks)	$h = 0.6 \text{ mm}$	
set of gravity discs	$D_{gr} = 57.5, 68, 73.5,$ $78, 78.75, 79.5,$ $83, 93.5. \text{ mm}$	
wing set	18 wings	3.19

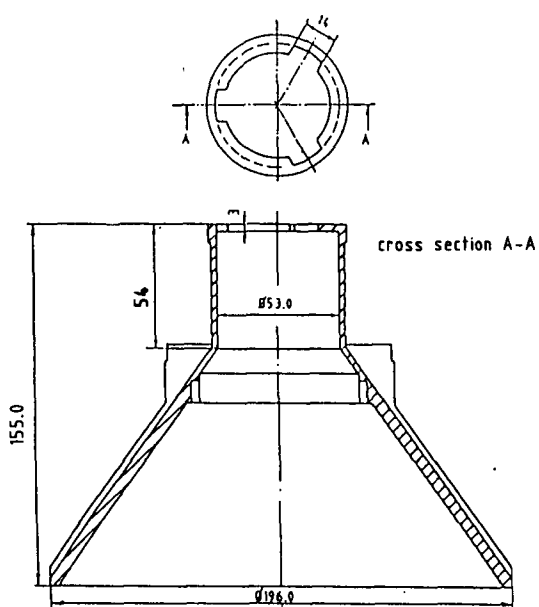


Fig.3.14 Top disc (standard)

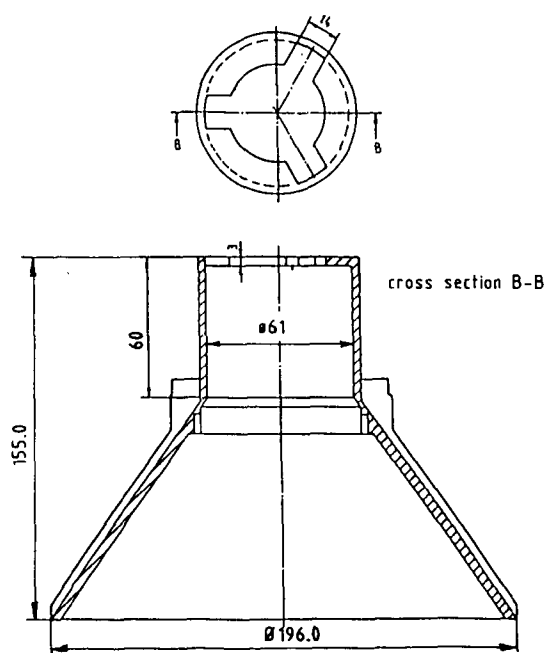


Fig.3.15 Top disc (increased capacity)

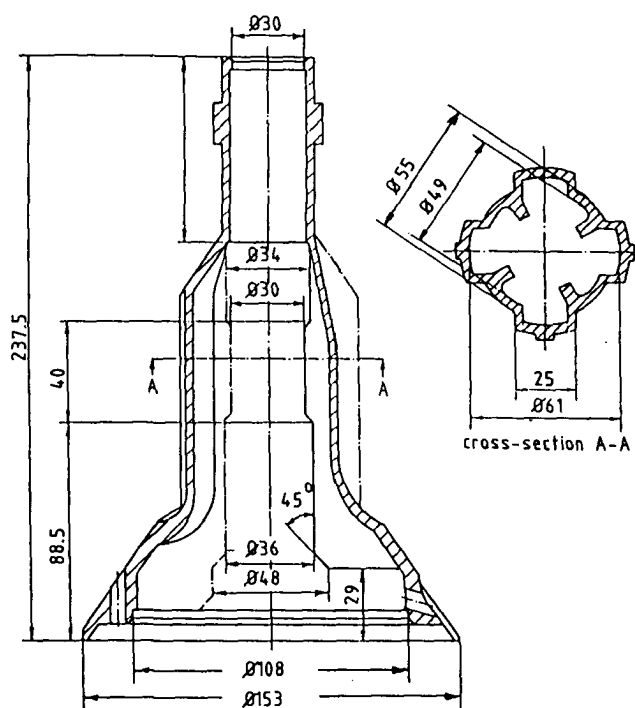


Fig.3.16. Distributor (standard).

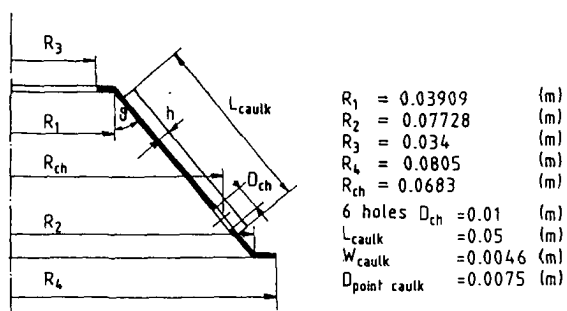


Fig.3.17 Disc geometry.

Table 3.3 Composition of the disc-stacks

caulk thickness h [mm]	number of discs *) [-]
0.4	62
0.6	47
0.8	40
1.0	34

Note: *) In the case of peripheral feed,
the distribution channels are
blinded by the blind disc.
In the case of channel feed
this blind disc is placed
directly under the top disc.

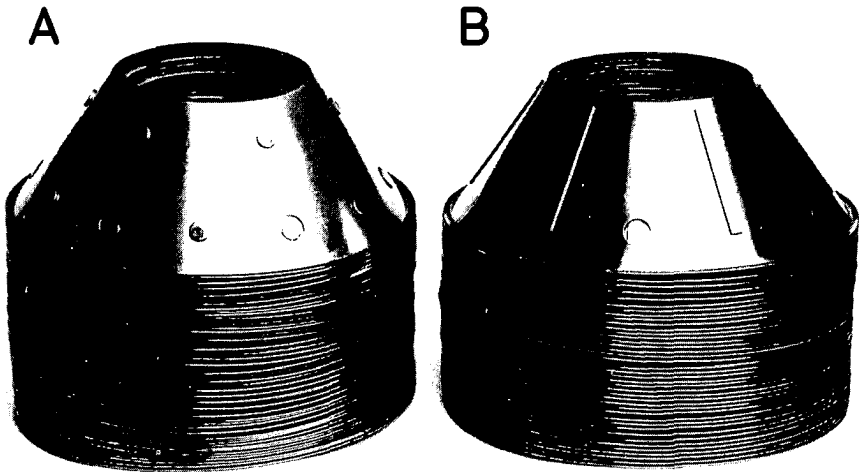


Fig.3.18. Caulk type. A. point caulks.B. long caulks.

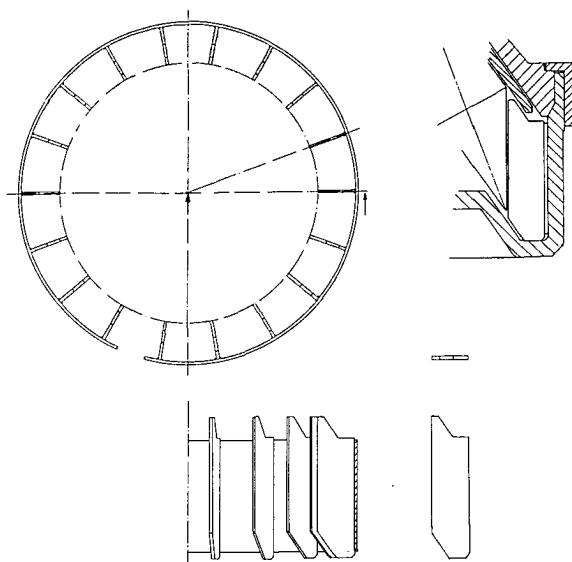


Fig.3.19 Wing set.

3.4.2 Measurement techniques and experiment procedures

3.4.2.1 Interface experiments

Volumetric method

The basic idea behind the volumetric method is the existence of a geometrical relationship between the amount of water present in the rotating bowl and the interface radius. Determining this amount of water is executed after an immediate interruption of the feed flow. Before the below-presented technique was available, preliminary experiments were made with the volumetric method in order to affirm the significance of pressure drop present within the separator.

Pulse-echo-method

An extensive description of the pulse-echo-method can be found in paragraph 4.3.

Experiments

The experiment procedure has been as follows. After filling the rotating separator bowl with thermostated water, calibration of the pulse-echo-detector was executed. Very carefully a small oil (pure oil) feed was introduced which was increased step by step until overflow of the separator occurred. At all circumstances the interface position was determined by reading off both signals (caulk + channel) no sooner than the moment at which no water was produced. In this way certainly no pressure drop would occur in the water phase, so that the pressure drop in the oil phase could be calculated afterwards. In most cases one series of experiments consisted of two or three identical subseries in order to check upon reproducibility. Flow was in all cases varied from 250 l/h (pump limit) to the point where hydraulic capacity would be exceeded or the maximum flow rate of about 2600 l/h would be reached. Rotation speed was held constant during all experiment series. Experiment series were produced at rotation speeds in between 2250 and 7300 rpm.

Viscosity was varied via the feed temperature. Especially in the early series, feed temperatures were chosen in between 20 and 90°C, whereas in later experiment series (from JP 34 on) 50°C was chosen as working temperature.

Various disc geometries were tested in order to gain knowledge of the influence of caulk thickness as well as of caulk type (long caulks or point caulks).

With the aid of a blind disc the feed type could be chosen (channel feed or peripheral feed (see also paragraph 3.4.1)). Both the standard top disc, and the increased capacity top disc, were used.

Two experiment series have been devoted to the effects of water flow (AL 94) and the effects of a dispersed feed instead of pure oil feed (AL 95).

Appendix D contains the experimental conditions of 114 experiment series.

Only in a restricted number of experiments (approximately 500) dual position measurements were made both at the caulk and the channel position. The numbers of the experiments during which dual measurements have been actually made, can be found in the footnote of the experimental conditions table in Appendix D.

The possible presence of a slip effect outside the disc-stack such as discussed in paragraph 3.3.1 was verified by the insertion of a set of wings and was tested for both feed types.

Table 3.4 Experimental conditions "winged disc" series

exp. code	winged disc	n rpm	T °C	R _o mm	D _{gr} mm	h	feed type *)	caulk type **)
WD 1	no	5500	50	30.5	83	1.0	ch ch pe pe	1
WD 2	yes							
WD 3	no							
WD 4	yes							

Notes: *) ch = channel feed, pe = peripheral feed
 **) 1 = long caulks

A detailed description of the set of wings, which basically consists of 18 radial baffles covering the entire outer disc space is given in paragraph 3.4.1, figure 3.19.

3.4.2.2 Weir head experiments

First series

Under various conditions (flow, rotation speed, viscosity) photographs were made of the oil weir flow, measured with the high capacity top disc (paragraph 3.4.1). In order to achieve this, the cover of the separator was removed and replaced by a perspex one. With a Leica camera (type M4) with a 90 mm lens ($f = 2.8$) mounted on a tripod, pictures with a reasonable magnification factor were obtained (1:1 on the negative) (See figure 3.20).

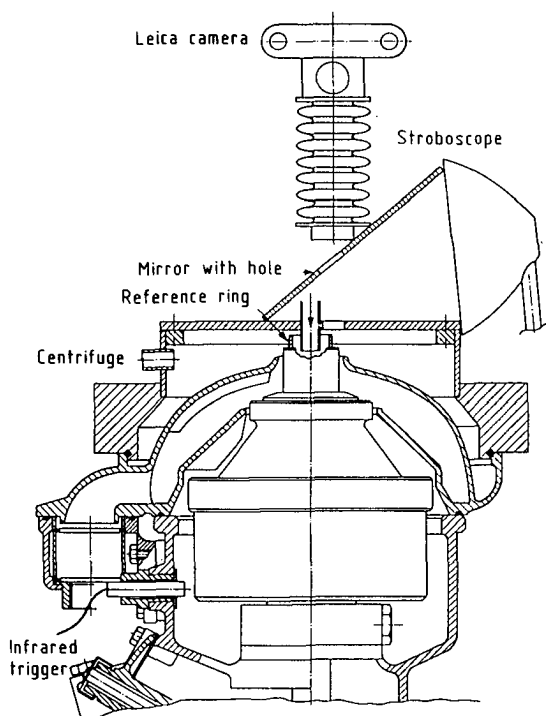


Fig.3.20 Experimental setup.

With a stroboscope (Drello, Drelloscop 1018), triggered with an infrared sensor mounted near the bowl, a steady picture was obtained. The shutter time was chosen in such a way that approximately 3 flashes were used. The negatives were projected in the dark room on a white sheet. The liquid depth was measured from the sheet with a ruler. The magnification factor, with which the above-mentioned measured length had to be multiplied, was taken the ratio of the weir length w measured both at the top disc and at the sheet. A problem which had to be solved, was the optical distortion of the weir by the presence of a curved oilsheet in between the weir and the camera. This can quite clearly be seen from picture W1-8 (figure 3.22 A).

In the first series of experiments (W1) this problem has been overcome by making a drawing on the projection sheet of the situation without feed. In order to prevent interpretation problems in the rest of the experiments, a special reference ring was placed near the outlet as shown in figure 3.21.

The outer diameter of the reference ring belonging to the increased capacity top disc ($R_o = 30.5$) and the standard top disc ($R_o = 26.0$) were 53 mm and 45.8 mm respectively.

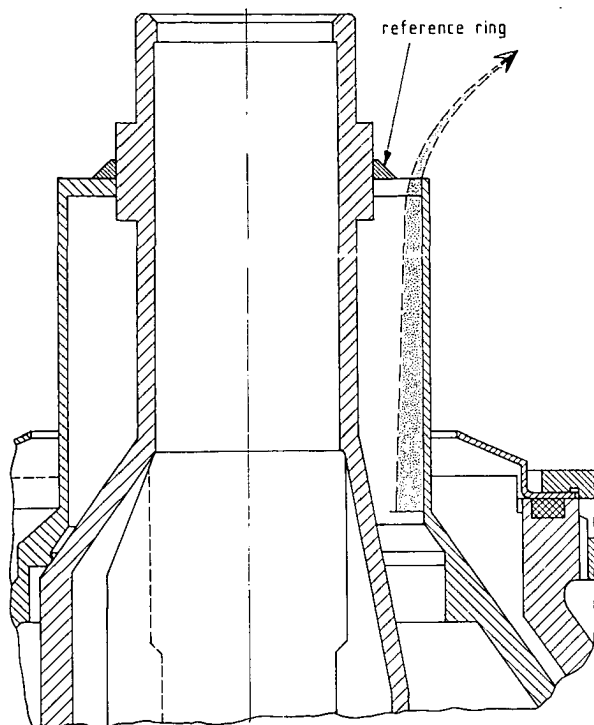


Fig.3.21 Outlet region of the separator with reference ring.

The positive effect can be observed in the rest of the pictures (figures 3.22 B-D). Flow was measured with calibrated rotameters. In table 3.5 an overview of the experimental conditions is presented.

Table 3.5 Photographs of weir experiments, Drost [18]

exp nr.	n rpm	Q l/h	R _o mm	T _o °C	reference ring	figure
W1- 8	2048	496	0.63	18	no	3.22 A
W3-30	5057	2260	2.30	26	yes	3.22 B
W7-23*	2765	1211	3.06	22	yes	3.22 C
W7-24	2663	1213	2.22	22	yes	3.22 D

Note : *) focused on "higher-liquid level"
upstream the crest region.

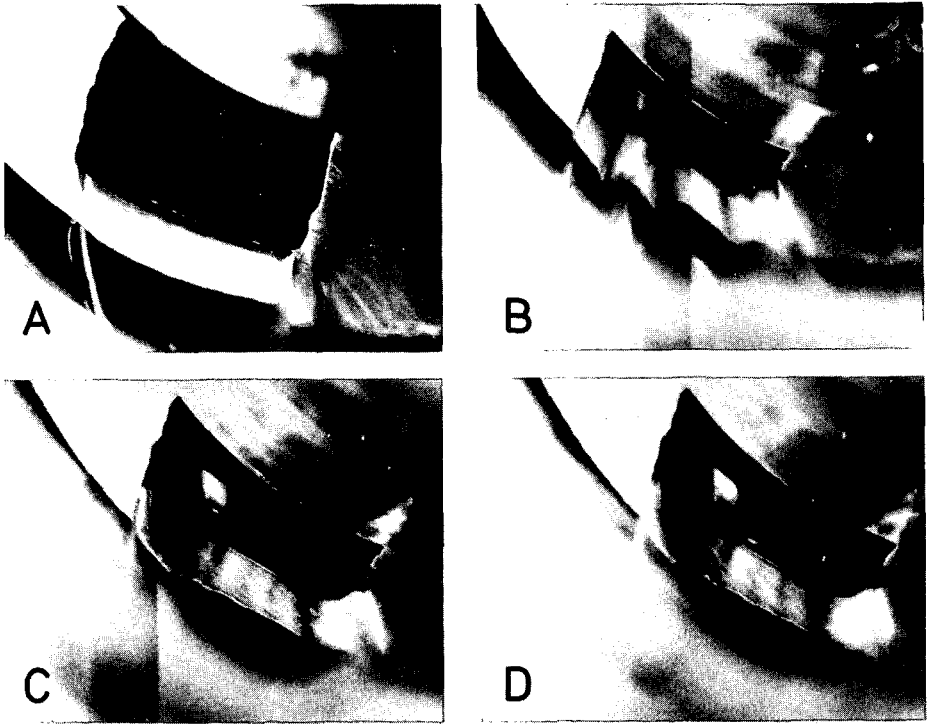


Fig.3.22. Weir experiments, data see table 3.5

Second series

Due to the fact that in experiment series W7 of the first series more surface levels were observed, and because spreading in results made an extensive data analysis doubtful, it was decided to set up a second experiment series. In this series almost the same experiment procedure was followed except that flow was measured with the turbine flowmeters (Appendix A) of which the viscosity influence was negligible compared to the above-mentioned rotameters.

Furthermore, the measurements were made directly from the photographic prints instead of the dark room projection.

Table 3.6 Conditions of the second experiment series MK 1-28,
Krombeen & Wolff [43]

exp code	exp nrs	n (rpm)	T _o (°C)	R _o mm	exp code	exp nrs	n (rpm)	T _o (°C)	R _o mm
MK 1	1- 10	2000	20	30.5	MK15	126-133	4000	65	30.5
MK 2	11- 19	3000			MK16	134-142	5000		
MK 3	20- 27	4000			MK17	143-151	6000		
MK 4	28- 36	5000			MK18	152-160	7000		
MK 5	37- 44	6000			MK19	161-169	2000	90	
MK 6	45- 53	7000			MK20	110-177	3000		
MK 7	54- 63	2000	MK21		178-186	4000			
MK 8	64- 71	3000	MK22		187-194	5000			
MK 9	72- 80	4000	MK23		195-203	6000			
MK10	81- 89	5000	MK24		204-211	7000			
MK11	90-101	6000	35		MK25	-		20	26.0
MK12	100-108	7000			MK26	212-216		35	
MK13	109-117	2000			MK27	217-219	5000	60	
MK14	118-125	3000			MK28	220-222		85	
				65					

In table 3.6 the experimental conditions are presented. All experiments consisted of dual measurements: one photograph focused at the edge, a second photograph focused at the surface level far upstream the edge. The location of the latter was measured by taking the distance which the focused camera had to traverse downward from the point at which the edge would be in focus (or at which the outer edge of the reference ring would be in focus). Four questions were to be answered. First, what is actually measured? Second, what is the location of the plane in which the measurement is made? Third, what is the viscosity effect on weir head? Fourth, what is the relationship between the weir head measured at both locations?

3.4.2.3 Hydraulic capacity experiments

After a period of time, during which the separator could come to its working temperature, the experiment was started. At a chosen rotation speed the flow would be increased very carefully until the moment that a very thin oil sheet would leave the top of the distributor. The latter could be observed

visually through the perspex hood of the collecting cover (figure 3.20). All experiment series were made twice in order to check upon reproducibility. Before starting an extensive experiment programme, preliminary experiments were made in order to find out the significance of various geometrical variables, such as: oil outlet radius, gravity disc and feed type. The oil outlet radius was varied from 22 mm to 30.5 mm with increments of 1 mm. This was accomplished during manufacture of the increased capacity top disc which was machined millimetre by millimetre in between the various experimental series. It has been verified whether the hydraulic capacity equation (3.9) is in reality indeed independent of the interface equation (3.8) by measuring the hydraulic capacity with various gravity discs, hence different interface radii. Finally, different internal geometries were tested and compared: first the standard disc-stack ($h = 0.6$ mm) with both channel feed and peripheral feed, second, the dummy stack and last the empty bowl. Experimental conditions of the hydraulic capacity measuring programme can be found in Appendix E.

Within this programme viscosity was varied via the feed temperature. Feed temperatures in between 20°C and 90°C were chosen.

Various disc geometries were tested in order to gain knowledge on the influence of caulk thickness as well as of caulk type (long caulks or point caulks). With the aid of a blind disc the feed type could be chosen (channel feed or peripheral feed) (see also paragraph 3.4.1). Both the standard top disc as well as the increased capacity top disc were used. The gravity discs were selected in such a way that the interface position would be outside the disc-stack, in order to prevent maldistribution effects.

3.4.2.4 Endoscope experiments

In paragraph 3.3.3 the hydraulic capacity equation was presented in which the inlet radius R_e is introduced. When the hydraulic capacity of the separator has not been exceeded, R_e is the feed liquid radius within the distributor and is a function of flow. The hydraulic capacity is the flow corresponding to the minimum R_e which just fits into the distributor. When the experimental conditions belonging to the starting point of overflow are inserted into the capacity equation (3.9), the total pressure drop in the oil phase can be calculated. It must be emphasized, however, that the

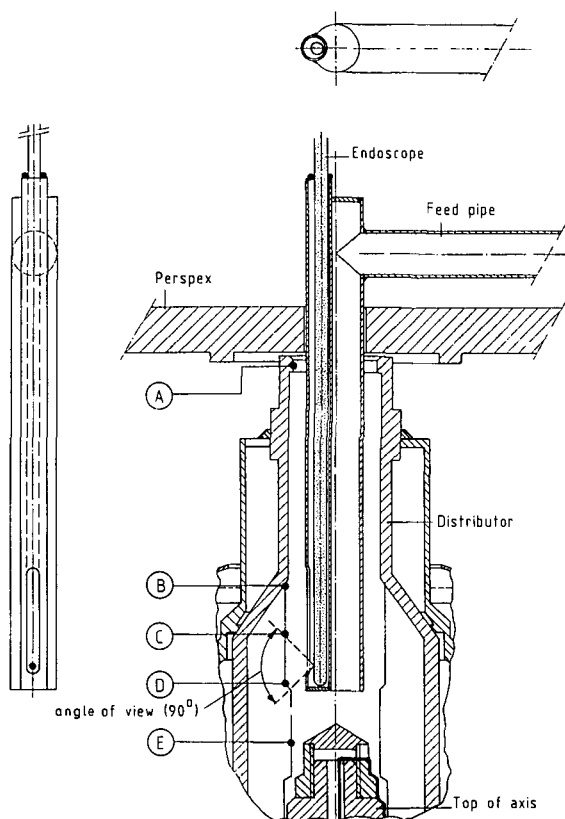


Fig.3.23 Distributor with endoscope

precision of this calculated value strongly depends upon the inserted value for the inlet radius. It is evident that at the point of exceeding the hydraulic capacity the local value for R_e , the inlet radius of liquid surface is identical to the distributor's inner radius at the top (15 mm). The question, however, is if the liquid head within the distributor, being the driving force for the transport, is proportional to ω^2 across the entire range from 15 mm to R_0 , or, in other words, if solid body rotation is also valid in the entire range. Some doubt on this point arises when observing the distributor's guiding fins, which are provided with a recess having a tip radius of 17 mm (see figure 3.16, paragraph 3.4.1). For this reason endoscope experiments were made in order to gain more certainty on this particular point. Besides, a qualitative impression could be obtained of the

distributor flow. With a special designed inlet, which allowed the endoscope (Wolf Technoscope ϕ 8 mm type 6.08050.09, angle of view 90°) to be penetrated into the distributor of the rotating separator, it could be observed what happened close to the tips of the guiding fins, just above the top nut. The special inlet was mounted on the perspex separator cover shown in figure 3.20 , and its details can be observed in figure 3.23. The endoscope is provided with a separate fibre light conductor which is to be connected with a stroboscopic light source. At three locations ($R_e = 17, 19.4$ and 21.2 mm) markers were fixed to the guiding fins, so that the liquid surface radius could be measured, together with rotation speed and flow. Moreover, at four locations marked A-D in figure 3.23 the flow was determined at which overflow would just take place. This was done for rotation speeds in between 3000 and 7300 rpm. As soon as overflow occurred at location D, it appeared impossible to discriminate details of guiding fins deeper in the distributor (location E) on further increase of feed flow. In this situation oil flowed in the axial direction in between the fin tips (location E) and the endoscope. For this reason the point of overflow could not be determined at location E. The endoscope experiments were made with the standard top disc, a dummy stack, a gravity disc diameter of 83 mm (interface positioned outside the dummy) and a feed temperature of 50°C .

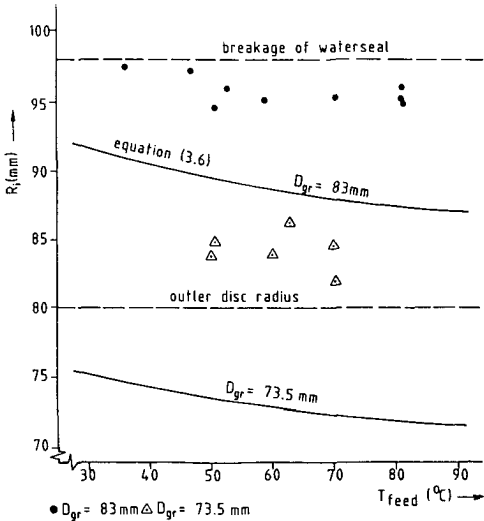


Fig.3.24 Validity of static interface equation.

3.5 Results and observations

3.5.1 Interface experiments

Figure 3.24 shows the results of preliminary experiments made with the volumetric method. The plotted lines were calculated with the static interface equation (3.6). It can be quite easily observed that equation (3.6) underestimates the interface position significantly. Both spreading in results and slow data acquisition made the volumetric method unuseful to determine parameter influence on the interface position. Furthermore, the separation process had to be stopped which was far from desirable.

Experiments with the pulse-echo-method

Due to the strong effects of various parameters on the interface position, which could only be measured in a restricted area, the interface had to be positioned in the measuring area ($80.5 < R_i < 98 \text{ mm}$). This was accomplished by the proper choice of gravity disc which at the same time makes it impossible to show parameter influences in a plot of the interface radius versus flow rate. In these cases plots are shown of the pressure drop $\Delta p_{o,i}$ in the oil phase versus flow rate.

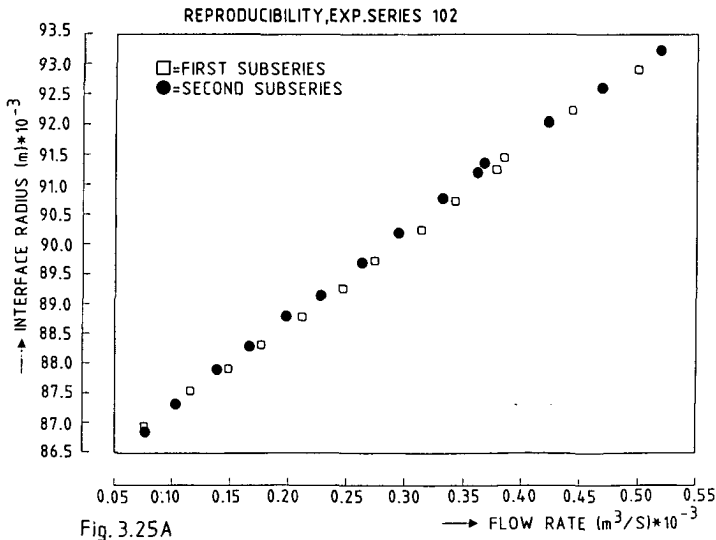


Fig. 3.25A

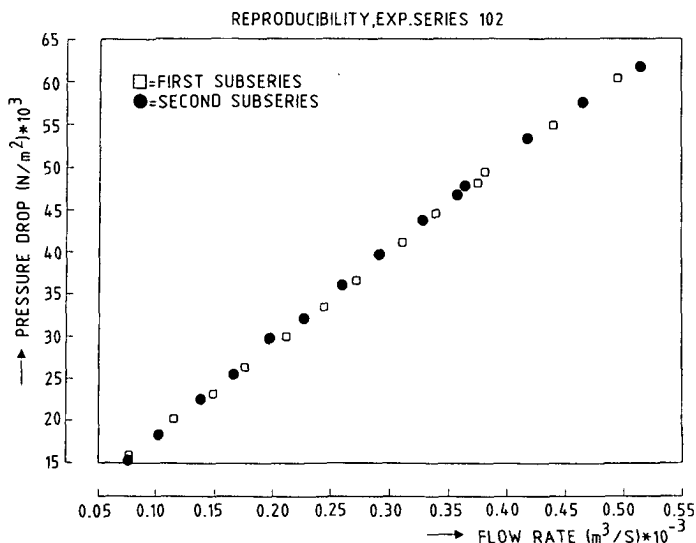
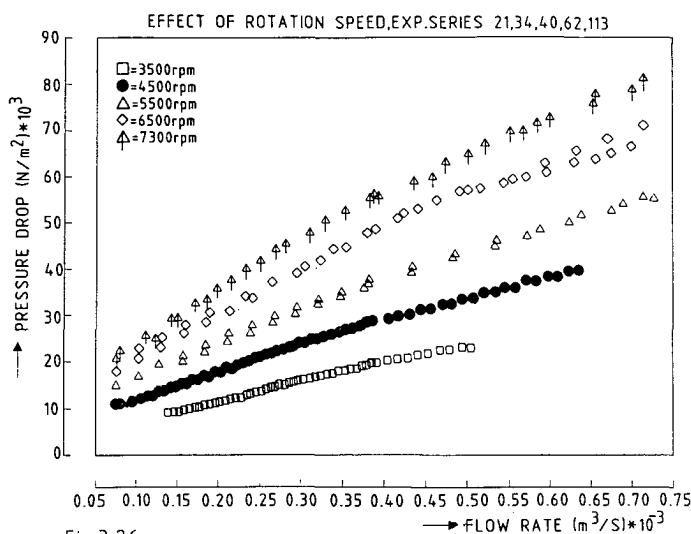


Fig.3.25B

Reproducibility is illustrated in figure 3.25 which is typical for most of the experiment series. Within one experiment series at least two subseries have always been measured in which the flow was varied in between the limiting values described above.

In figure 3.25 A the interface radius which is directly measured is plotted against flow rate, while figure 3.25 B shows the oil pressure drop, calculated with equation (3.8) setting $\Delta p_w = 0$. Close observation learns that the experimental points apparently follow the line better for the pressure drop compared to the interface radius. This is caused by a small, but important temperature difference in between the subseries, taken into account via the density evaluation (in this case $\approx 1.5^\circ\text{C}$). The effect of rotation speed on pressure drop is presented in figure 3.26. Raising the rotation speed from 3500 to approximately twice as much (viz. 7300 rpm) causes an increase of the pressure drop of two to three times. This means that the increase of the static pressure (proportional to n^2) is bound to overrule the increase in dynamic pressure drop, hence the interface moves to the axis at higher rotation speed.



Contrary to the above statement, care must be taken when the effect of caulk thickness is point of interest. Focusing attention on equation (3.22), the radial solution, in which the caulk thickness is in the pressure drop to the power -3, together with the number of spaces N_s to the power -1, it might be expected that narrow disc spacing inevitably leads to higher pressure drops. According to equation (3.22) the calculated pressure drops belonging to the caulk thicknesses of 0.4, 0.6 and 1.0 mm appear to be in proportion to 8.57 : 3.35 : 1.00 respectively. The corresponding proportions according to equation (3.21) for the symmetric case amount to 6.93 : 2.78 : 1.00. Comparison with figure 3.27 A shows that more pressure drop must exist apart from the disc-stack in order to justify the calculated proportions. Figure 3.27 B illustrates the situation for the higher λ -values. From the plot a clear minimum for the pressure drop as function of caulk thickness can be observed which is also caused by the number of disc spaces being a function of caulk thickness (see table 3.2 paragraph 3.4.1). This is predicted by equation (3.21) which gives the proportions of 1.52 : 0.909 : 1.01.

EFFECT OF CAULK THICKNESS, EXP. SERIES 17,19,20

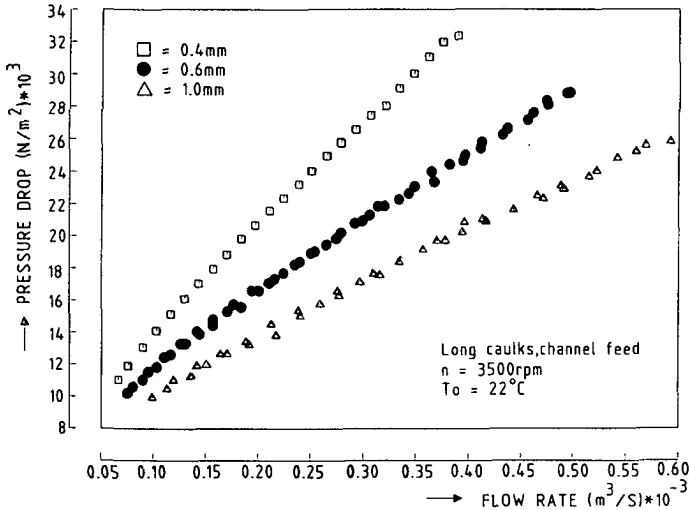


Fig 3.27A

EFFECT OF CAULK THICKNESS, EXP. SERIES 34,35,36

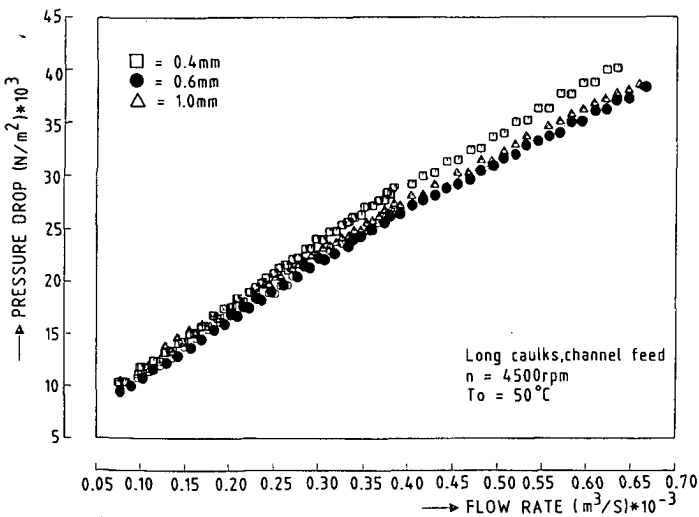


Fig.3.27B

The effect of temperature is presented in figure 3.28 for which the calculated proportions of the disc-stack pressure drop amount to 6.39 : 1.82 : 1.00. This does not mean, however, that raising temperature will cause the interface to shift inward: the opposite is the case, because the effect of density ratio on the static pressure is stronger than the viscosity effect on the interface position via the pressure drop.

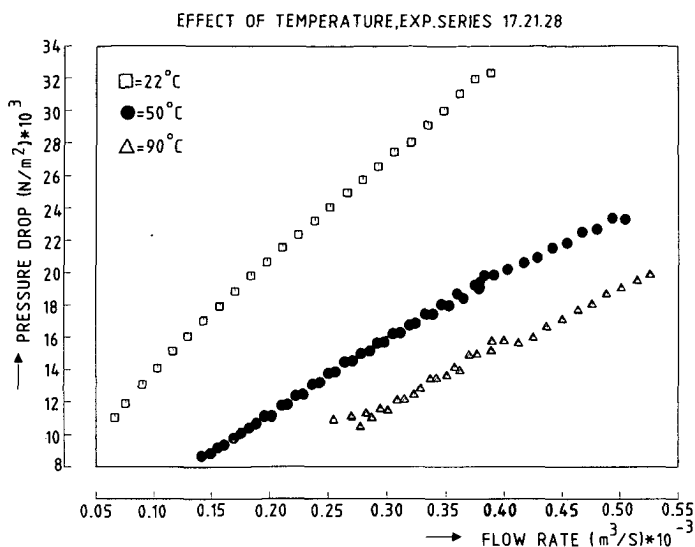


Fig.3.28

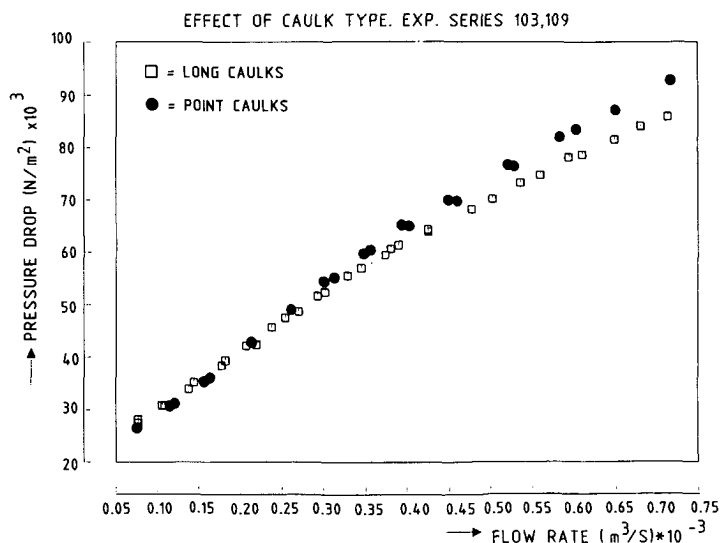


Fig.3.29

The effect of caulk type is shown in figure 3.29. Indeed, pressure drop reduction is obtained inserting long caulks instead of point caulks such as discussed in paragraph 3.3.4. The stream parameter λ has the value of 1.77 in this particular case, for which the correction formula (3.23) produces the value of 0.86. Figure 3.30 ultimately shows the effect of feed type.

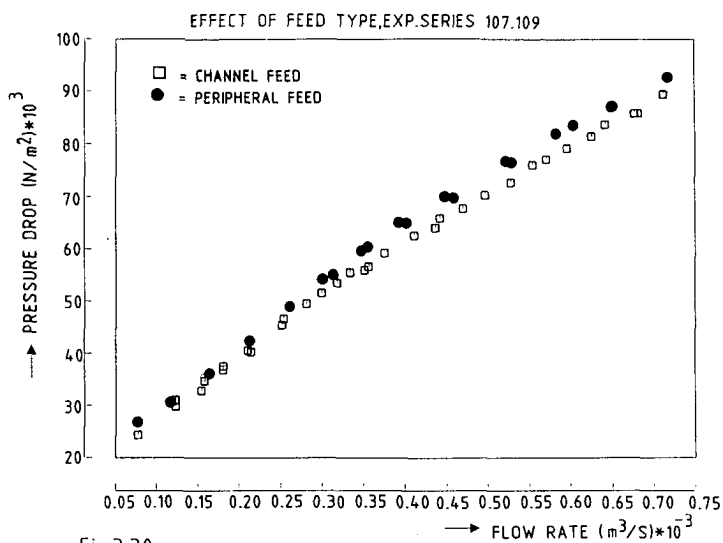


Fig.3.30

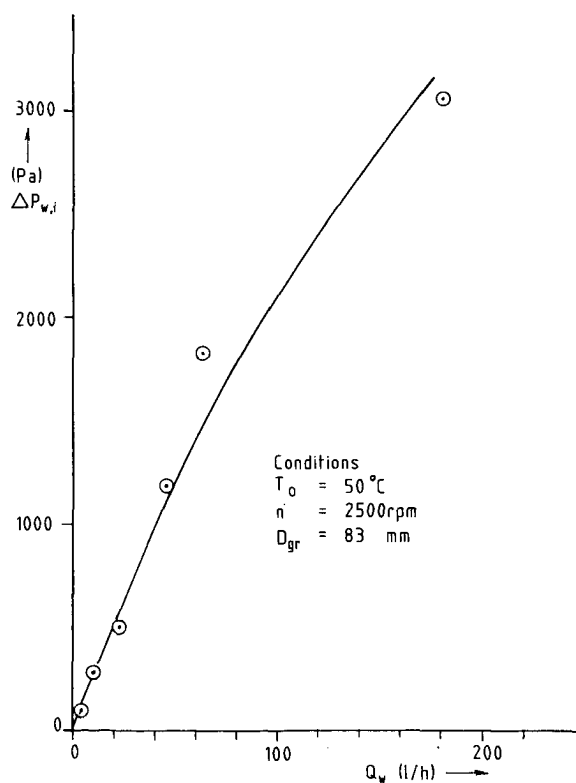


Fig.3.31 Pressure drop in the waterphase.

Symmetry

The interface radius measured opposite the channel appeared some 0.2 mm higher than opposite the caulk, averaged over the available dual measurements. No clear correlation was observed with flow and the absolute value is high compared with what might be expected from equation (3.24), so that this effect is dedicated to a systematic error.

Effect of water flow

In order to evaluate the pressure drop with $\Delta p_{w,i}$ with maximum precision, experiments have been made with a low rotation speed of 2500 rpm and rather high water flow rates up to 180 l/h. At an established set of conditions without water flow interface position was measured, after which water flow was step-wise increased while measuring interface position. At a water flow of 180 l/h the interface position had shifted 3.8 mm in inward direction. Therefore it can safely be stated that the importance of the water pressure drop compared with the oil pressure drop is negligible. For instance, at a flow of 1 m³/h with 1% water one can expect some 0.2 mm at 2500 rpm which at the standard rotation speed of 7300 rpm will be even lower.

The first experiment was made without water flow, providing for $\Delta p_{o,i}$, which was calculated with equation (3.8) and served as a reference for the calculation of $\Delta p_{w,i}$. Oil flow, temperature and rotating speed were held constant during the entire experiment series. The numeric results are presented in figure 3.31 together with the relevant experiment conditions.

Effect of dispersed feed

During the entire experiment programme presented above, the separator was fed with pure oil in order to be certain about the densities of both phases present within the rotating bowl. When feeding the separator with a dispersed feed, one might expect that due to presence of water droplets in the dispersion, its effective density would be higher, hence resulting into an interface being positioned more to the outside compared with the pure oil situation.

Careful observations, however, proved the opposite: the interface radius moved 1 mm inward when feeding a water-in-oil dispersion instead of an unmixed water and oil feed with identical phase ratio and flow rate. The experiment has been performed with two knife mixers running at an agitating speed of 1350 rpm, a separator rotation speed of 7300 rpm, a 0.4 mm spaced disc-stack provided with long caulks and channel feed. Oil feed rate has been 1460 l/h with feed temperature of 54°C. Water feed rate has been 56 kg/h. The observed shift in the interface position corresponded to a reduction of pressure drop $\Delta p_{O,i}$ of 9700 Pa, whereas the pressure drop in the disc-stack under the circumstances mentioned above amounts to 6020 Pa (symmetrical solution and therefore an overestimation).

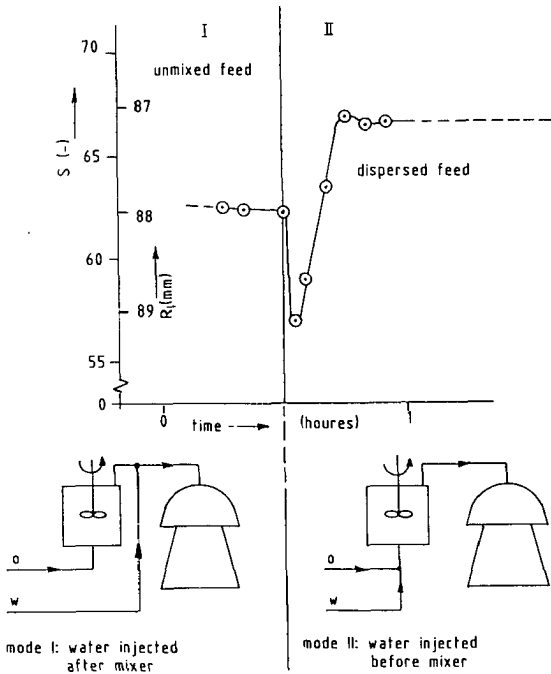


Fig.3.32 Effect of dispersed feed on interface position.

The interface as function of experiment time is shown in figure 3.32. Due to the high power input of the mixers and the corresponding temperature effect, the agitators could not be simply turned on and off, because the temperature effect on viscosity is rather important. Only by a switch of the location of injection, a switch from unmixed to dispersed feed could be realised, while keeping the feed temperature constant within 1 - 2°C. The initial dip in the plotted curve can be explained by a temporary absence of water production which is connected with the residence time of the feed in the agitators (in this case some 2.5 minutes for both agitators).

Before the result can be explained, one must bear in mind that the observed reduction in pressure drop amounts to some 10 percent of the calculated pressure drop itself, of which the accuracy is restricted. For instance, a difference in temperature of 1°C between the two phases gives rise to a 1% change in pressure drop calculation, which corresponds to some 800 Pa. Because this experiment was made during one run, working with identical separator internals and identical pulse-echo-detector calibration, no systematic errors could be expected. In other words, in spite of the sensibility of the calculated pressure drop for the operating temperature, it can therefore be assumed that it is significantly higher than the disc pressure drop. It can therefore be stated that the pressure reduction cannot be caused by effects, only finding its origin within the disc-stack. An explanation for the reduction can be the secondary flow occurring in the region in between stack and the interface, due to the outward directed jet type flow of the water phase coming from the 6 channels. The idea that the dispersion flows directly towards the interface is based upon observations making use of a perspex single disc separator.

Winged disc experiments

Four experiment series were produced for both feed types, with and without wings. The observed difference in interface or pressure drop appeared to be quite low, which is illustrated in figure 3.33.

Compared with the channel feed experiments the effect of wings in the peripheral feed experiments is significant, and lies in the order of 2000 Pa for the higher flow rates ($Q = 0.7 \cdot 10^{-3} \text{ m}^3/\text{s}$). For this flow rate the

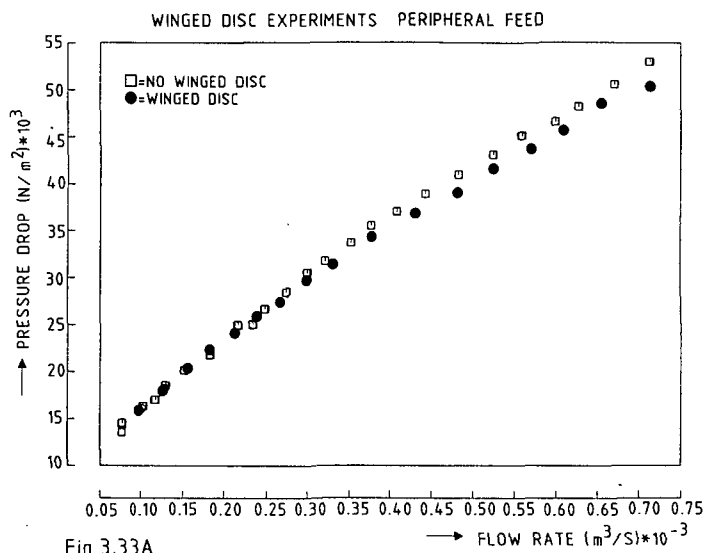


Fig.3.33A

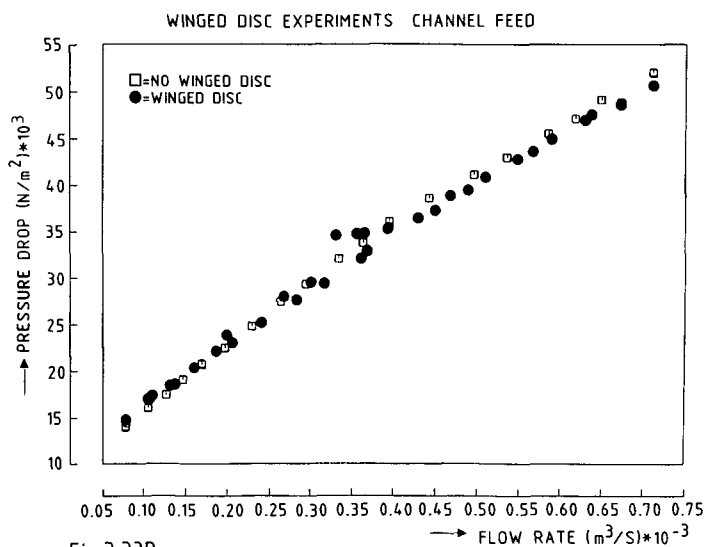


Fig.3.33B

pressure drop in the disc-stack amounts to 8400 Pa (symmetrical case: equation (3.21)).

The static pressure difference across the region in which solid body rotation might be violated, namely the outer disc space ($80.5 < r < R_1 = 94$ mm), amounts to 3.32 bar of which 2000 Pa is 0.6 %.

Evaluation of equation (3.4) substituting realistic values for m and the actual radius ratio, deviations of the static pressure from the solid body case (equation (3.2)) are found of several percents (see also figure 3.1). Therefore it can safely be stated that under the circumstances solid body rotation is valid.

3.5.2 Weir head experiments

First series

In the case of higher weir heads, undular flow was observed which had a negative effect on the quality of the photographs. For these heads the liquid level was never cylindrically shaped, but rather curved (see figure 3.22 B).

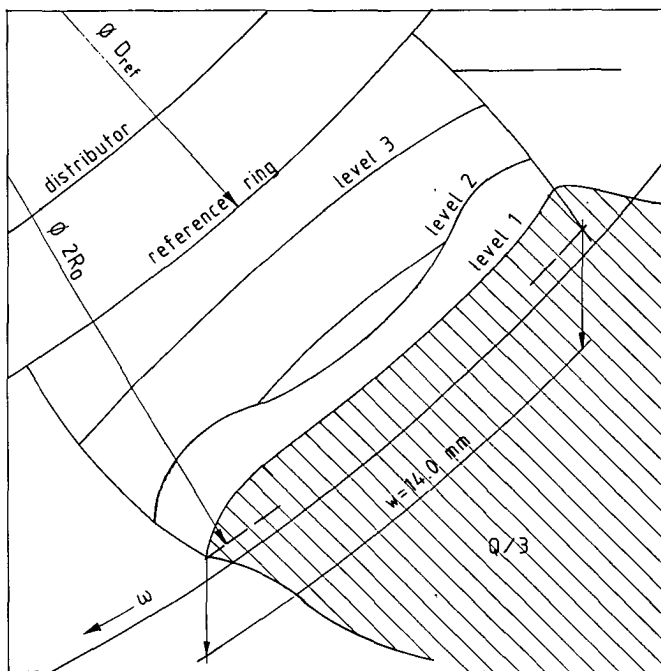


Fig.3.34 Light phase outlet shown from above.

Lowering the camera deeper into the outlet region a "second liquid level" was observed, shown in the figures 3.22 C and D showing experiments W7-23 and W7-24 respectively. From the results, obtained in the first series, no strong viscosity influence on the weir head could be observed. The phenomena observed in both experiment series will be described in detail first.

Second series

Figure 3.34 shows an outline of typical situations shown in most of the photographs. The photographs shown in figure 3.22 C and D have served as an example. At moderate to high flow rates, local liquid surface curvatures become more and more pronounced, deviating from the cylindrical shaped surface observed at the low flow rates. Moreover, a vague transition could be observed from laminar to wavy laminar on increasing Reynolds number which, within the entire experiment series was in the range of approximately 4 to 600. Within the experimental series more liquid surface levels could be observed in most cases. Most interpretation problems are in the high temperature series; on the one hand by lack of contrast in the photographs, on the other by the typical appearance of the flow picture itself.

Visual observations affirmed the existence of more levels, also for the higher temperature series, whereas only a limited number of photographs would underline this.

Level 1 is at all times situated at the crest and was observed on the photographs as a white to grey curve against a darker background. Level 1 could be observed best when the camera had been focused on the outer edge of the reference ring. About 50 percent of the photographs gave rise to the interpretation problems with respect to level 1 and had to be abandoned in the numerical analysis.

Level 2 was at all times measured together with the corresponding focal depth and was clearly visible, especially during the lower temperature series, where deviations from the cylindrical shape was most easily visible. Level 2 corresponds to the measurements performed by Drost [18] described above.

Level 3, of which the position was measured only at 90°C, did not deviate much from the cylindrical shape. However, in most cases its surface could not clearly be observed along the full circumference.

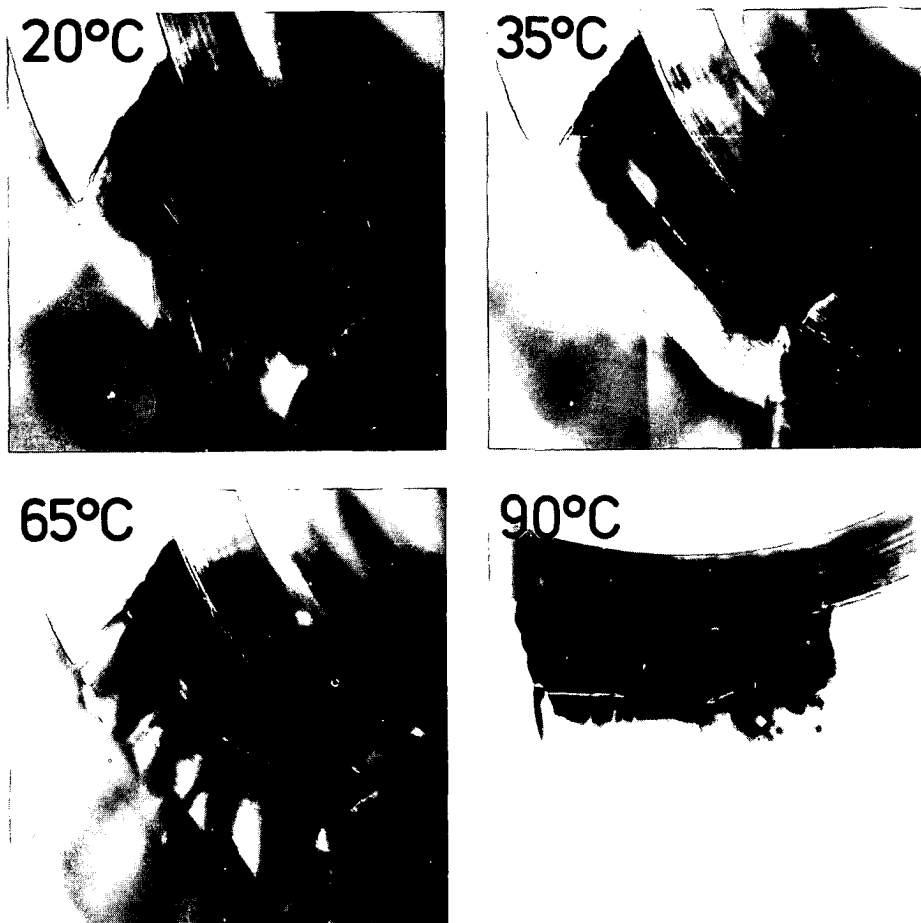
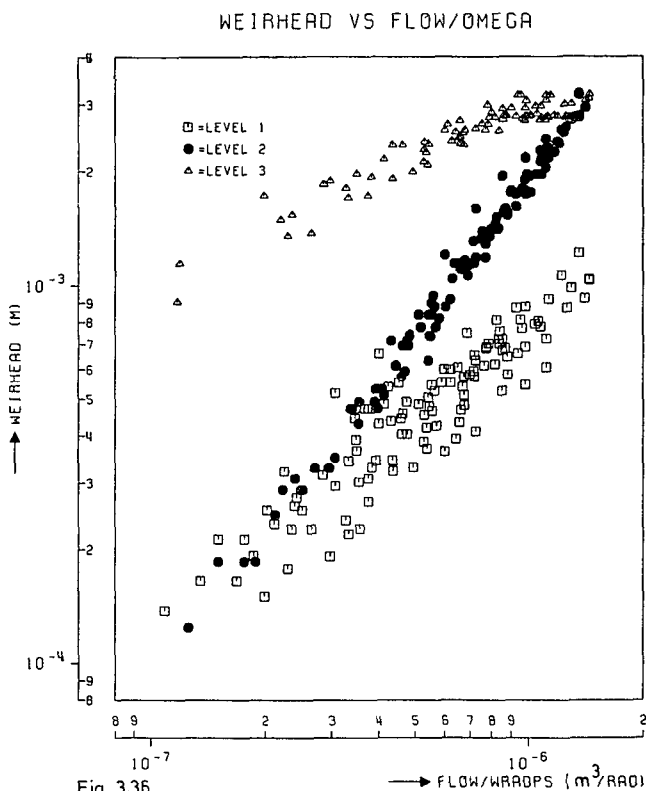


Fig.3.35. Onset of undular flow.

Figure 3.35 shows four situations at a rotation speed of 3000 rpm and a flow of $1 \text{ m}^3/\text{h}$ at 4 different temperatures which illustrate both the onset of undular flow, and the disappearance of level 2 described above.



In figure 3.36 the weir heads belonging to the three levels have been depicted in one graph. Remarkable is the convergence of level 2 and 3 for higher liquid loads. Most probably this is caused by the moving location. Level 2 is a local curvature positioned at both weir ends, caused by the severe contraction effect. Level 3 is expected to be identical with some friction effect included. The locations of both phenomena will be positioned more and more near the crest on increasing flow rate which has been observed. Hence the mutual distance will also decrease on increasing flow rate. The slope discontinuity at $Q/\omega = 9 \cdot 10^{-7}$ for the level 3 measurements is most probably caused by filling of the flow passage with liquid at the cylinder entrance.

POSITION OF THE WEIR HEAD MEASUREMENT

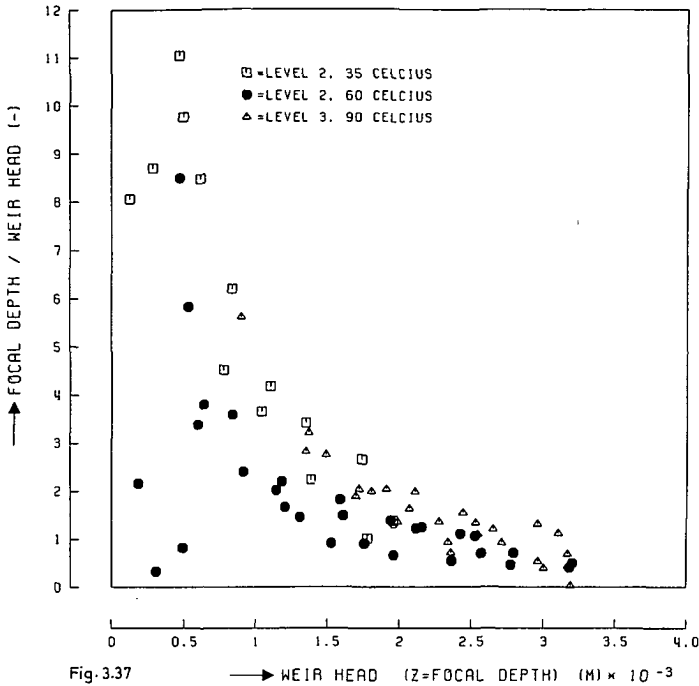


Fig.3.37

Focal depth

In the early experiment series focusing was performed once at the first photograph, hence the focal depth produced constant values within these series. In the later series (MK 9, 11-16 and 19-23) focusing took place for all separate data points. Only the data taken from these experiments were plotted in figure 3.37. Because literature reports a constant ratio (3-4) of focal depth and weir head measured at the critical spot, it was chosen to plot this ratio versus weir head. The experiments within this study indicated over and over a decrease in focal depth on an increase in flow rate. Focal depths bigger than 6 mm have never been observed.

Numeric analysis

In accordance with the work of Slocum [59] an exponential empirical relationship was used for fitting experimental data. Slocum used the weir height forming a dimensionless group together with the weir head.

Because the case in question is a free overfall (weir height = 0) this choice appeared not to be feasible. For this reason the oil outlet radius R_o was chosen, yielding the below-presented equation:

$$\frac{\Delta R_o}{R_o} = \alpha \left(\frac{Q}{3_w \omega R_o^2} \right)^\beta \left(\frac{v}{\omega R_o^2} \right)^\gamma \quad (3.55)$$

Other options for the characteristic length scale failed to improve the fit and are therefore not reported. Numeric results obtained with a least square analysis programme are presented in table 3.7.

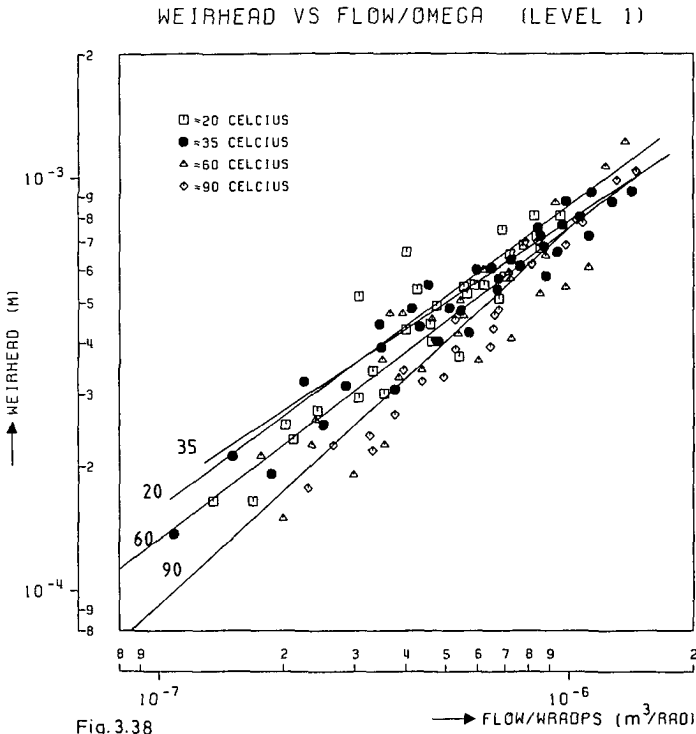
Table 3.7: Numeric results of the least square analysis. Krombeen & De Wolff [43]

subject	data	number of data points	α	β	γ	Cor	avarage fit error(%)
level 1	20°C MK 1- 6	29	.508	.794	0	.901	11.1
	35°C MK 7-12	34	.347	.715	0	.959	9.9
	60°C MK 13-18	28	.491	.821	0	.891	18.6
	90°C MK 19-24	23	.883	.982	0	.985	7.4
	MK 1-24	114	.435	.780	0	.921	14.6
	MK 1-24	114	.767	.779	.0605	.920	13.5
level 2	20°C MK 1- 6	46	9.04	1.36	0	.996	4.5
	35°C MK 7-12	45	7.98	1.33	0	.996	5.6
	60°C MK 13-18	31	9.46	1.36	0	.983	8.7
	MK 1-18	122	8.79	1.35	0	.992	5.9
	MK 1-18	122	8.66	1.35	-.002	.992	5.6
level 3	20°C MK 1- 6	14	.889	-.007	0	.114	0.6
	35°C MK 7-12	25	.257	.281	0	.926	2.8
	60°C MK 13-18	23	.474	.422	0	.969	4.9
	90°C MK 19-24	26	.568	.490	0	.972	5.1
	MK 1-24	88	.411	.405	0	.927	6.6
	MK 1-24	88	.363	.428	-.0022	.935	6.5

Figures 3.38-3.40 show all available data points in plots of weir head versus Q/ω for the levels observed. The fit curves drawn are those for which the viscosity power γ was fixed zero, corresponding to the various experiment temperatures.

Spreading in results appeared extremely high for the level 1 weir measurements which was caused by the interpretation problems due to the restricted quality of the photographs.

In figure 3.40 it can be observed that friction significantly raises the weir head which is expected from the numerical results presented in Appendix B.



WEIRHEAD VS FLOW/OMEGA (LEVEL 2)

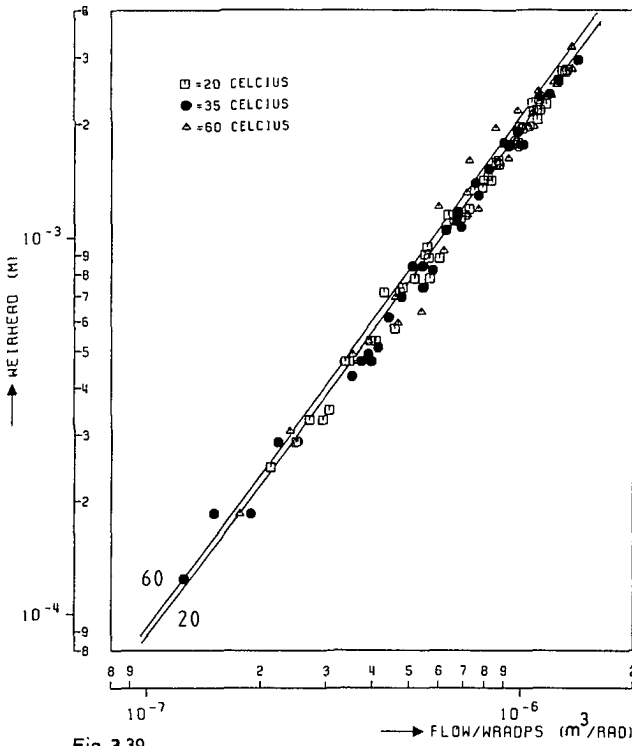


Fig. 3.39

WEIRHEAD VS FLOW/OMEGA (LEVEL 3)

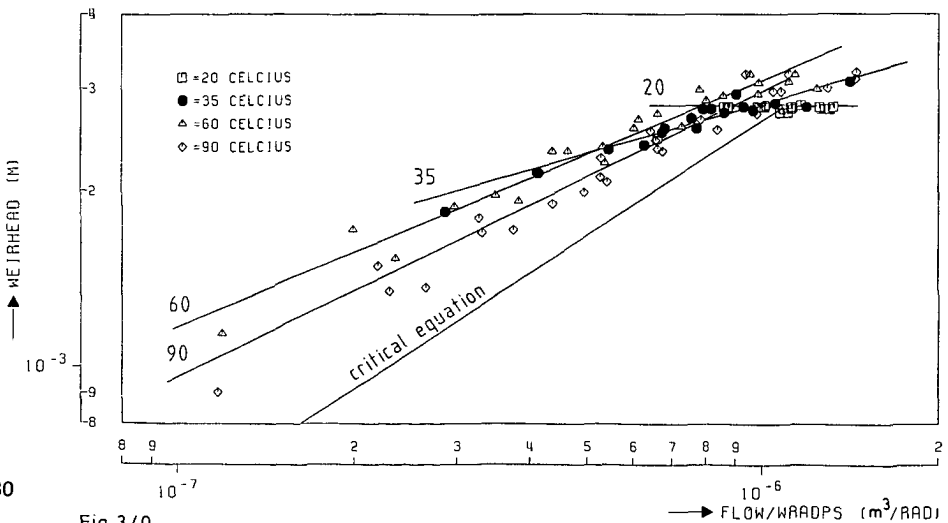


Fig. 3.40

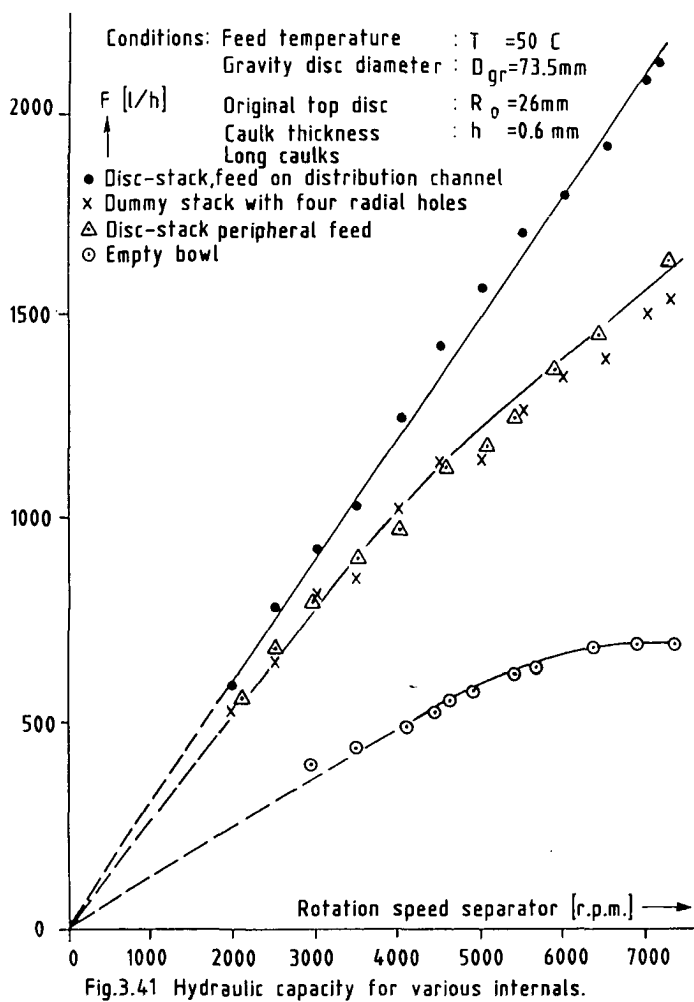


Fig.3.41 Hydraulic capacity for various internals.

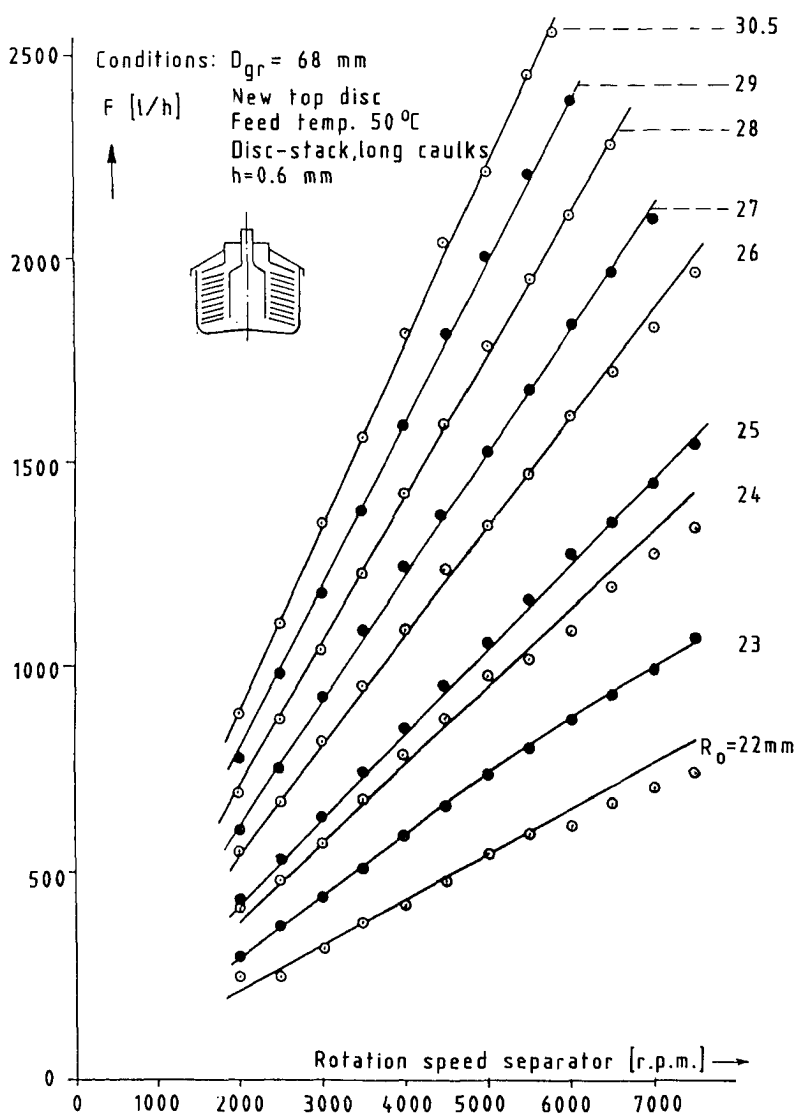


Fig.3.42 Hydraulic capacity for various outlet radii R_0 in case of a disc-stack.

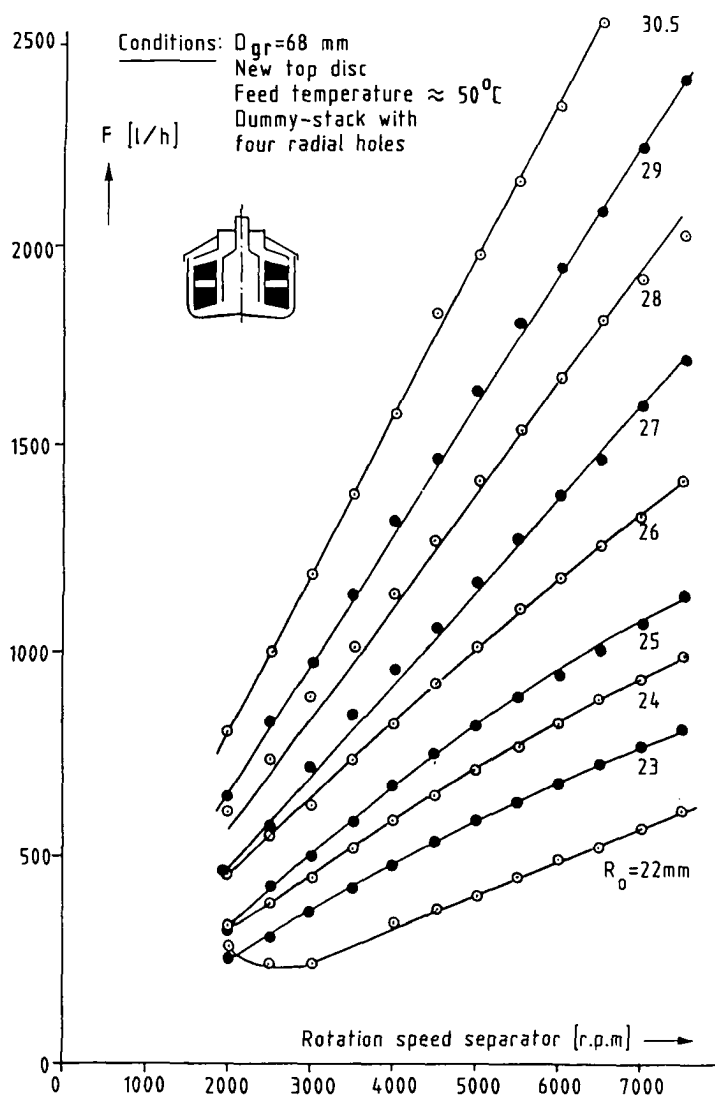


Fig.3.43 Hydraulic capacity for various outlet radii R_0 in case of a dummy stack.

3.5.3 Hydraulic capacity experiments

Preliminary experiments with four different internal configurations are presented in figure 3.41. It is quite clear that capacity of the channel fed disc-stack is higher than the peripherally fed disc-stack. The extra pressure drop in the latter case can be found both in the disc-stack (bigger radius ratio) and in the extended trajectory of the accelerated feed in the flared lower end of the distributor. The hydraulic capacity of the dummy stack coincides with that of the peripherally fed disc-stack in this particular case. Most remarkably is that the empty bowl capacity is far lower than the capacity with internals, which is most likely caused by the fact that solid body rotation is not valid anymore in the oil phase in between the feed radius and the outlet, resulting in spin-up effects such as discussed in paragraph 3.3.1.

Figures 3.42 and 3.43 show the significant effect of the oil outlet radius which directly controls the available head needed to overcome the various pressure drops within the bowl. The data belonging to these figures was obtained by machining the top disc outlet port bit by bit, ultimately obtaining the extended top disc shown in figure 3.15.

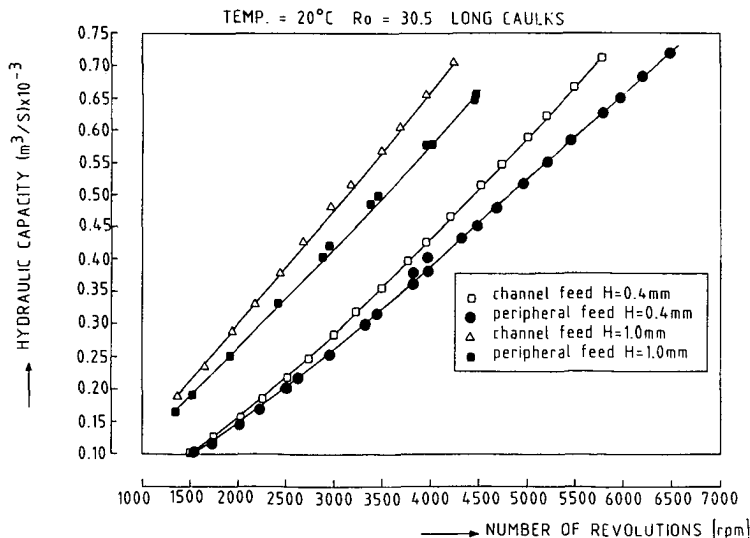


Fig.3.44

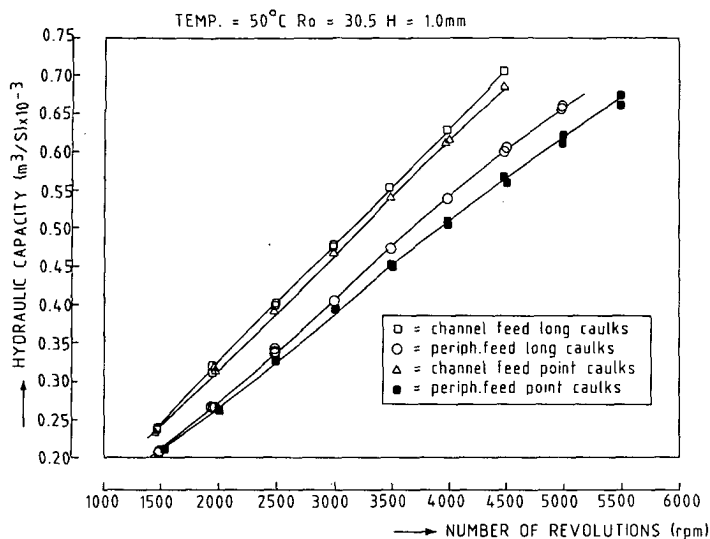


Fig.3.45

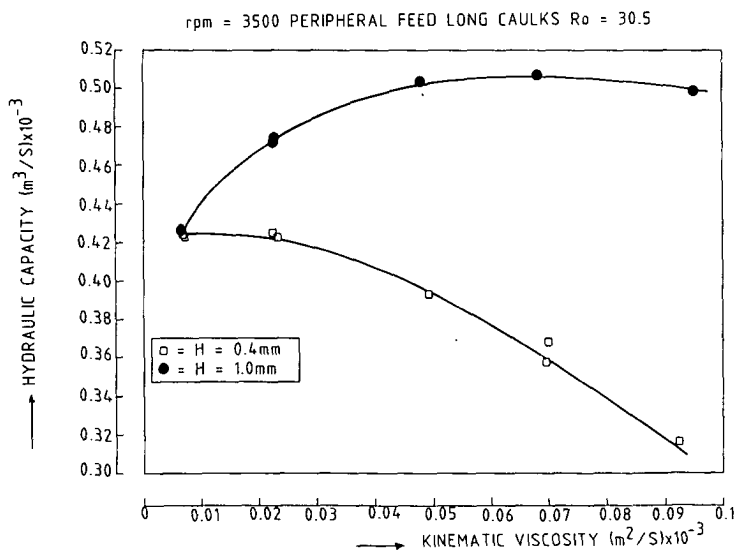


Fig.3.46

Figure 3.44 shows the important effect of caulk thickness and feed type. The caulk type effect is illustrated in figure 3.45. Figure 3.46 finally shows the decreasing importance of the disc-stack pressure drop on decreasing viscosity.

Generally speaking the hydraulic capacity appeared rather sensitive towards the chosen type of internals compared to the interface position.

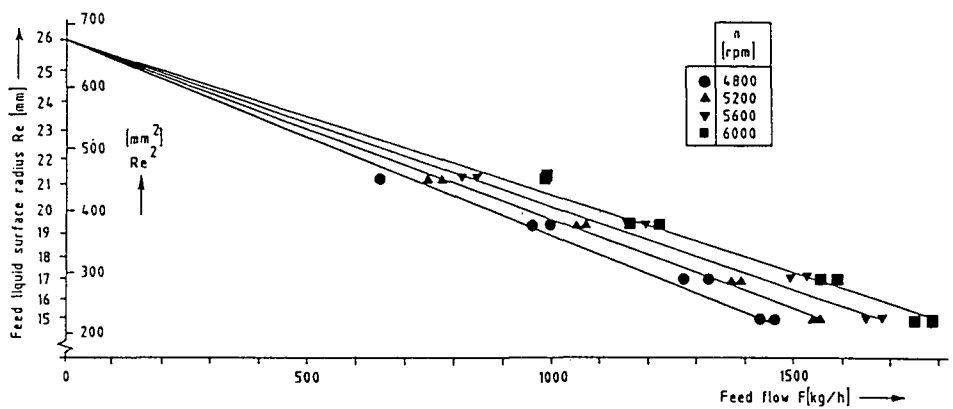


Fig.3.47. Feed liquid surface radii as function of feed flow.

3.5.4 Endoscope experiments

Figure 3.47 shows the results of the liquid surface radius measurements the square of which was plotted versus feed flow.

In view of the difficult measuring conditions it can be stated that the consistency of the results is not too bad. Assuming the total pressure drop in the oil phase $\Delta p_{O, cap}$ being proportional with flow rate and the validity of solid body rotation within the entire radius range of 15 mm to $R_O = 26$ mm we expect straight lines in between the points ($F = 0$, $R_e = R_O$) and (F_{max} , $R_e = 15$ mm).

It can be observed that the experimental values slightly deviate from this which is caused by several effects. First of all, the above-mentioned assumption is a simplification, whereas we have observed a non-proportional weir. Inserting the $\frac{2}{3}$ power into the pressure drop a slightly concave shaped curve in between the above-mentioned co-ordinates would be obtained, which would not fit the measured data better. Second, on decreasing R_e the available liquid cross section area increases which on the one hand lowers the axial velocity and on the other intensifies circulations within the axial channels. With respect to this point it must be emphasized that the liquid level was measured near the guiding fin, not being able to quantify the possible existence of a nonsymmetric fluid surface level. Third, a slip effect occurred when the liquid surface level radius passed the local recess in the guiding fin, as discussed in paragraph 3.4.2.4. Traversing the endoscope down into the rotating distributor the locations B, C and D were scanned of which the corresponding overflow rates were made dimensionless with F_a , the hydraulic capacity.

Figure 3.48 shows the overflow ratio plotted versus rotation speed. The flow ratio can be estimated by calculating the ratio of available pressure within the distributor to overcome the present pressure drop. From the figure 3.16 in paragraph 3.4.1 the radius at location A is found to be 15 mm, and at locations B, C and D 17 mm. Flow ratio between F_C and F_A is (left-hand side of equation (3.9) paragraph 3.3.3) $(R_O^2 - R_e^2) / (R_O^2 - R_A^2) = (26^2 - 17^2) / (26^2 - 15^2) = 0.859$. The arithmetic average of the measured ratios is 0.856 with standard deviation of 0.02.

The mutual deviations of the ratios measured at the locations A, C and E are not too high, nor very consistent. The overflow ratio slightly increases on increasing rotation speed (or flow) which is a possible indication of the observed slip effect. The experimental data of the above-presented work are reported by Van der Donk [16].

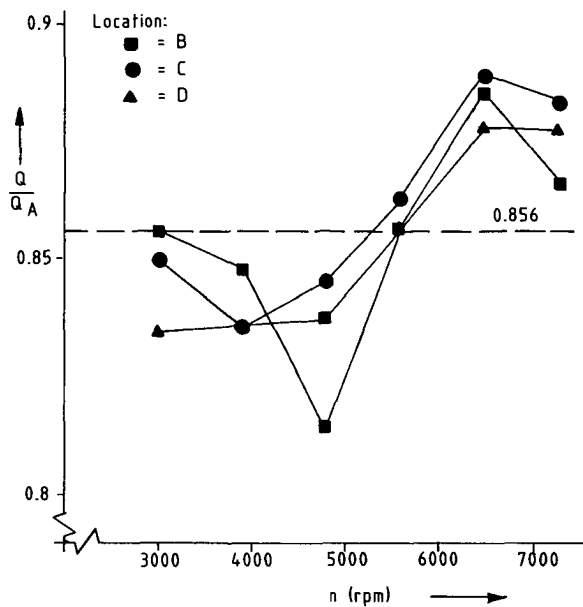


Fig.3.48 Overflow ratios

3.6 Prediction of interface position and hydraulic capacity

3.6.1 Approach

In order not to be confronted with too many pressure terms at once, the numerical treatment of the pressure drop $\Delta p_{o,i}$ was started with, making use of the dataset of the interface experiments. Having produced a satisfactory model description for this pressure drop, this would be subtracted from $\Delta p_{o, cap}$, the pressure drop determining hydraulic capacity, yielding the pressure drop within the distributor, $\Delta p_{o, dis}$. For the latter action the dataset of the hydraulic capacity experiments would be used.

3.6.2 Interface position

In a centrifugal separator the interface position is influenced by pressure drop in both phases, such as expressed in equation (3.8). Through measurement of the interface radius, the pressure drop of the oil phase $\Delta p_{o,i}$ (which does not include the distributor) was obtained by substitution of R_i into equation (3.8). Assuming the pressure drop in the water phase $\Delta p_{w,i}$ to be zero and writing $\Delta p_{o,i}$ in equation (3.8) explicitly yields:

$$\Delta p_{o,i} = \frac{1}{2} \rho_w \omega^2 (R_i^2 - R_w^2) - \frac{1}{2} \rho_o \omega^2 (R_i^2 - R_o^2) \quad (3.56)$$

The density of water is calculated with an equation presented by Weast [68]. The density of the turbine oil is calculated with equation (A4) presented in Appendix A. In case dual interface measurements were available (see Appendix D, footnote) the arithmetic average was taken of the values measured at the caulk and the channel position.

In paragraph 3.5.1 the quantitative results clearly indicated that the disc-stack pressure drop has certainly not been the one and only one, but must be completed by more pressure drop effects.

Before going into detail on the choice of the pressure drop models, the numerical procedure with which the available dataset was treated is shortly described. Under the assumption that a linear flow problem is encountered, it may be stated that the total pressure drop in the oil phase will be a linear combination of the consisting terms:

$$\Delta p_{o,i} = K_{disc} \Delta p_{disc} + K_{weir} \Delta p_{weir} + K_{grad} \Delta p_{grad} \quad (3.57)$$

The magnitude of the correction factors is expected to be 1. Positive deviation from this value can be an indication of an incorrect model or the existence of pressure drop at locations not taken into account by the models used. Equation (3.57) into which the measured values of n experiments will be substituted provides for n equations and 3 unknowns which will be treated with a least square analysis, hence minimising the residual errors in the pressure drop.

First, attention will be focused on the available pressure drop models, to be inserted into equation (3.57).

Disc-stack

For the disc-stack pressure drop equation (3.21) describing the symmetrical case, is used. For the non-symmetrical case, the correction factor derived by Carlsson is used (equation 3.23)). The disc-stacks used in this study are provided with horizontal flanges (cone angle $\theta = 90^\circ$) which amount to a few millimetres in the axial direction (see figure 3.17, paragraph 3.4.1). Presence of these flanges is accounted for with the same equation and added to the pressure drop corresponding to the conical part of the discs. In the peripheral feed situation the complete disc is accounted for in the range from R_3 to R_4 . In the channel feed situation only part of the disc is accounted for in the range from R_3 to R_{ch} .

Weir

Under the assumption of solid body rotation in the cylindrical part of the top disc, the pressure drop related to the weir head ΔR_o can be calculated with the below-presented equation:

$$\Delta p_{weir} = \rho_o \omega^2 \Delta R_o (R_o - \frac{1}{2} \Delta R_o) \quad (3.58)$$

For the substitution of the weir head ΔR_o into the above-presented equation more alternatives were available: the fit curves for level 1, level 2,

level 3, as well as the critical depth equation (3.34), discussed in paragraph 3.3.5, substituting $\omega^2 R_o$ for g and $Q/3w$ for q . At the end of the cylinder a transition takes place of potential energy into kinetic energy. The increase in fluid depth is at that location expected to be half the critical depth (paragraph 3.3.5). This factor was inserted into the weir pressure (eq. 3.58) by substituting the 1.5 fold critical depth for ΔR_o .

Gradient

Apart from the flow type (four suggestions can be found in figure 3.13, paragraph 3.3.6) a choice was to be made for the boundary conditions, which must be in strict relationship to the choice of the weir head equation, such as discussed already in paragraph 3.3.6. Apart from the possibilities mentioned, two more can be added: level 2 and level 3. The position of the latter, however, is undefined, but is certainly not the end of the cylinder because the focal depth measurements indicated that no clear details deeper than some 10 millimetres from the edge could be distinguished. The alternatives used are schematically presented together in table 3.8 and the insertion of the weir terms into the model is presented schematically in figure 3.49.

Table 3.8 Boundary conditions gradient model

weirmodel	z_o	δ_o
level 1 (table 3.7)	0	ΔR_o (level 1)
level 2 (table 3.7)	0 *)	ΔR_o (level 2)
level 3 (table 3.7)	0 *)	ΔR_o (level 3)
critical equation(eq.(3.34))	$3.5\delta_c$	δ_c

* It was chosen to set $z_o = 0$ instead of some fit value on the focal depth data presented in figure 3.37, because focal depth is negligible compared to the cylinder length.

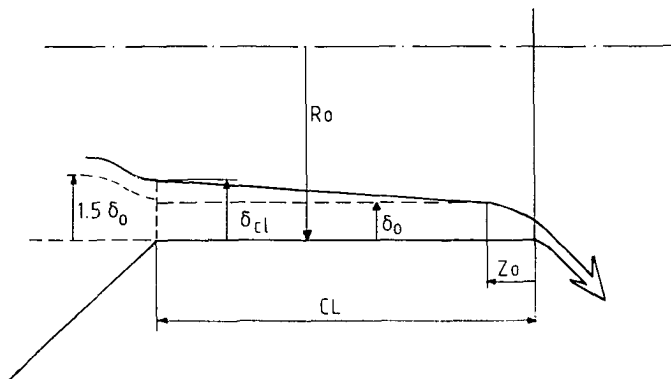


Fig.3.49 Model representation of weir and gradient.

Dataset

Experiments with the interface positioned closer than 1 mm to the disc-stack were always removed, in order to be certain that no maldistribution effect would affect the fit. Moreover, the experiments at the start of each series were removed, whereas the inlet temperature not always equalled the nominal temperature within the tolerated range of 1°C. This selection was accomplished by setting a flow criterion.

The complete dataset consisting of 114 experiment series, the experimental conditions of which can be found in Appendix D, was not numerically treated at once, but was subdivided into sub datasets with intent to check upon the correct model representation of the relevant parameters. For this purpose the complete dataset was reduced in such a way that all parameters would be equally represented. The results are presented in tabel 3.10.

Whereas in the complete dataset viscosity is far from equally represented, a special sub dataset was arranged, which contained equal portions of data, obtained at different temperatures. Selection of a rotation speed of 3500 rpm, long caulks, extended top disc and caulk thicknesses of both 0.4 and 1.0 mm, provided such a set, of which the results are presented in table 3.11.

Finally a subdivision has been made with respect to the feed type (channel/peripheral) as well as the caulk type (long/point), of which the correction factors were calculated together with those belonging to the complete dataset (see table 3.12).

Numeric results

In order to illustrate the necessity of incorporating more pressure terms, apart from the disc-stack pressure drop, it was chosen to start calculating with a rather simple version, namely equation (3.57) setting K_{weir} and $K_{\text{grad}} = 0$. For the dataset all available data belonging to the point caulk disc-stacks with peripheral feed were selected, hence the symmetrical solution (equation (3.21)) is valid. Results are presented in table 3.9.

Table 3.9 Results for the model version in which
only the disc-stack is taken into account

$K_d = 5.98$	data: point caulks peripheral feed number of datapoints: 506 $K_{\text{weir}} = K_{\text{grad}} = 0$	
parameter	correlation coefficient (%)	average fit error (%)
pressure drop $\Delta p_{o,i}$	93.8	20.9
interface radius R_i	81.9	1.61

Both the high value for the disc correction factor, together with the expected value of 1, and the high fit errors clearly indicate the necessity of extending the pressure drop model. At this moment it was chosen to extend the model with the weir pressure drop, of which the existence was already proven with the photographic results presented in paragraph 3.5.2, and to extend the model with the gradient. Because it can be conceived from the foregoing that the weir pressure would be the most important pressure drop,

selecting a proper weir expression was started. The plot of $\Delta p_{o,i}$ versus flow appeared concave in all cases, as can be observed in figures 3.25-3.31. Only the critical equation approached the experimental points contrary to the other 3 options listed in table 3.8, application of which resulted both into unrealistic high values for K_{weir} and worse predictions. Without further comment the critical equation will be used below.

The results presented in table 3.10 show that in spite of satisfactory predictions, problems arise in the disc representation, whereas both caulk thickness and rotation speed affect the correction factor for the disc-stack pressure drop significantly. The wide range of calculated disc correction factors is also explained by the magnitude of the disc-stack pressure drop, which, according to table 3.9, amounts to one sixth of the measured pressure drop.

Table 3.10 Results for various selections from a balanced dataset

dataset	interface radius R_i		K_{disc}	K_{weir} **)	pressure drop $\Delta p_{o,i}$		number of data points
	fit error (%)	cor (%)			fit error (%)	cor (%)	
complete *)	.596	97.6	1.08	1.23	6.62	99.3	1540
channel peripheral	.538	98.0	1.27	1.18	6.01	99.4	864
	.660	97.2	.827	1.29	7.29	99.2	676
long caulks point caulks	.562	98.1	1.36	1.17	6.12	99.3	812
	.631	96.9	.950	1.25	7.08	99.3	728
$R_o = 26.0$ mm $R_o = 30.5$ mm	.469	95.4	1.59	1.10	6.76	99.0	512
	.666	97.8	.953	1.26	6.53	99.4	1028
$h = 0.4$ mm $h = 1.0$ mm	.510	98.6	.417	1.37	5.85	99.4	777
	.464	98.4	1.93	1.06	5.36	99.2	763
$n = 3500$ rpm	.490	99.0	.631	1.18	4.48	97.6	257
$n = 5500$ rpm	.363	98.1	1.71	1.01	4.45	98.3	308
$n = 7300$ rpm	.322	98.0	1.54	1.20	4.38	98.4	325

Notes *) $T = 50^\circ\text{C}$; $h = 0.4$ mm and $h = 1.0$ mm
 **) $K_o^{grad} = 1.0$; cylinder flow type according to equation (3.51)
 weir type: $\Delta R_o = 1.5$ fold critical depth (equation (3.58))

For the complete data set the disc correction factor produces an acceptable value, whereas the weir correction factor is slightly more than expected. The latter observation can be explained either by the end contraction, which amounts to some 20% of the circumference, as shown in figure 3.13D, or by possible existence of pressure effects, not yet accounted for. For instance, filling of the flowpassage, as discussed in paragraph 3.5.2, might lead to extra pressure drop.

Table 3.11 shows correction factors approaching unity with less spreading compared to the previous results. Incorporation of the gradient model seems to have a marginal effect on the calculated factors and does not improve the prediction. The combination of both the disc and weir factor increase on increasing viscosity which favours the conclusion that a viscosity dependent term should be added.

Table 3.11 Results for a dataset balanced with respect to viscosity

dataset *)	interface radius R_i		K_{disc}	K_{weir} **)	K_{grad} ***)	pressure drop $\Delta p_{o,i}$		number of data points
	fit error (%)	cor (%)				fit error (%)	cor (%)	
T=50°C	.500	99.0	.846	1.15	1.0	4.5	99.0	138
	.364	99.3	.832	1.20	0.0	3.31	99.3	
T=22°C	.286	99.9	.883	1.18	1.0	1.72	99.5	68
	.317	99.5	.942	1.30	0.0	1.79	99.5	
T=90°C	.508	97.8	1.22	.911	1.0	4.58	97.7	91
	.481	97.9	1.21	.928	0.0	4.33	97.9	
complete	.761	97.3	.977	1.07	1.0	6.41	97.0	313
	.932	94.0	1.12	1.09	0.0	7.69	94.9	

Notes: *) $n = 3500$ rpm; long caulks; $R_o = 30.5$ mm;
 $h = 0.4$ mm and $h = 1.0$ mm

**) weir type: $\Delta R_o = 1.5$ fold critical depth (equation (3.58))

**) cylinder flow type according to equation (3.51)

Table 3.12 Results for the four sub datasets

dataset *)	flow type **)	interface radius R_i		K_{disc}	K_{weir} ***)	K_{grad} ****)	pressure drop $\Delta p_{o,i}$	
		fit error (%)	cor (%)				fit error (%)	cor (%)
lc ch 839 data points	-	.690	97.3	.992	1.27	0.0	6.3	99.4
	sin	.678	98.7	.872	1.24	1.0	6.51	99.5
	lin	.647	98.4	.915	1.25	1.0	6.21	99.5
	3 w	.679	98.7	.872	1.24	1.0	6.52	99.5
	$2\pi R_o$.642	98.1	.934	1.26	1.0	6.13	99.5
lc pe 493 data points	-	.957	96.3	.702	1.36	0.0	9.19	99.1
	sin	.949	98.0	.902	1.27	1.0	9.21	99.3
	lin	.926	97.7	.847	1.30	1.0	9.04	99.3
	3 w	.950	98.0	.902	1.27	1.0	9.22	99.3
	$2\pi R_o$.927	97.4	.804	1.31	1.0	9.02	99.3
pc ch 403 data points	-	.473	98.1	.541	1.39	0.0	5.30	98.0
	sin	.570	97.4	1.04	1.23	1.0	6.43	99.3
	lin	.540	97.7	.885	1.27	1.0	6.10	99.3
	3 w	.570	97.4	1.04	1.23	1.0	6.44	99.3
	$2\pi R_o$.521	97.8	.783	1.31	1.0	5.88	99.3
pc pe 335 data points	-	.593	97.2	.358	1.46	0.0	6.56	99.3
	sin	.678	96.5	.770	1.30	1.0	7.59	99.3
	lin	.653	96.8	.644	1.35	1.0	7.30	99.3
	3 w	.679	96.5	.772	1.30	1.0	7.59	99.3
	$2\pi R_o$.637	97.0	.559	1.38	1.0	7.10	99.3
complete 2070 data points	-	.720	97.0	.942	1.30	0.0	7.05	99.3
	sin	.746	98.2	.916	1.25	1.0	7.46	99.4
	lin	.713	97.9	.929	1.26	1.0	7.18	99.4
	3 w	.747	98.2	.916	1.25	1.0	7.47	99.4
	$2\pi R_o$.705	97.8	.939	1.28	1.0	7.08	99.4

Notes:
 *) lc = long caulks ; pc = point caulks;
 ch = channel feed; pe = peripheral feed
 **) sin : b according to equation (3.51)
 lin : " " " "
 3 w : " " " "
 $2\pi R_o$: " " " "
 ***) critical equation (3.34)
 ****) fixed values

The following remarks with respect to the results in table 3.12 are to be made.

1. The flow types "sin" and "3 w" result into almost identical correction factors, which is a result of the fact that their resemblance directly upstream the outlet ports is high, which is the most important zone with respect to frictional losses. The above-mentioned resemblance can be observed in figure B3 (Appendix B) in which the plots belonging to the "3 w" and "sin" type are almost identical.
2. Deviation of the disc and weir correction factors from unity is strongest for the point caulk experiments when the gradient model was not included.
3. As was already observed in table 3.10 for the complete dataset the weir correction factor is also higher than unity.
4. Careful observations of the model predictions learned that pressure drop was underestimated for the lower rotation speeds. Besides, the underestimation appeared stronger for the higher caulk thickness. Under no circumstances instability of flow could be expected, whereas typical Reynolds values would never exceed the value of 10 in the complete data set (Reynolds according to the notation of equation 3.27). This observation made us believe that the misfit was entirely due to an imperfection of the disc-stack model representation. Existence of pressure drop in the distribution channel, not being a function of rotation speed, could explain the above-mentioned trends.
5. In order to check upon the statement made above, concerning the disc-stack representation, the complete distribution model was incorporated within the analysis. However, the fit was not improved to such an extent that the necessary extra computation time appeared worthwhile. This is mainly caused by the fact that the lacking pressure effect is only a small part of the total pressure drop which is measured up to a limited accuracy. E.g. the average fit error of 0.746% in the interface radius equals an average deviation of some 0.5 mm which is fairly close to deviations to be expected when even small temperature changes occur.

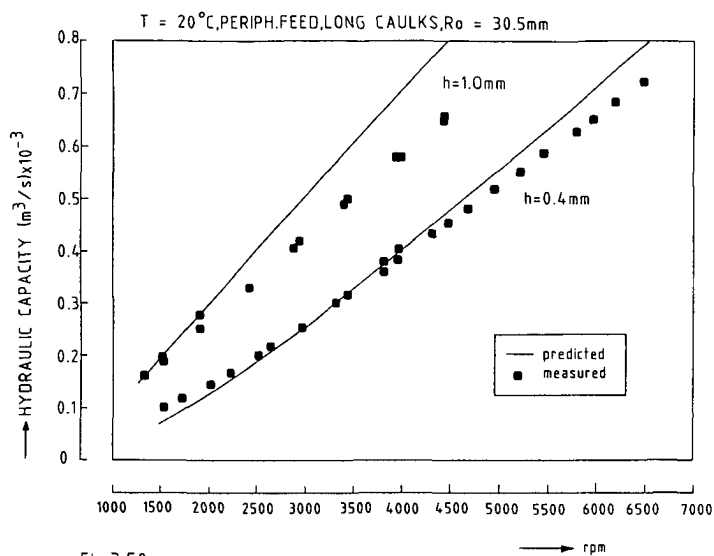


Fig.3.50

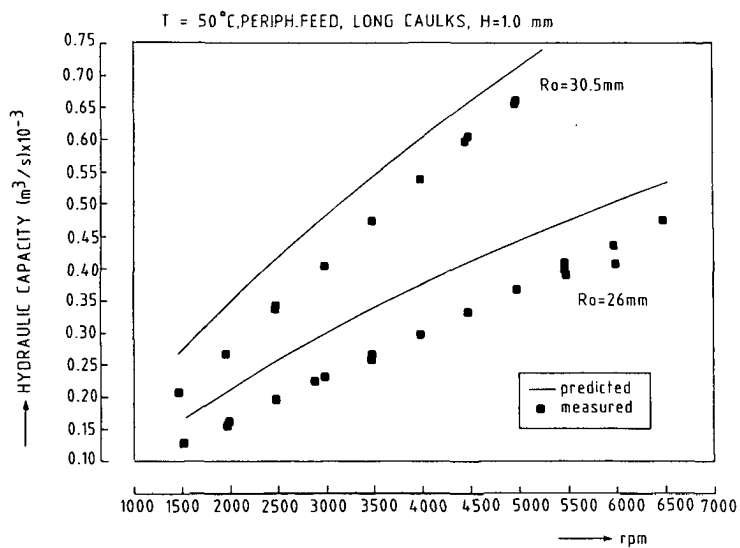


Fig.3.51

3.6.3 Hydraulic capacity

With the quantitative knowledge of $\Delta p_{o,i}$ obtained in paragraph 3.6.2, an expression could be presented for the overall pressure drop occurring in the light phase from inlet to outlet, which apart from $\Delta p_{o,i}$ would also contain the distributor pressure effect Δp_{dis} :

$$\Delta p_{o,cap} = \Delta p_{o,i} + \Delta p_{o,dis} \quad (3.59)$$

Through the experimental conditions belonging to the hydraulic capacity, $\Delta p_{o,cap}$ could be calculated with the aid of equation (3.9).

From the information obtained with the endoscope experiments, a slip effect is known to take place in the distributor, which does not favour the validity of solid body rotation in the range of $R_e = 15$ to 17 mm within the distributor. However, for the time being, $R_e = 15$ mm will be substituted into equation (3.9). The best available approximation for the pressure effect in the distributor, $\Delta p_{o,dis}$, is the disc-stack pressure drop equation (3.21), inserting $R_2 = 54.0$ mm; $R_1 = 30.5$ mm; $h = 23.5$ mm; $N_s = 1$ and $\theta = 35^\circ$. In this case of high values for λ , the influence of h on the predicted pressure effect appears to be marginal. With an identical least square analysis, as mentioned above, the dataset belonging to the hydraulic capacity experiments was treated with the below-presented equation:

$$\Delta p_{o,cap} - \Delta p_{o,i} = K_{dis} \cdot \Delta p_{dis} \quad (3.60)$$

After having evaluated K_{dis} in equation (3.60), the predicted hydraulic capacity was calculated backwards and compared with the measured value. The latter calculation was performed with a numeric procedure, whereas equation (3.60) is implicit with respect to flow. With respect to the representation of the disc pressure effects two alternatives were tested. First, the straight forward disc pressure drop such as already explained in paragraph 3.6.2. Second, the extended disc model such as described in Appendix G. The results of computer calculations can be found in table 3.13.

Figures 3.50-3.53 show some experiments together with model curves, applying the extended disc model. In the above-stated procedure the weir factor was fixed at a value of 1.2 and the gradient factor at a value of 1.0.

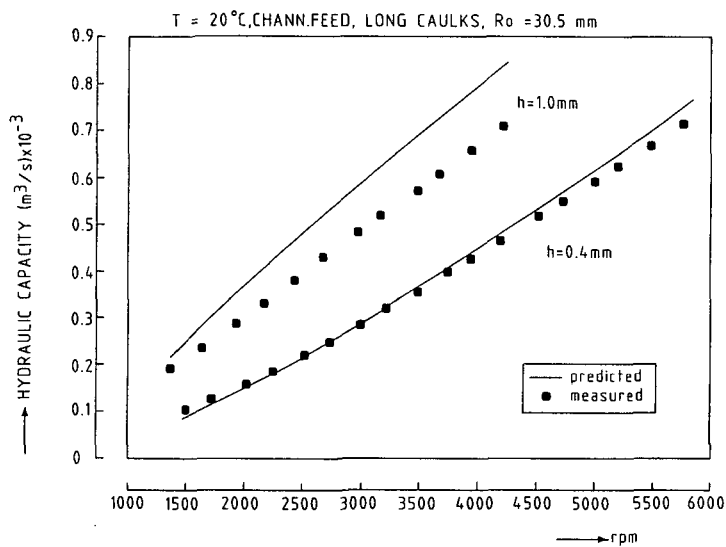


Fig.3.52

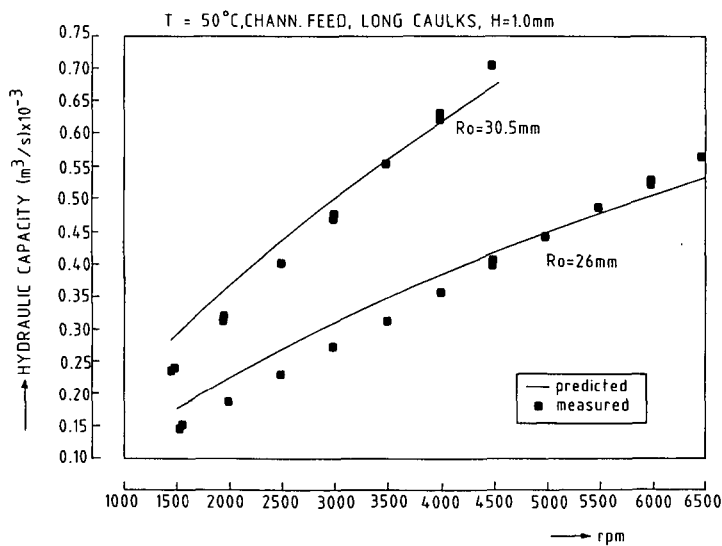


Fig.3.53

Table 3.13 Hydraulic capacity prediction

dataset *)	disc model **)	R_e (mm)	K_{dis} (-)	hydraulic capacity		number of data points (-)
				fit error (%)	cor (%)	
h=0.4 or 1.0 mm	n	15.0 16.0 17.0	.173 .151 .127	15.9 14.6 13.6	92.1 92.8 93.5	631
2000<n<7300 rpm	n	15.0	.176	14.8	89.9	616
	ext		.170	12.0	93.1	
3000<n<7300 rpm	n	15.0	.175	13.6	85.9	441
	ext		.169	11.5	89.4	
complete	n	15.0	.176	15.6	92.4	724
	ext		.170	12.2	95.0	
complete; $\alpha_F = .44 \cdot 10^9 n$	ext	15.0	.155	11.0	95.5	724

Notes: *) see Appendix E

**) n = disc pressure drop: eq. (3.21) and (3.23)
ext = extended disc model (Appendix G)

Fit errors with respect to the predicted hydraulic capacity are somewhat higher than the fit errors belonging to the pressure drop in the previous section. This is explained, among other things, by the existence of a slip effect within the distributor. For this reason R_e was lowered in order to simulate the reduced static head in the distributor. The numeric results appear to improve slightly. Precise analysis of the fit errors learned that the disc representation was incorrect, whereas fit errors appeared significantly higher for the 1.0 mm disc-stacks compared to the 0.4 mm disc-stacks. For this reason the extended disc model was incorporated in the model which improved the fit according to table 3.13. Best results were obtained when the distributor foot resistance factor was increased with a

factor of 5, which was verified with the effect of flow type on the fit error.

Summarizing:

The interface radius can be calculated with equation (3.8), into which $\Delta p_{o,i}$ is to be substituted.

The pressure drop $\Delta p_{o,i}$ consists of three terms:

1. Disc pressure drop; equation (3.21) for the symmetrical case and equation (3.23) for the assymmetrical case.
2. Weir pressure drop; 1.5 fold the critical depth according to equation (3.34), substituting $\omega^2 R_o$ for g and $Q/3w$ for q , combined with equation (3.58). In practice this pressure drop must be corrected with a factor of approximately 1.2.
3. Hydraulic gradient; application of the critical depth mentioned above as the boundary condition at the edge, an integration procedure will provide for the upstream liquid depth. With equation (3.58) the pressure effect can be estimated.

The hydraulic capacity can be calculated with equation (3.9), when $\Delta p_{o, cap}$ is expressed as a function of flow.

Pressure drop $\Delta p_{o, cap}$ consists of $\Delta p_{o,i}$ and the distributor pressure drop $\Delta p_{o, dis}$, according to equation (3.59).

The distributor pressure drop can be estimated with equation (3.21) which has to be corrected with a factor of approximately 0.17, which is typical of the separator used within this study.

3.7 Conclusions

1. The interface experiments prove to reproduce reasonably well (paragraph 3.5.1).
2. Pressure drop in a centrifugal separator has a considerable effect on interface position which becomes more and more important in case of low density differences (paragraph 3.5.1).
3. The interface position is hardly affected by waterflow, because of the high weir length and the low water to oil phase ratio, which is typical of oil purification (paragraph 3.5.1).
4. Frictional losses in the light phase outlet have a considerable effect on the effective weir head (Appendix B, paragraph 3.5.2).
5. The contribution of the disc-stack to the total pressure drop in a centrifugal separator is of minor importance (paragraph 3.6).
6. The hydraulic capacity of a centrifugal separator appears to be roughly proportional to the separator rotation speed (paragraph 3.5.3).
7. Increasing the light phase outlet radius is an effective tool in improving the hydraulic capacity of a centrifugal separator (paragraph 3.5.3).
8. When calculating the interface position, no valid reason can be found why the empirical power expression presented by Schilp [55] should be used in order to describe the pressure gradient in a separator, hence accounting for non-rigid rotation (paragraphs 3.3.1 and 3.5.1).
9. Although there is still room for improvement concerning the hydraulic capacity, incorporation of the extended disc model, which accounts for non-uniform liquid loading, raises the accuracy of the disc-stack representation (paragraph 3.6.3).

10. The liquid surface radius within the distributor can be estimated by an interpolation, assuming proportionality between the square of this radius and the ratio between feed flow and hydraulic capacity (paragraph 3.5.4).

CHAPTER 4

IN-LINE SEPARATION-MONITORING

4.1 Introduction

To improve the performance of centrifugal separators from which a high degree of separation is expected, more precise measurement techniques are required, which can withstand the severe circumstances, typically encountered within these devices. Especially when the parameters which determine the optimum separation must be maintained in close limited ranges, whereas instationary feed conditions occur, indirect measurements often fail to be of practical use. Being confronted with this problem in the early stage of the disc-stack centrifuge project, as commercially available systems could not meet the necessary requirements, it was decided to develop adequate measuring techniques within the project.

In this chapter two developments are mentioned: first, the pulse-echo-method, with which the position of the interface could be measured in a rotating bowl and second, the capacitance technique, with which low water content in oil could be measured.

Experiments are performed with a three terminal capacitive sensor of which the latest design sensor is able to discriminate changes in water content of 10 ppm, which is made possible by application of the dual cell principle in combination with high sensitivities. Special arrangements must be made in order to make the high sensitivity profitable, whereas the stability of the output signal depends entirely on the thermal behaviour of the measuring system. Besides temperature effects, presence of air severely reduces the measuring range. Contrary to temperature effects, presence of air cannot be compensated for in a simple way, which therefore is the severest restriction of the measuring technique discussed.

4.2 Objectives

Providing knowledge of the general design rules as well as the limitations, for both the pulse-echo interface measurement technique and for the capacitive system, including the dielectric behaviour of a water-in-oil dispersion.

4.3 Interface-monitoring, pulse-echo-method

4.3.1 Basic principle

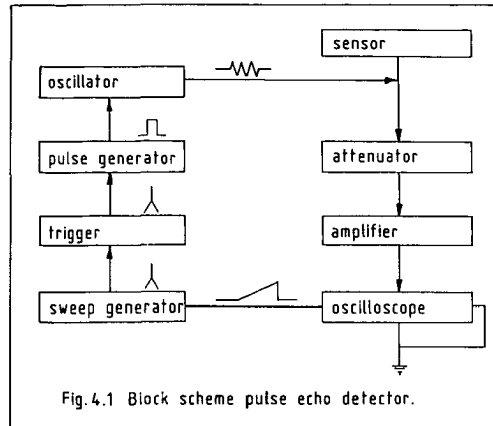
The working principle of the pulse-echo-method is the existence of a discontinuity in acoustic impedance at the water oil interface which partly reflects acoustic signals. The acoustic signals are produced by a transducer containing a piezo element, which transforms electric pulses into mechanic pulses and the other way around. High resolution can be obtained by applying high frequencies in combination with high damping factors resulting in a dirac-like pulse form. Working principle is described as follows. First a short pulse is emitted with the aid of an ultrasonic transducer. The reflection will cause an electric pulse in an ultrasonic detector being connected with the vertical beam deflector of an oscilloscope causing a vertical peak of which the height is a measure for the peak intensity. At the time of the emission of the pulse a sweep generator is activated steering the horizontal beam deflector of the oscilloscope. Together with the known frequency of the sweep generator the position of the above-mentioned peak is a measure for the distance in between the ultrasonic transducer and the reflecting obstacle. Schematically this is presented in figure 4.1.

4.3.2 Description of monitoring system

4.3.2.1 Transducer

In co-operation with the echo-acoustics group of the instrumentation department within the Technisch Fysische Dienst in Delft, special transducers were developed which could withstand the severe conditions of 30 bars, 6000 g and 20-90°C, in water and oil. A maximum damping factor was strived for which was realized by the application of backing material with high acoustic impedance, a compound of heavy metal powder and araldite, centrifugally cast in high vacuum thus preventing inclusions of air. In the first design no matching layer ($1/4 \lambda$) was used in order to obtain an optimum resolution. For mechanical reasons a $5/4 \lambda$ matching layer was

incorporated in the second design. The crystal diameter has been 6 mm and the transducer frequency has been 5 MHz.



4.3.2.2 Transducer position

Since the interface is positioned in between the disc-stack (outer radius $R_4 = 80.5$ mm) and the top disc (outer radius 98 mm), it can be stated that the measuring area is rather limited. With the internal diameter of the bowl $D_w = 214.07$ mm it has been found that the interface position relative to the inner bowl wall is in between approximately 9 and 27 mm. The intensity field coming from a plane radiator is never homogeneous, but oscillates due to interference effects. The zone in which this phenomenon takes place is called the Fresnell zone, which extends to the zero order maximum in the intensity, which in our case is some 3 cm away from the above-described crystal. For this reason we have positioned the measuring area outside the Fresnell zone by means of a 45° mirror "folding" the sound path from the axial direction towards the radial direction (see figure 4.2). Additional advantage is that no deposition of separated particles at the transducers' front surface will occur, which might lead to loss of signal intensity.

4.3.2.3 Constructional aspects

Two transducers were installed: one opposite the caulk and the other opposite the distribution channel, thus almost diametrically positioned in the bowl. In this way possible axisymmetry could be checked upon, making dual measurements. Figure 4.2 shows a detailed drawing of the modified separator bowl. The transducers were directed in the axial direction and were mounted in aluminium holders. The holders, as well as the 2 mm thick coaxial cable, were attached to the bowl with araldite. In order to be able to interchange the internals and the distributor in particular, the cable has been guided in a groove which was machined into the distributor seating. The topnut was modified slightly in order to guide the cable into the hollow axis. The aluminium holder forms one piece with the mirror which reduces deflections of the transducer axis with the trigger surface centre.

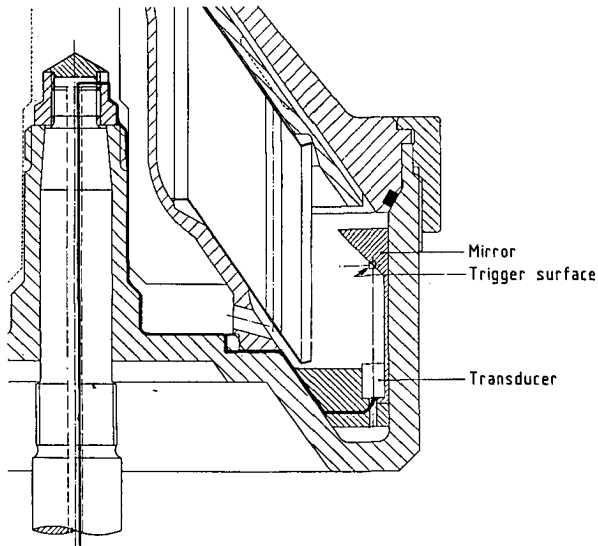


Fig. 4.2 Assembly drawing of the ultrasonic transducer in the separator bowl

Figure 4.3 shows the spindle details. The slipring assembly is rigidly connected to the separator frame. In order to be able to cope with the small axial and radial displacements of the spindle a claw coupling is used. A special double sealing ring is used under the axial bearing in order to prevent leakage of lubrication oil. A pneumatic brush lifting device extends the operational life of the high speed slipring assembly.

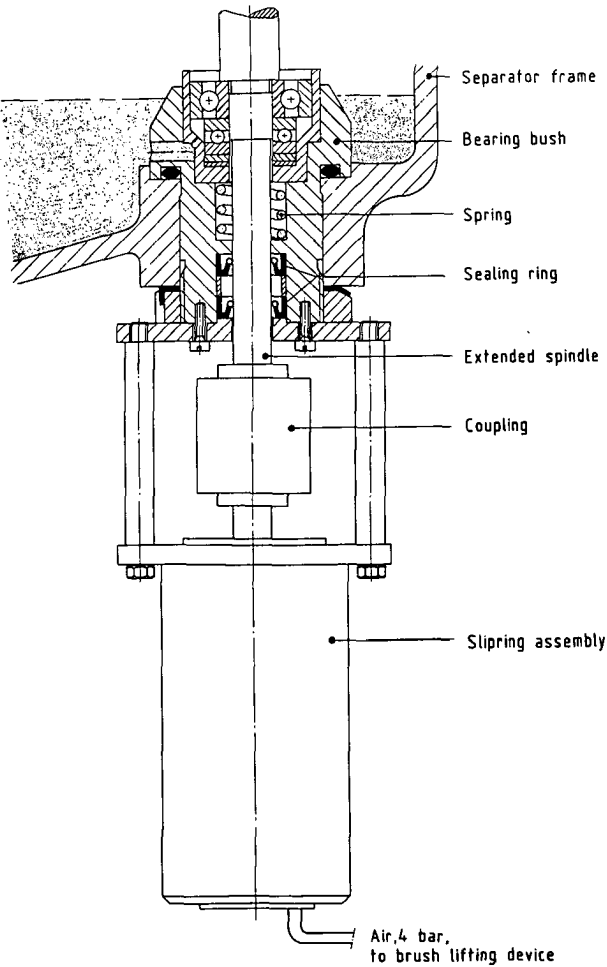


Fig. 4.3 Details of the spindle design.

4.3.2.4 Signal interpretation

In order to increase the dynamic range of the measurement, a reference reflection was created by means of a so-called trigger surface machined on the mirror.

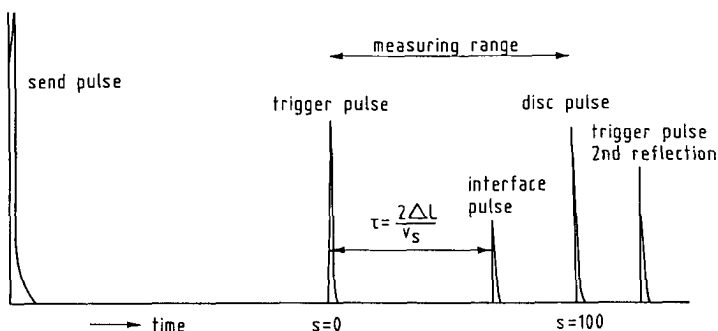


Fig.4.4 Typical response of the ultrasonic transducer.

Figure 4.4 shows the typical response of the ultrasonic system. The ultrasonic signal emitted by the crystal travels to the mirror. Part is reflected by the trigger surface and produces the so-called trigger pulse. The rest of the emitted sound is deflected 90° in the radial direction and arrives at the interface where partial reflection takes place producing the so-called interface pulse. The rest, which is transmitted by the interface, penetrates in the oil phase and produces the disc pulse, a reflection at the outer disc diameter. After the disc pulse, multiple reflections can be observed with decaying intensity. The reflection pattern was analysed with a pulse-echo-detector Krautkrämer USIP 11. The speed of sound in water depends upon temperature, pressure and salinity and is reported by various workers [6, 19, 69, 71]. According to Edmonds [19] the value at 25°C is 1402.73 m/s . Willard [69] reports a formula which gives the velocity of sound in water, v_{sw} as function of temperature:

$$v_{sw} = 1557 - 0.245 (74 - T)^2 \quad (4.1)$$

in which T is temperature in $^\circ\text{C}$ and v_{sw} in m/s .

Wilson [71] gives a formula for the speed of sound as function of temperature, pressure and salinity. The influence of pressure is not too high: + 0.012 %/bar. For reasons of accuracy and simplicity two reference points have been used: first, the trigger surface and second, the edge of the disc-stack. This is accomplished, in practice, by both a trigger option on the pulse-echo-detector and an adjustable timescale. Calibration of the signal is executed during the start-up of the separator, when the bowl only contains water. In this way only one medium (water), with one and the same speed of sound, is present, so that linear interpolation is valid. With the proper adjustments the trigger pulse can be got left in the picture tube ($S = 0$ units) and the disc pulse right in the picture tube ($S = 100$ units) (see also figure 4.4). The position of the interface can now easily be measured by reading off an aluminated linear scale, S , subdivided into 100 units. The interface radius is obtained by substituting the value for S into a geometrically relationship of which the derivation is presented in Appendix C and is identical for both the caulk transducer and the channel transducer:

$$R_i = 100.42 - 0.1992 S \quad (4.2)$$

with R_i the interface radius in mm and S in between 0 and 100. For values of S smaller than $S = 12.1$, breakage of water seal could be expected ($S = 12.1$ corresponds to the outer radius of the top disc).

4.3.3 Experience gained with the interface-monitoring system

Signal-to-noise ratios measured, have been quite sufficient (> 40 dB) to perform experimental work under various conditions. Signal intensity oscillated a bit, especially the signal coming from the transducer mounted opposite the channel, which is explained by local interface disturbances caused by the feed liquid. Feed temperature, as well as grade of dispersion, appeared not to affect measured intensities noticeably. Generally, most stable signals were obtained at the higher rotation speeds.

During the course of the experimental programme transducer failure occurred twice: once due to a fracture in the unprotected coaxial cable, caused during exchange of separator internals and once due to a fracture in between the crystal and the backing material. The latest version was redesigned and has been functioning until the end of the project.

4.4 Water-content monitoring, capacitance technique

4.4.1 Background theory

4.4.1.1 Dielectric behaviour of dispersions

In alternating fields, a temporal phase shift may occur between the driving field and the resulting polarization, and a loss current component appears. The conduction term need not stem from a migration of charge carriers, but can represent any other energy consuming process. It has therefore become customary to refer to the existence of a loss current in addition to a charging current by the introduction of a complex relative permittivity or relative dielectric constant ϵ^* :

$$\epsilon^* = \frac{\sigma^*}{j\omega\epsilon_0} = \epsilon + \frac{\sigma}{j\omega\epsilon_0} \quad (4.3)$$

where σ is the dielectric conductivity ($1/\Omega \text{ m}$), ϵ_0 the dielectric constant of vacuum and ω the angular frequency. This dielectric conductivity contains all dissipative effects and may represent both an actual ohmic conductivity caused by migrating charge carriers and an energy loss associated with a frequency dependence (dispersion) of ϵ , for example, the friction accompanying the orientation of dipoles.

Heterogeneous mixtures composed of two phases, which differ from each other in dielectric constant and electrical conductivity, show a dielectric dispersion due to the so-called interfacial polarization.

Maxwell [49] explained the dielectric dispersion due to the interfacial polarization of a heterogeneous system by means of a stratified model (see also Von Hippel [36]). Maxwell [49] derives the overall relative dielectric constant ϵ^* of a two-layer condenser, consisting of two parallel sheets of material, both characterized by their relative dielectric constant ϵ , conductivity σ and thickness d . The final result is written in a compact form in which the parameters ϵ_1 , ϵ_h , σ_1 and τ can be expressed as functions of the dielectric properties of the consisting materials (see Hanai [30]):

$$\epsilon^* = \epsilon_h + \frac{\epsilon_1 - \epsilon_h}{1 + j\omega\tau} + \frac{\sigma_1}{j\omega\epsilon_0} \quad (4.4)$$

The static dielectric constant, ϵ_1 , the limiting value of ϵ at lower frequencies, is larger than the optical one, ϵ_h , the limiting value of ϵ at higher frequencies, because of the completion of transport of mobile charge carriers. As the frequency increases, the interfacial polarization begins to lag. The relative dielectric constant ϵ decreases to the midpoint between the static and optical value when $\omega = 1/\tau$, where τ is the relaxation time. An important shortcoming of the Maxwell theory is that it is unable to explain the considerable changes of dielectric constants and conductivities on phase inversion of emulsions, since no distinctions are made between the continuous medium and the disperse phase of emulsions.

Wagner [66] showed that, for a dispersion system where spherical particles are sparsely distributed throughout the dispersion medium, the complex dielectric constant ϵ^* and conductivity σ^* of a heterogeneous mixture are given by the following expressions:

$$\epsilon^* = \epsilon_c^* \frac{2\epsilon_c^* + \epsilon_d^* - 2\phi(\epsilon_c^* - \epsilon_d^*)}{2\epsilon_c^* + \epsilon_d^* + \phi(\epsilon_c^* - \epsilon_d^*)} \quad (4.5)$$

$$\sigma^* = \sigma_c^* \frac{2\sigma_c^* + \sigma_d^* - 2\phi(\sigma_c^* - \sigma_d^*)}{2\sigma_c^* + \sigma_d^* + \phi(\sigma_c^* - \sigma_d^*)} \quad (4.6)$$

where c denotes the continuous medium, d the disperse phase and ϕ the volume fraction of the disperse phase.

Inserting equation (4.3) for both phases into equations (4.5) and (4.6) the compact form of equation (4.4) can be obtained resulting in the below-presented expressions for the static and optical relative dielectric constant, the static conductivity and the relaxation time:

$$\epsilon_1 = \frac{\epsilon_c(2\sigma_c + \sigma_d)^2 + [(9\epsilon_d - 2\epsilon_c)\sigma_c^2 - 8\epsilon_c\sigma_c\sigma_d + \epsilon_c\sigma_d^2]\phi + 2\epsilon_c(\sigma_c - \sigma_d)^2\phi^2}{[2\sigma_c + \sigma_d + \phi(\sigma_c - \sigma_d)]^2} \quad (4.7)$$

$$\epsilon_h = \epsilon_c \frac{2\epsilon_c + \epsilon_d - 2\phi(\epsilon_c - \epsilon_d)}{2\epsilon_c + \epsilon_d + \phi(\epsilon_c - \epsilon_d)} \quad (4.8)$$

$$\sigma_1 = \sigma_c \frac{2\sigma_c + \sigma_d - 2\phi(\sigma_c - \sigma_d)}{2\sigma_c + \sigma_d + \phi(\sigma_c - \sigma_d)} \quad (4.9)$$

$$\tau = \epsilon_0 \frac{2\epsilon_c + \epsilon_d + \phi(\epsilon_c - \epsilon_d)}{2\sigma_c + \sigma_d + \phi(\sigma_c - \sigma_d)} \quad (4.10)$$

In case of water-in-oil dispersions (for which the conductivity, σ_d , of the water phase is far greater than that of the oil, σ_c) and for modest frequencies (viz. lower than the optical frequency), the real part of ϵ^* may be reduced to:

$$\epsilon_1 = \epsilon_c \frac{1 + 2\phi}{1 - \phi} \quad (4.11)$$

In case of oil-in-water dispersions for which $\sigma_c \gg \sigma_d$ equation (4.7) reduces into:

$$\epsilon_1 = \frac{2(1 - \phi)(2 + \phi)\epsilon_c + 9\epsilon_d\phi}{(2 + \phi)^2} \quad (4.12)$$

Hanai [30, 31] developed a theory for concentrated disperse systems, based on Wagner's theory, with the below-presented general result:

$$\frac{\epsilon^* - \epsilon_d^*}{\epsilon_c^* - \epsilon_d^*} \left(\frac{\epsilon_c^*}{\epsilon^*} \right)^{\frac{1}{3}} = 1 - \phi \quad (4.13)$$

For a w/o type emulsion ($\sigma_d \gg \sigma_c$) the following expressions are obtained for ϵ_1 and ϵ_c , provided the particle conductivity σ_d is much smaller than the static conductivity of the dispersion σ_1 :

$$\epsilon_1 = \epsilon_c \frac{1}{(1 - \phi)^3} \quad (4.14)$$

$$\frac{\epsilon_d - \epsilon_h}{\epsilon_d - \epsilon_c} \left(\frac{\epsilon_c}{\epsilon_h} \right)^{\frac{1}{3}} = 1 - \phi \quad (4.15)$$

For an o/w type emulsion ($\sigma_c \gg \sigma_d$) provided $\sigma_1 \gg \sigma_d$ Hanai finds:

$$\frac{2\epsilon_1 - 3\epsilon_d}{2\epsilon_c - 3\epsilon_d} = (1 - \phi)^{\frac{1}{2}} \quad (4.16)$$

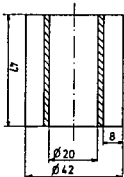
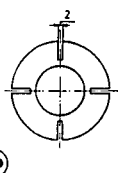
In a later study Hanai [32] measured the dielectric properties of emulsions of water prepared by him in a mixture of Nujol and carbon tetrachloride with emulsifiers. It was found that the limiting value of the dielectric constant at low frequencies, ϵ_1 , decreased on increasing shear rate towards the value predicted by equation (4.14), whereas ϵ_h appeared insensitive to shear rate. This phenomenon was explained by the contribution of conductivities to the dielectric constants of the dispersion system.

Kurkova [45] tested the agreement between the Wagner and Hanai theories in relation to petroleum emulsions of the w/o type over wide ranges of frequencies (10 kHz - 14 MHz) and of concentrations of water in petroleum (0-70%). Typical drop sizes were in the range of 10-20 μm . Contrary to Kurkova's conclusion, the experimental values of ϵ_1 fit Wagner's equation (4.11) better and for a wider range in concentration, compared to the Hanai equation (4.14).

4.4.1.2 Dual cell principle

In the presented study the dielectric constant of oil is measured comparatively with that of dry oil as a reference. The sensor basically consists of two identical capacitors, one being filled with dry oil and the other being flown with a water-in-oil dispersion, thereafter denominated reference cell and process cell. In the case when both empty cell capacitances, C_o , are identical the difference in capacitance ΔC is a unique function of water concentration and temperature difference only:

$$\begin{aligned} \Delta C &= C_{\text{process}} - C_{\text{reference}} \\ &= C_o (\epsilon_{\text{process}} - \epsilon_{\text{reference}}) \\ &= C_o \left\{ \left(\epsilon + \frac{d\epsilon}{d\phi} \phi + \frac{d\epsilon}{dT} T_{\text{process}} \right) - \left(\epsilon + \frac{d\epsilon}{dT} T_{\text{reference}} \right) \right\} \\ &= C_o \left(\frac{d\epsilon}{d\phi} \phi + \frac{d\epsilon}{dT} \Delta T \right) \end{aligned} \quad (4.17)$$



OPM: na inkten gat uitdraaien op Ø 28,5 mm

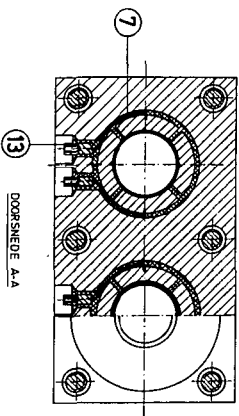


Fig.4.5.5. Water fraction sensor (first design)

[illegible]

It is quite evident why temperature plays an important role. Reason is that the mass related dielectric constant decreases at increasing temperature on decreasing density, which can be estimated with the Clausius-Mosotti equation [36]:

$$\Pi = \frac{N_o \alpha}{3\epsilon_o} = \frac{\epsilon-1}{\epsilon+2} \frac{M}{\rho} \quad (4.18)$$

in which Π stands for the molar refraction and M designates the molecular weight [kg], ρ the density in [kg/m³], N_o the number of molecules per mole, Avogadro's number and α the polarizability. Differentiating towards temperature T results in:

$$\frac{3 \frac{d\epsilon}{dT}}{(\epsilon+2)^2} = \frac{N_o \alpha}{3\epsilon_o M} \frac{d\rho}{dT} \quad (4.19)$$

Substitution of (4.18) into (4.19) yields:

$$\frac{d\epsilon}{dT} = \frac{(\epsilon-1)(\epsilon+2)}{3} \frac{1}{\rho} \frac{d\rho}{dT} \quad (4.20)$$

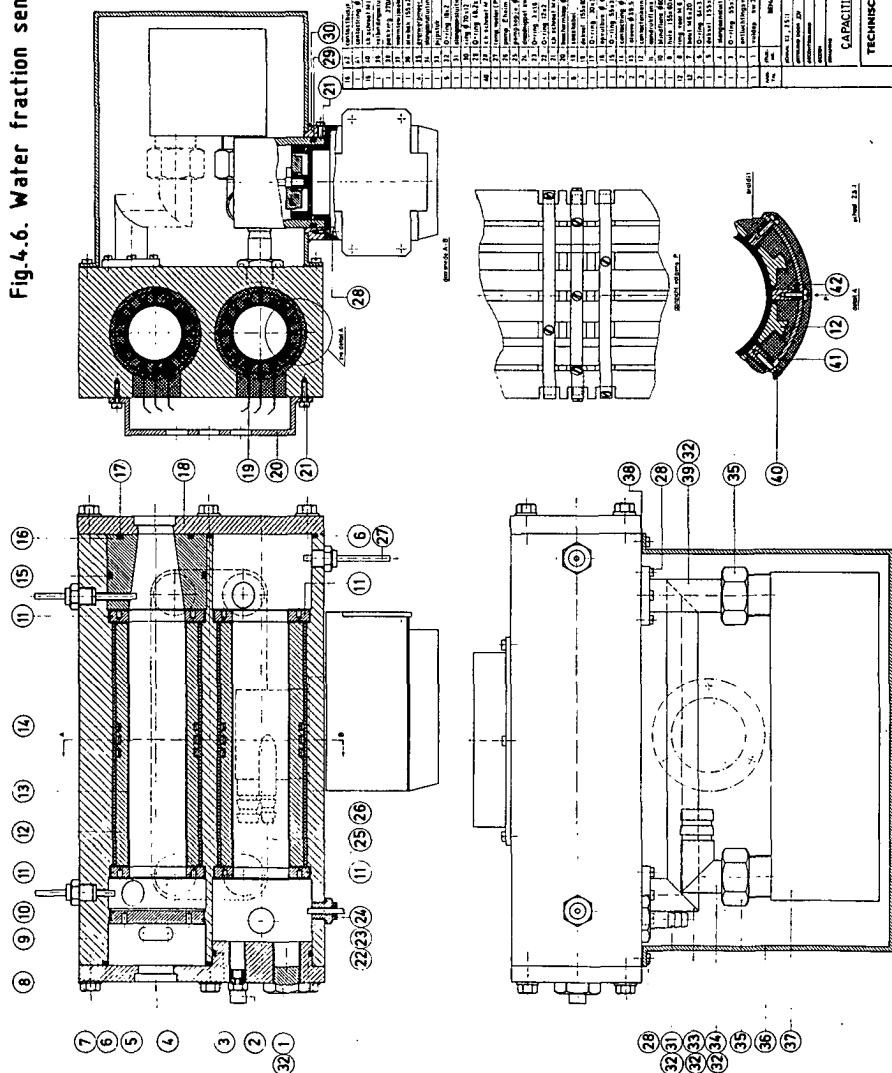
The value of $d\epsilon/d\phi$ depends on the applied frequency such as pointed out in paragraph 4.4.1.1. In the case of low frequencies and for a water-in-oil dispersion equations (4.11) or (4.14) can be used, which for small water content yields identical results:

$$\frac{d\epsilon}{d\phi} = 3 \epsilon_c \quad (4.21)$$

4.4.1.3 Sensor design

The sensors used within this study (figures 4.5 and 4.6) both possessed a cylindrical shape, the capacitor electrodes being part of the cylindrical wall, protected by a thin dielectric sleeve, resistant to the chemicals involved (polytetrafluorethylene). Heerens [34] derives the capacitance of cylindrical geometries which under certain conditions achieve an accuracy better than 1ppm. Applying the multi-terminal principle the parasitic capacitances can be eliminated, which demands presence of guard electrodes.

Fig 4.6. Water fraction sensor (second design)



№	Наименование	Материал	Значение	Примечание
1	Корпус	Латунь	100	
2	Пружина	Сталь	100	
3	Пружина	Сталь	100	
4	Пружина	Сталь	100	
5	Пружина	Сталь	100	
6	Пружина	Сталь	100	
7	Пружина	Сталь	100	
8	Пружина	Сталь	100	
9	Пружина	Сталь	100	
10	Пружина	Сталь	100	
11	Пружина	Сталь	100	
12	Пружина	Сталь	100	
13	Пружина	Сталь	100	
14	Пружина	Сталь	100	
15	Пружина	Сталь	100	
16	Пружина	Сталь	100	
17	Пружина	Сталь	100	
18	Пружина	Сталь	100	
19	Пружина	Сталь	100	
20	Пружина	Сталь	100	
21	Пружина	Сталь	100	
22	Пружина	Сталь	100	
23	Пружина	Сталь	100	
24	Пружина	Сталь	100	
25	Пружина	Сталь	100	
26	Пружина	Сталь	100	
27	Пружина	Сталь	100	
28	Пружина	Сталь	100	
29	Пружина	Сталь	100	
30	Пружина	Сталь	100	
31	Пружина	Сталь	100	
32	Пружина	Сталь	100	
33	Пружина	Сталь	100	
34	Пружина	Сталь	100	
35	Пружина	Сталь	100	
36	Пружина	Сталь	100	
37	Пружина	Сталь	100	
38	Пружина	Сталь	100	
39	Пружина	Сталь	100	
40	Пружина	Сталь	100	
41	Пружина	Сталь	100	
42	Пружина	Сталь	100	
43	Пружина	Сталь	100	

КАПИТАЛЬНАЯ ВОДЯНАЯ СЕНСОР
ТЕХНИЧЕСКАЯ ДОКУМЕНТАЦИЯ
ДЕЛЕТ

№ 111

АВЛ. ИРБИТСКО-УРАЛЬСКИЙ

ИРБИТ

ИРБИТ

ИРБИТ

ИРБИТ

ИРБИТ

ИРБИТ

ИРБИТ

ИРБИТ

ИРБИТ

ИРБИТ

ИРБИТ

ИРБИТ

ИРБИТ

ИРБИТ

ИРБИТ

ИРБИТ

ИРБИТ

ИРБИТ

ИРБИТ

ИРБИТ

ИРБИТ

ИРБИТ

ИРБИТ

ИРБИТ

ИРБИТ

ИРБИТ

ИРБИТ

ИРБИТ

ИРБИТ

ИРБИТ

ИРБИТ

ИРБИТ

ИРБИТ

ИРБИТ

ИРБИТ

ИРБИТ

ИРБИТ

ИРБИТ

ИРБИТ

ИРБИТ

ИРБИТ

ИРБИТ

ИРБИТ

ИРБИТ

In order to maintain a compact and sensitive sensor, a multiple electrode configuration was chosen for the second design shown in figure 4.6 (4 measuring electrodes, 4 detector electrodes and 8 guard electrodes).

The second design sensor is equipped with a plate heat exchanger and a small centrifugal pump which provides a thermal coupling in between both cells. Four PT100 probes connected to a strain gauge bridge amplifier provided a stable temperature difference signal.

4.4.2 Description of apparatuses

The electronic bridge circuit, being developed for this purpose, with which the difference in cell capacitances could be measured directly, is extensively described by Heerens [33]. Applied frequency has been 1430 Hz. The capacitance bridge was calibrated with the aid of precision capacitors, one fixed and the other adjustable (fixed: General Radio Co. type 1403-K, 1.00011 pF; adjustable: General Radio Co. type 1422-CD, 11-1.1 pF). Both capacitors were connected in the bridge and the output signal was measured. Excellent linearity was obtained up to 6.8 Volt, resulting in correlation coefficients of .99999 for all 9 amplification factors, which could be chosen in between 0.0288 V/pF and 11.44 V/pF (data see Den Ouden [51]).

Dispersions of water-in-oil were prepared in a 10 litre agitated vessel (inner diameter and height, $D = 0.236$ m). It consisted of two concentric cylinders mounted in between two flat stainless steel flanges. Both the inner cylinder as well as the four baffles ($0.1 D$) were made out of perspex, in order to prevent preferential wetting of the dispersed phase. The standard Rushton turbine agitator (diameter 82 mm) was operated at a height $h/D = 1/7$. Phase inversion was never observed. The vortex was suppressed by eliminating gas-liquid interface. The dispersed phase fraction could be adjusted with high precision injectors by changing plunger height. Temperature was controlled by an in-line plate heat exchanger in combination with a temperature controlled bath.

4.4.3 Experiments

In order to find out if the above-presented theory is applicable for both design purposes and interpretation of monitoring trials, experiments were performed. Empty cell capacitance was measured and compared with calculated values. The effects of temperature, air content, flow rate and water content were quantified. The results of this work are briefly described in the subsequent paragraph.

4.4.4 Results and observations

Cell capacitances

The measured capacitances of the process and reference cells of the first design sensor amount to 0.0716 and 0.0723 pF respectively, whereas the calculated value is 0.0745 pF.

For the second design these values amount to 3.82 and 3.78 pF respectively with 3.70 pF as the calculated value.

The small deviations can be explained by the fact that end effects are omitted within the capacitance formula, as well as by finite machining tolerances.

Temperature effect

The process cell of the sensor, built in a circulating oil loop together with the agitated vessel, together with the above-described adjustable precision capacitor were connected in the bridge circuit. From a balanced situation the output signal has been measured together with temperature. The experimental value appeared constant within the trajectory 25-90°C and the average was found to be $-(1.272 \pm 0.024) \cdot 10^{-3}$ (data see Den Ouden [51]).

Together with the $d\epsilon/d\phi$ which has the expected value of 6.75 (equation 4.21) we find for the temperature factor in terms of ppmv water 188 (ppmv/°C).

Substitution of the physical constants belonging to the turbine oil taken at 20°C for $\rho = 868$ (kg/m³), $d\rho/dT = -0.613$ (kg/m³ °C) and $\epsilon = 2.249$ (Appendix A) into equation (4.20) yields $d\epsilon/dT = -1.249 \cdot 10^{-3}$ (1/°C).

Effect of air

Experimental work performed by Van de Korput [42] and Warnar [67], who measured the volumetric effect of dispersed air in oil, resulted in $d\epsilon/d\phi_{\text{air}} = -1.20$.

The volumetric contribution of air can be estimated provided the air is homogeneously dispersed within the liquid by insertion of $\epsilon_c = 1$ into equation (4.12) or (4.16). Together with the above-mentioned value for the dielectric constant of oil, $d\epsilon/d\phi_{\text{air}} = -1.11$ is found in both cases, so that the volumetric contribution is approximately minus one sixth of the volumetric contribution of water.

Effect of flow rate

Adjusting the circulation pump, flow was varied from zero to maximum flow rate (40 l/h). Both for clean oil and for water dispersed in oil (0.1%) no effect on output signal could be observed.

Effect of volume fraction water

More workers on the water fraction sensor produced data whose mutual consistency was not perfect. Only the results therefore, measured by Den Ouden [51], who had the opportunity to check his results against Karl Fischer analysis, are presented. Water fractions were varied up to 20% by volume. Four series of measurements are presented at different temperatures of the dispersion (viz. 33.4, 41.3, 42.9 and 49.1°C). Figure 4.7 presents the results belonging to one of the series (42.9°C), together with the curves representing Wagner's equation (4.11) and Hanai's equation (4.14). A slightly better prediction is given by Wagner's equation for the higher concentrations.

4.4.5 Experience gained with the capacitance technique

Apart from various experiments performed with the sensors in development, the capacitance technique was tested in a realistic situation, monitoring an industrial separator. For this purpose a hermetic separator, Alfa-Laval

WSPX-207 was installed and connected to the centrifuge pilot plant. This separator appeared to be capable of discharging the separated oil, free from air by the application of a paring disc. Results of the test procedure indicated that fast responses were obtained, whereas outlet concentrations were never higher than 5000 ppm.

Comparison of the temperature compensated sensor with its predecessor, clearly indicated the importance of the thermal behaviour, when stable signals would be necessary.

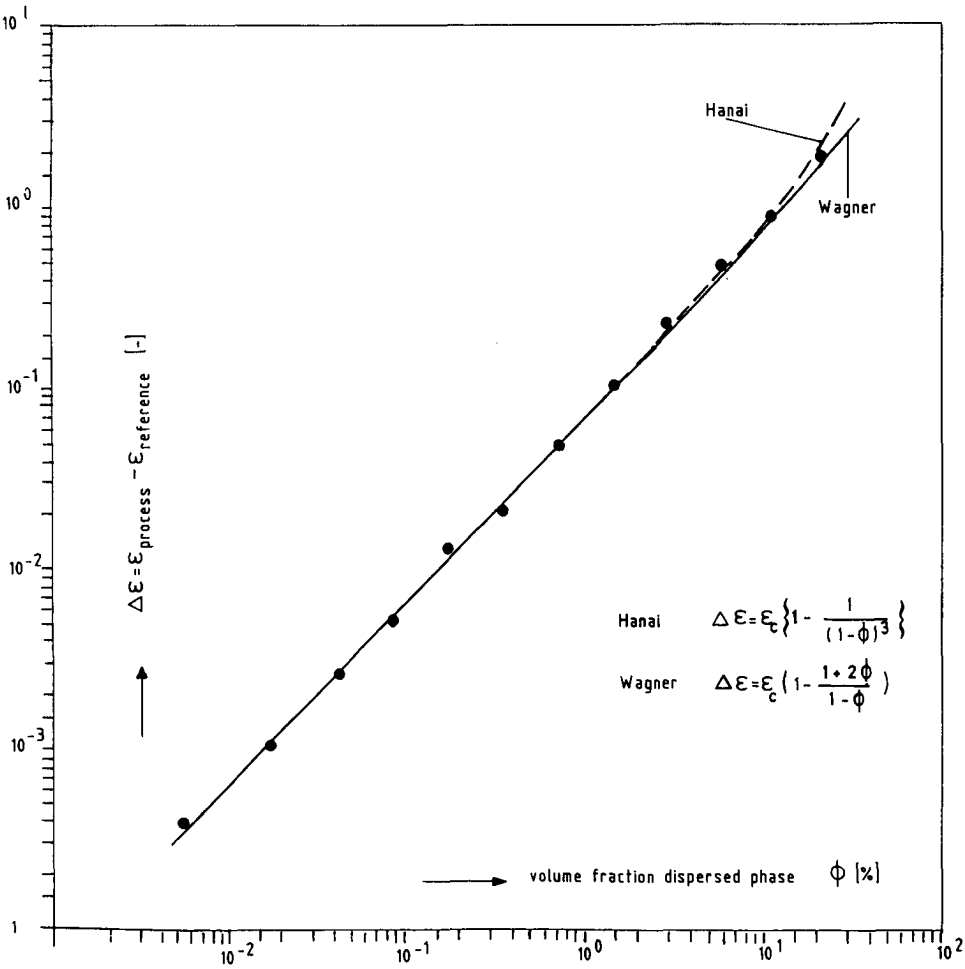


Fig.4.7 Dielectric behaviour of a water-in-oil dispersion.

4.5 Conclusions

- 1) The echo acoustic principle has proven to be quite feasible for determining the position of the oil-water interface in a centrifugal separator (paragraph 3.4.2.1).
- 2) With respect to the temperature effect and the dispersed phase fractions of both air and water, the theory fairly well predicts the measured values (paragraph 4.4.4).
- 3) Presence of air affects the dielectric properties substantially, hence limiting the measuring range of the capacitance technique (paragraph 4.4.4).
- 4) The output signal of the capacitance monitoring system depends upon temperature difference between the process and reference cell, which becomes more and more important when low water content is to be measured (paragraphs 4.4.1.2 and 4.4.4). Thermal coupling between both the process cell and the reference cell of the capacitive sensor is therefore the most obvious solution, which in practice provides satisfactory results.
- 5) The volumetric flow rate through the capacitive sensor does not affect the measurement significantly (paragraph 4.4.4).
- 6) The capacitance of cylindrical geometries is predicted well by the equations presented by Heerens [33] (paragraph 4.4.4).

REFERENCES
AND
APPENDICES

REFERENCES

- 1- Ambler, C.M., "The fundamentals of separation, including Sharples "Sigma value" for predicting equipment performance", Ind. Eng. Chem. 53 (1961), 6, p.430-433
- 2- Ambler, C.M., "The evaluation of centrifuge performance", Chem. Eng. Progr. 48 (1952), 3, p.150-158
- 3- Ambler, C.M., "The theory of scaling up laboratory data for the sedimentation type centrifuge", Journ. Biochem. Microbiol. Techn. Eng. I (1959), 2, p.185-205
- 4- Ambler, C.M., "The centrifuge, its process potentials", Chem. Eng. Progr. 46 (1950), 11, p.549-555
- 5- Bell, D.J., K.H. Brunner, "A method of evaluation of floc breakup in centrifuges", Filtr. & Separ. (1983), July/August, p.274-301
- 6- Bergmann, L., "Der Ultraschall, und seine Anwendung in Wissenschaft und Technik", Stuttgart, Hirzel, 6. Auflage (1954)
- 7- Brunner, A., "Über das Reinigen von Schweröl mittels der Zentrifuge", Dissertation ETH, Zurich (1956)
- 8- Brunner, A., "Versuchsarbeiten über das Zentrifugieren von Schweröl", M.T.Z. 14 (1953), 10, p.292-300
- 9- Brunner, K.H., "Theoretische und experimentelle Untersuchung der Feststoffabscheidung in Tellerseparatoren", Dissertation, Universität Erlangen-Nürnberg (1979)
- 10- Brunner, K.H., O. Molerus, "Theoretical and experimental investigation of separation efficiency of disc centrifuges", Ger. Chem. Eng. 2 (1979), p.228-233
- 11- Carlsson, C.G., Personal communication, Research & Development group staff Technical calculation and systems analysis, Alfa-Laval, Tumba, Sweden.
- 12- Carlsson, C.G., "Separation efficiency and the flow of two liquid layers in a disk stack centrifuge", Dissertation, Chalmers Tekniska Högskola, Göteborg, (1979)
- 13- Datar, R., "Centrifugal and membrane filtration methods in biochemical separation", Filtr. & Separ. (1984), Nov./Dec., p.402-406
- 14- Dioguardi, F., "Bepaling van de dichtheid van Shell Turbo Oil T32 in het temperatuurstraject van 30 tot 80 gr. C", Delft University of Technology, Laboratory for Process Equipment, Delft, Nov. 1984, students report
- 15- Donk, H.W.L. van der, J.P. van der Linden, "Data book dispersion experiments", Delft, University of Technology, Laboratory for Process Equipment, Delft, October 1986, internal report

- 16- Donk, H.W.L. van der, J.P. van der Linden, "Data book endoscope experiments", Delft University of Technology, Laboratory for Process Equipment, Delft, October 1986, internal report
- 17- Donk, H.W.L. van der, J.P. van der Linden, "Data book separation experiments", Delft University of Technology, Laboratory for Process Equipment, Delft, October 1986, internal report
- 18- Drost, J.C.G., "Metingen aan de kritische diepte van de olie uitlaat van een centrifugaalseparator", Delft, University of Technology, Laboratory for Process Equipment, July 1985, Students report
- 19- Edmonds, P.D., "Methods of experimental physics", Academic Press Inc. 19 (1981). Ultrasonics
- 20- Falbe, J., U. Hasserodt, "Katalysatoren, Tenside und Mineralöhladditive", Georg Thieme Verlag, Stuttgart, 1978
- 21- Faller, A.J., "An experimental study of the instability of the laminar Ekman boundary layer", Journ. Fluid Mech. 15 (1963), 4, p.560-576
- 22- Frese, F., "Versuche über den Abfluss des Wassers bei vollkommenen Ueberfällen", Zeitschrift des Vereines Deutscher Ing. 34 (1890), 49, p.1285-1293, ibid. 34 (1890), 50, p.1309-1315, ibid. 34 (1890), 51, p.1337-1342, ibid. 34 (1890), 52, p.1365-1376
- 23- Fumoto, H., R. Kiyose, "Interface characteristics in settler of centrifugal extractor", Journ. of Nucl. Sci. and Techn. 17 (1980), 9, p.694-699
- 24- Fumoto, H., R. Kiyose, "Drop formation characteristics in high speed agitation of centrifugal extractor", Journ. of Nucl. Sci. and Techn. 17 (1980), 8, p.627-633
- 25- Gol'din, E.M., "Hydrodynamic model for distribution holes in a disc-stack-separator", Izv. Vuzov. Pishshevaya Tekhnologiya (1966), 3
- 26- Gol'din, E.M., "Hydrodynamics of clarifying separators with guiding fins and peripheral feed", Theor. Found. Chem. Eng. 5 (1971), 2, p.246-252
- 27- Grace, H.P., "Dispersion phenomena in high viscosity immiscible fluid systems and application of static mixers as dispersion devices in such systems", Chem. Eng. 14 Comm. (1982), p.225-277
- 28- Greenspan, H.P., "The theory of rotating fluids", Cambridge, Univ. Press (1968)
- 29- Gusev, A., F.H. Bark, "Stability of rotation-modified plane poiseuille flow", Phys. Fluids 23 (1980) 11, p. 2171-2177
- 30- Hanai, T., "Theory of the dielectric dispersion due to the interfacial polarization and its application to emulsions", Kolloid Zeitschr. 171 (1960), Heft 1, p. 23-31

- 31- Hanai, T., "A remark on the "Theory of the dielectric dispersion due to the interfacial polarization"", Kolloid Zeitschr. 175 (1961) Heft 1, p. 61-62
- 32- Hanai, T., "Dielectric properties of emulsions: Part III; Dielectric behaviour of W/O emulsions", Kolloid Zeitschr. 177 (1961) Heft 1, p. 57-61
- 33- Heerens, W.Chr., "Basic principles in designing highly reliable multi terminal capacitors and the performance of some laboratory test models", Sensors and Actuators 2 (1982/83), p. 137-148
- 34- Heerens, W.Chr., F.W. Wedman, G. Keizer, "Theorie und Praxis Kapazitiver Stab- und Rohrsensoren mit mehreren Anschlusspunkten für Verwendung in der Chemischen Industrie Und Verwendeten Industrie Zweigen", Sensor'83, Conference Proc. (1983), May, chapter 9.2, part 5, p.27, Basel
- 35- Hinze, J.O., "Fundamentals of the hydrodynamic mechanism of splitting in dispersion processes" AICHE Journ. 1 (1955), 3, p.289-295
- 36- Hippel, A.R. von, "Dielectrics and waves", New York, John Wiley, (1954)
- 37- Hrubec, O., J.P. van der Linden, "Data book hydraulic capacity experiments, Delft University of Technology, Laboratory for Process Equipment, Delft, October 1986, internal report
- 38- Hrubec, O., J.P. van der Linden, "Data book interface experiments", Delft University of Technology, Laboratory for Process Equipment, Delft, October 1986, internal report
- 39- Jury, S.H., W.L. Locke, "Continuous centrifugation in a disk centrifuge", A.I.Ch.E. Journ. 3 (1957), December 4, p.480-483
- 40- Kolmogorov, A.N., "The break-up of droplets in a turbulent stream", Dokl. Akad. Nauk. 66 (1949), 5, 825-828
- 41- Konno, M., M. Aoki, S. Saito, "Scale effect on breakup process in liquid-liquid agitated tanks", Journ. Chem. Eng. Japan 16 (1983), 4, p.312-319
- 42- Korput, A.P. van de, "Capacitieve sensor voor het meten van water-in-olie dispersies", Delft, University of Technology, Laboratory for Process Equipment, June 1986, students report
- 43- Krombeen, M., J.J. de Wolff, "De weirhoogte van de olie-uitlaatstroom van de disc-stack-centrifuge", Delft, University of Technology, Laboratory for Process Equipment, May 1986, students report
- 44- Krombeen, M., "Herijking van turbine-flowmeters type HM 7/15 F en HM 11/25 F", Delft University of Technology, Laboratory for Process Equipment, January 1986, students report

- 45- Kurkova, Z.E. (et al.), "Correlation of experimental data on dielectric dispersion in an emulsion of the water-in-oil type with the theory of interface polarization", Zhurnal Prikl. Khim. 56 (1983) nr. 5, p. 1034-1037
- 46- Leibovich, S., S.K. Lele, "The influence of the horizontal component of earth's angular velocity on the instability of the Ekman layer", Journ. Fluid Mech. 150 (1985), p.41-87
- 47- Lenz, A.T., "Viscosity and surface tension effects on V-notch weir coefficients", Trans. Am. Soc. of Civil Engrs. 108 (1943), p.759-802
- 48- Lewis, C.P.G., personal communication, Residual fuel oils Quality & Handling, Koninklijke/Shell -Laboratorium, Amsterdam (Shell Research B.V.)
- 49- Maxwell, J.C., "Electricity and magnetism", Oxford, Clarendon Press, 1(1892), p. 452
- 50- Ouden, Th.A.F. den, "Pycnometrische dichtheidsbepaling van turbine olie", Delft University of Technology, Laboratory for Process Equipment, Delft, Aug. 1986, students report
- 51- Ouden, Th.A.F. den, J.P. van der Linden, "Data book capacitance technique" Delft, University of Technology, Laboratory for Process Equipment, Delft, October 1986, internal report
- 52- Paz Balmaseda, J. de, "Sensibility threshold of disc centrifuges in clarification processes, a theoreticall approach", 198th Event of the European Federation of Chemical Engineering. Antwerp. (1978), 6-7 June, p.149-157
- 53- Richardson, J.F., W.N. Zaki, "Sedimentation and fluidisation: part I", Trans. Inst. Chem. Engrs. 32 (1954), p.35-53
- 54- Rouse, H., "Discharge characteristics of the free overfall", Civil Eng. 6 (1936), 4, p.257-260
- 55- Schilp, R., "Fluiddynamik in Zentrifugalextraktoren", IDEA-Verlag, Dissertation Technische Universität München (1983)
- 56- Schmitz, F.J., "Die Verteilung der Milch im Tellerraum der Separatoren", Milchwissenschaft 12 (1950), dec, p.418-425
- 57- Schoder, E.W., L.K. Turner, "Precise weir measurements", Trans. Am. Soc. of Civil Engrs. 93 (1929), p.999-1110
- 58- Shinnar, R., "On the behaviour of liquid dispersions in mixing vessels", Journ. of Fluid Mech. 10 (1961), 2, p.259-275
- 59- Slocum, E.W., "Flow of viscous fluids over weirs", Can. Journ. of Chem. Engr. 42 (1964), p.196-200

- 60- Svensson, S., B. von Schultz, "Centrifugal separation and the cleaning of modern low grade heavy fuel oils", The Motor Ship (1980), July
- 61- Tatro, P.R., E.L. Mollo-Christensen, "Experiments on Ekman Layer instability", Journ. Fluid Mech. 28 (1967), part 3, p.531-543
- 62- Taylor, G.C., "The formation of emulsions in definable fields of flow", Proc. Roy. Soc. A146 (1934), p. 501-523
- 63- Thylefors, H.W., Alfa-Laval AB, Tumba, Sweden, "Vollmantelzentrifuge", Deutsches Patentamt, Patentschrift 1 632 266, 1973
- 64- Trowbridge, M.E.O'K., "Centrifugal purification of oils for marine service", Trans. Ins. Mar. Eng. 72 (1960), p.1-32
- 65- Vennard, J.K., "Elementary fluid mechanics", New York, John Wiley, 2nd ed. (1952)
- 66- Wagner, K.W., "Erklärung der dielektrischen Nachwirkungsvorgänge auf Grund Maxwell'scher Vorstellungen", Arch. Elektrotechn. 2(1914) 9. Heft, p. 371-387
- 67- Warnar, J.W., "Capacitieve waterfractie bepaling bij centrifugaal separatie", Delft, University of Technology, Laboratory for Process Equipment, May 1985, students report
- 68- Weast, R.C., "Handbook of Chemistry and Physics", Boca Raton, CRC Press Inc., 61th ed. (1980-1981)
- 69- Willard, G.W., "Temperature coefficient of ultrasonic velocity in solutions", Journ. Ac. Soc. Am. 19 (1947), 1, p.235-241
- 70- Willus, C.A., B. Fitch, "Flow patterns in a disc centrifuge", 74th National Meeting AIChE, New Orleans, March 15, 1973, Symposium on centrifugation, hydrocycloning
- 71- Wilson, W.D., "Speed of sound in sea water as a function of temperature, pressure and salinity", Journ. Ac. Soc. Am. 32 (1960), 6, p.641-644

Appendix A

PHYSICAL AND CHEMICAL PROPERTIES AND MEASUREMENT PROCEDURES

Kinematic viscosity

Viscosity of the turbine oil is measured with Ubbelohde viscosity metres. In all cases measuring time exceeded 200 seconds resulting in a relative error of less than 0.5%. This has been accomplished by using four different Ubbelohde metres as specified below. Temperature was held constant by placing the metres in a thermostated water bath. Temperature was measured with a calibrated mercury thermometer and time with a digital chronometer. Table A1 contains the measured data.

Table A1 viscosity data

T_o [°C.]	$\bar{\tau}$ [s]	multiplication constant [mm ² /s ²]	v_o [mm ² /s]
20.0	323.5	0.2965	95.92
20.2	318.1	0.2965	94.32
25.0	240.9	0.2965	71.43
30.1	456.0	0.1199	54.67
30.5	444.3	0.1199	53.27
35.3	353.2	0.1199	42.35
39.8	286.4	0.1199	34.34
45.3	227.4	0.1199	27.27
49.8	388.1	0.0554	21.50
55.6	331.8	0.0554	18.38
59.5	282.0	0.0554	15.62
64.9	236.9	0.0554	13.12
69.8	204.4	0.0554	11.34
79.9	272.5	0.03155	8.60
89.9	214.3	0.03155	6.76

Table A2 Ubbelohde constants

Type	No	multiplication constant [mm ² /s ²]
ASTM5	64303	0.2965
ASTM4	63	0.1199
ASTM3	64557	0.0554
ASTM4	64587	0.03155

With a least square programme the constants of a fifth order polynom were calculated with an average error of 0.3%:

$$v_o = a + b T_o + c T_o^2 + d T_o^3 + e T_o^4 + f T_o^5 \text{ (mm}^2/\text{s)} \quad (\text{A1})$$

with $a = 315.14$, $b = -18.5178$, $c = 0.503109$, $d = -7.34779 \cdot 10^{-3}$

$$e = 55.4766 \cdot 10^{-6} \text{ and } f = -169.404 \cdot 10^{-9}$$

Density

For the density of water a correlation presented by Weast [68] is applied:

$$\begin{aligned} \rho_w = & (999.83952 + 16.945176 \cdot T_w - 7.9870401 \cdot 10^{-3} T_w^2 + \\ & - 46.170461 \cdot 10^{-6} T_w^3 + 105.56302 \cdot 10^{-9} T_w^4 - 280.54253 \cdot 10^{-12} T_w^5) / \\ & (1 + 16.879850 \cdot 10^{-3} T_w) \text{ (kg/m}^3\text{)} \end{aligned} \quad (\text{A2})$$

The density of oil is measured with pycnometers [14]. The volumes of two pycnometers are determined as function of temperature using a precision balance and deionised water as a calibration liquid with a density according to equation A2. Regression analysis on 20 measurements in a temperature range from 30 to 80°C produces the following result for the oil density:

$$\rho_o = 880.715 - 0.6125 T_o \text{ (kg/m}^3\text{)} \quad (\text{A3})$$

The average fit error was 0.47 kg/m³ with a standard deviation of 0.58 kg/m³. Directly after completion of the interface measuring programme Den Ouden [50] measured oil density again with identical measuring procedure, in the range from 20 to 90°C, with the following result obtained from 14 experimental data points:

$$\rho_o = 881.207 - 0.6130 T_o \quad (\text{kg/m}^3) \quad (\text{A4})$$

Average fit error was 0.16 kg/m³ with a standard deviation of 0.19 kg/m³. With a probability of at least .995 it can be stated that the increase of density is significant (t-test). Measuring accuracy for the above-mentioned density data is better than 0.1%. In our opinion this density increase is caused by flashing the lighter components.

Dielectric constant

The dielectric constant was measured, comparing the capacitances of both an empty cell and a cell filled with oil, applying the multiterminal principle, hence eliminating parasitic effects. With the application of precision capacitors and an electronic capacitance bridge, Den Ouden [51] finds:

$$\epsilon_o = 2.274 - 1.272 \cdot 10^{-3} T_o \quad (\text{A5})$$

with T_o temperature in °C.

Flow

The oil flow is measured with two turbine metres both calibrated in the temperature range from 21 to 92°C. [44]. For the small turbine metre (Endress & Hauser, type HM 7/15 F), which is used for flows up to about 1400 l/h, a correlation was produced on a dataset consisting of 49 experiments, with average fit error of 0.48% and a standard deviation of the fit error of 0.76%:

$$Q_o = 67.82 \cdot 10^{-6} U_{\text{out}} + 0.2466 v_o + 1.552 \cdot 10^{-6} \quad (\text{m}^3/\text{s}) \quad (\text{A6})$$

For the big turbine metre (Endress & Hauser, type HM 11/25), which is used for flows in between 1250 and 2600 l/h, a correlation was produced on a dataset consisting of 42 experiments, with average fit error of 0.28% and a standard deviation of the fit error of 0.37%:

$$Q_o = 127.6 \cdot 10^{-6} U_{out} + 0.3125 v_o + 1.952 \cdot 10^{-6} \quad (\text{m}^3/\text{s}) \quad (\text{A7})$$

The output signal U_{out} was read off from a digital voltmeter Solartron (type LM 1420.2).

Rotation speed

Rotation speed of the separator is measured with a Rheintacho tachometer type DT 96-4 which, during the period of 5 seconds, counts electronic pulses produced by an inductive probe, Rheintacho MD9 14. The latter is mounted on the separator frame watching a toothed wheel connected to the horizontal axis of the separator.

Chemical properties turbine oil, (Shell Turbo T32), Lewis [48]

paraffinic carbon 65% (w)
aromatic carbon 7% (w)
naphthenic carbon 28% (w)
average carbon number about 28
sulphur 0.7% (w)
boiling range about 380-490°C
additives: anti-oxidant
 rust-preventer
 metal deactivator

The chemical composition of the additives is reported by Falbe & Hasserodt [20].

Appendix B

HYDRAULIC GRADIENT MODEL FOR THE CYLINDRICAL PART OF THE TOP DISC

Assumptions:

1. No effects induced by the contraction near the edge.
2. Solid body rotation and hence two dimensional approach.
3. Symmetrical case.
4. Fully developed flow.
5. Small liquid gradient and hence radial velocities small compared to the axial velocities.

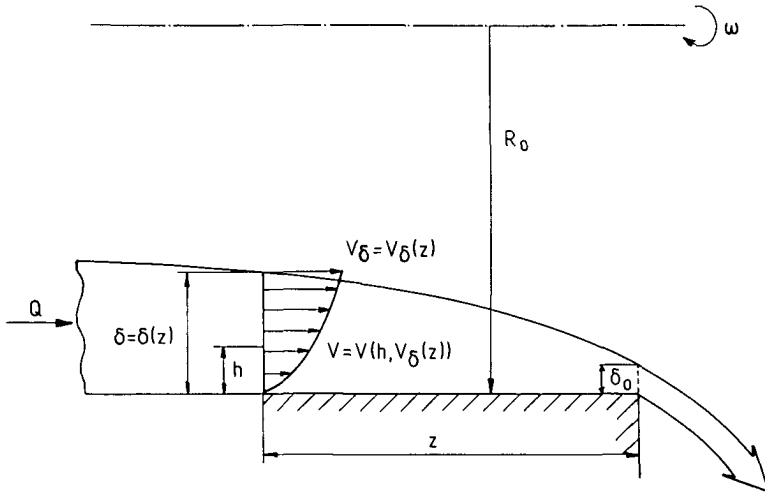


Fig.B1 Simplified situation.

In figure B1 the situation is shown. A parabolic velocity profile is assumed:

$$v = v_{\delta} \left(2 \frac{h}{\delta} - \frac{h^2}{\delta^2} \right) \quad (B1)$$

Continuity:

$$Q = b \int_0^{\delta} v \, dh = \frac{2}{3} b \delta v_{\delta} \quad (B2)$$

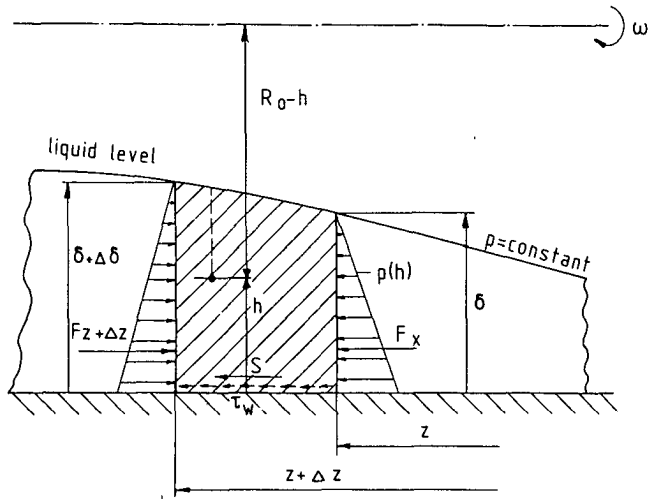


Fig.B2 Forces acting upon a volume element.

Upstream from the overfall the gradient will be calculated with the momentum equation, analogue to the derivation of the Chezy equation, but altered at some points. Therefore equations must be found for the different forces which act upon the volume element shown in figure B2. The momentum equation on this volume element is

$$F_{z+\Delta z} - F_z - S = -b \int_0^{\delta} \rho v_z^2 dh + b \int_0^{\delta+\Delta\delta} \rho v_{z+\Delta z}^2 dh \quad (B3)$$

The first two terms are induced by the hydrostatic pressure, the third term is the wall shear and the right hand side is the increase in momentum.

Hydrostatic pressure under the assumption of solid body rotation:

$$p(h) = \frac{1}{2} \rho \omega^2 \left[(R_0 - h)^2 - (R_0 - \delta)^2 \right] = \rho \omega^2 R_0 (\delta - h) \left(1 - \frac{h + \delta}{2 R_0} \right) \quad (B4)$$

According to this definition the pressure is zero at the liquid level.

The resulting force is obtained by integration of equation (B4):

$$F = b \int_0^{\delta} p(h) dh = \frac{1}{2} \rho \omega^2 R_0 b \delta^2 \left[1 - \frac{2}{3} \frac{\delta}{R_0} \right] \quad (B5)$$

As a result of the assumptions listed above, the wall shear can be estimated with:

$$\tau_w = \eta \left. \frac{dv}{dh} \right|_{h=0} = \frac{2 \eta v \delta}{\delta} \quad (B6)$$

The shear force S is calculated multiplying equation (B6) with the ground surface of the volume element $b \Delta z$ and elimination of v_δ with equation (B2):

$$S = \frac{3 \eta Q}{\delta^2} \Delta z \quad (B7)$$

The right-hand side of equation (B3) can be obtained by substituting equation (B1) and eliminating v_δ with equation (B2):

$$b \int_0^\delta \rho v \delta dh = \frac{\pi}{8} \rho \frac{Q^2}{b \delta} \quad (B8)$$

Substitution of equations (B5), (B7) and (B8) into equation (B3) yields:

$$\frac{1}{2} \rho \omega^2 R_o b \left\{ (\delta + \Delta \delta)^2 \left(1 - \frac{2(\delta + \Delta \delta)}{3 R_o} \right) - \delta^2 \left(1 - \frac{2 \delta}{3 R_o} \right) \right\} +$$

$$- \frac{3 \eta Q}{\delta^2} \Delta z + \frac{\pi}{8} \rho \frac{Q^2}{b} \left(\frac{1}{\delta} - \frac{1}{\delta + \Delta \delta} \right) = 0 \quad (B9)$$

After writing differential d instead of Δ and after some rearrangement the above obtains the differential equation for the fluid depth δ :

$$\frac{d\delta}{dz} = \frac{3 \eta Q}{\omega^2 R_o b \delta^3 \left(1 - \frac{\delta}{R_o} \right) + \frac{\pi}{8} \frac{Q^2}{b}} \quad (B10)$$

with boundary condition:

$$z = z_o \quad \delta = \delta_o \quad (B11)$$

As an illustration the quantitative results of the model are presented in a plot of fluid depth vs flow/angular velocity. For the boundary condition δ_o the critical depth d_c (equation 3.34) was chosen at $z_o = 0$ substituting $Q/3\omega$ for q and $\omega^2 R_o$ for g . Figure B3 shows four plots belonging to the 4 flow types presented in figure 3.13 paragraph 3.3.6 in which v/ω [m^2/rad] was chosen as parameter.

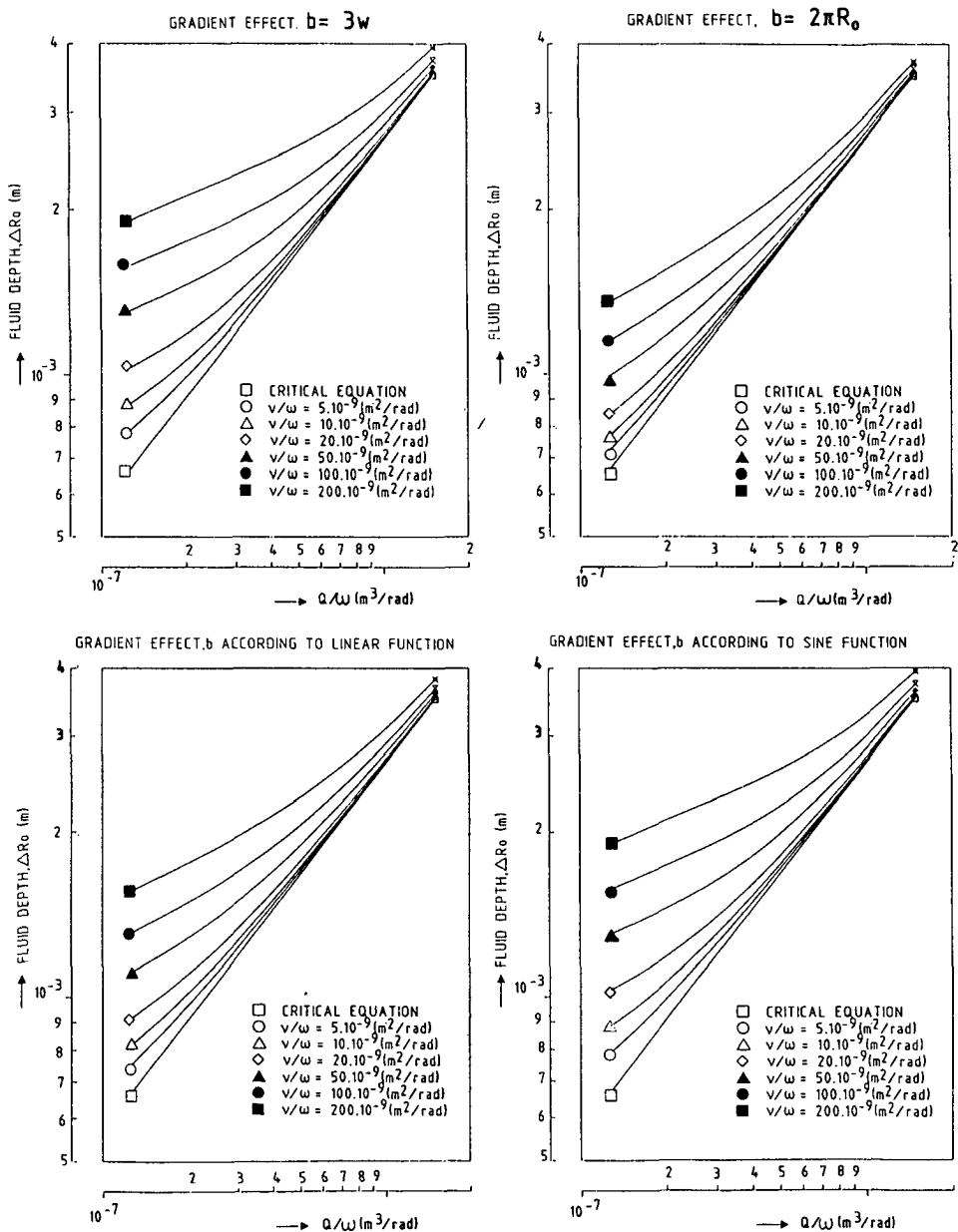


Fig.B3

Appendix C

INTERFACE CALIBRATION FORMULA

The reflection of the trigger pulse has covered the distance L_t (see figure C1):

$$L_t = 2 d_1 \quad (C1)$$

For the interface the evaluation is somewhat more complicated, because of the actual length of the trigger spot (in millimetres):

$$\begin{aligned} L_i &= 2 (d_1 + d_2 - 10.5 + \frac{1}{2} D_w - R_i - D_w + L_e + 10.5) \\ &= 2 (d_1 + d_2 - \frac{1}{2} D_w + L_e - R_i) \end{aligned} \quad (C2)$$

Once the trigger pulse is used as a reference, it is important to know the difference of the two length intervals L_t and L_i :

$$\Delta L = L_i - L_t = 2 (d_2 - \frac{1}{2} D_w + L_e - R_i) \quad (C3)$$

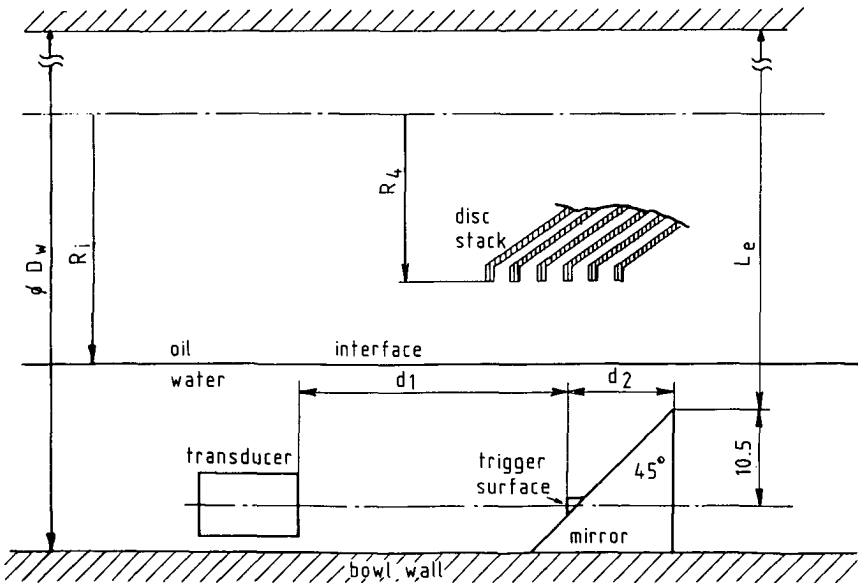


Fig.C1 Schematic drawing of the ultrasonic transducer.

By definition:

$$S = 0 \rightarrow \Delta L = 0 \quad (C4)$$

$$S = 100 \rightarrow R_i = R_4 = 80.5 \quad (C5)$$

Combination of equations (C3) and (C4) yields

$$R_i (S = 0) = d_2 - \frac{1}{2} D_w + L_e \quad (C6)$$

Careful measurements with a sliding gauge gave the following data on the geometry of the two transducer holders, presented in table C1.

Table C1 Geometry of the caulk and channel transducers

transducer	d_1 [mm]	d_2 [mm]	L_e [mm]
caulk	33.68	11.1	196.35
channel	33.50	11.3	196.15

Substituting the internal diameter of the separator bowl $D_w = 214.07$ mm and geometrical data found in table C1 the interface radius is expressed as function of the scalar value S. Quite by accident the same values are found within the accuracy of the measurements of the geometry factors:

$$R_{i, \text{caulk}} (S=0) = 11.1 - \frac{1}{2} \cdot 214.07 + 196.35 = 100.42 \text{ (mm)} \quad (C7)$$

$$R_{i, \text{channel}} (S=0) = 11.3 - \frac{1}{2} \cdot 214.07 + 196.15 = 100.42 \text{ (mm)} \quad (C8)$$

The final equation is thus:

$$R_i \text{ (mm)} = 100.42 - \frac{100.42 - 80.5}{100} \cdot S \quad (C9)$$

Appendix D

INTERFACE EXPERIMENTAL CONDITIONS

exp. code	exp. nr.	n [rpm]	\bar{T}_O [°C]	caulk type *)	feed type **)	h [mm]	D _{gr} [mm]	R _O [mm]
JP1	1- 43	2250	22	1c	ch	0.6	73.5	30.5
JP2	44- 55	2250	"	"	"	0.4	"	"
JP3	56- 93	2500	"	"	"	"	"	"
JP4	94- 123	"	"	"	"	0.6	"	"
JP5	124- 129	"	"	"	"	1.0	"	"
JP6	130- 182	"	"	"	"	"	78.0	"
JP7	183- 212	"	"	"	"	0.8	"	"
JP8	213- 257	"	"	"	"	0.4	"	"
JP9	258- 276	"	"	"	"	"	73.5	"
JP10	277- 299	"	"	"	pe	"	78.0	"
JP11	300- 319	"	"	"	"	"	73.5	"
JP12	320- 352	"	"	"	"	0.6	78	"
JP13	353- 369	"	"	"	"	1.0	"	"
JP14	370- 386	"	"	"	"	"	"	"
JP15	387- 408	"	"	"	"	"	73.5	"
JP16	409- 461	"	"	"	"	0.8	78.0	"
JP17	462- 486	3500	"	"	ch	0.4	"	"
JP18	487- 514	"	"	"	"	"	73.5	"
JP19	515- 565	"	"	"	"	0.6	78.0	"
JP20	566- 606	"	"	"	"	1.0	"	"
JP21	607- 654	"	50	"	"	0.4	79.5	"
JP22	-	-	-	-	-	-	-	-
JP23	655- 723	3500	50	"	ch	0.6	79.5	30.5
JP24	724- 773	"	"	"	"	1.0	"	"
JP25	774- 817	"	"	"	pe	0.4	"	"
JP26	818- 859	"	"	"	"	0.6	"	"
JP27	860- 900	"	"	"	"	1.0	"	"
JP28	901- 931	"	90	"	ch	0.4	"	"
JP29	932- 953	"	"	"	"	0.6	"	"
JP30	954- 987	"	"	"	"	1.0	"	"
JP31	988-1015	"	85	"	pe	0.4	"	"
JP32	1016-1041	"	90	"	"	0.6	"	"
JP33	1042-1071	"	"	"	"	1.0	"	"
JP34	1072-1138	4500	50	"	ch	0.4	83.0	"
JP35	1139-1208	"	"	"	"	0.6	"	"
JP36	1209-1278	"	"	"	"	1.0	"	"
JP37	1279-1341	"	"	"	pe	0.4	"	"

exp.	exp.	n	\bar{T}_O	caulk	feed	h	D _{gr}	R _O
code	nr.	[rpm]	[°C]	type (*)	type (**)	[mm]	[mm]	[mm]
AL38	1342-1377	2500	50	-	-	dummy	78.0	30.5
AL39	1378-1425	5500	"	-	-	"	"	"
AL40	1426-1465	"	"	lc	ch	0.4	83.0	"
AL41	1466-1483	"	"	"	pe	"	"	"
AL42	1484-1526	"	"	pc	ch	"	"	"
AL43	1527-1543	"	"	"	pe	"	"	"
AL44	1544-1587	"	"	lc	ch	1.0	"	"
AL45	1588-1612	"	"	"	pe	"	"	"
AL46	1613-1635	"	"	pc	ch	"	"	"
AL47	1636-1656	"	"	"	pe	"	"	"
AL48	1657-1675	"	"	"	"	"	79.5	26.0
AL49	1676-1712	"	"	"	ch	"	"	"
AL50	1713-1740	"	"	lc	ch	"	"	"
AL51	1741-1766	"	"	"	pe	"	"	"
AL52	1767-1793	"	"	lc	ch	0.4	78.0	"
AL53	1794-1818	"	"	"	pe	"	"	"
AL54	1819-1852	"	"	pc	ch	"	"	"
AL55	1853-1878	"	"	"	pe	"	"	"
AL56	1879-1907	6500	"	-	-	dummy	79.5	30.5
AL57	1908-1932	"	"	-	-	"	"	26.0
AL58	1933-1971	"	"	lc	ch	1.0	83.0	30.5
AL59	1972-2003	"	"	"	pe	"	"	"
AL60	2004-2033	"	"	pc	ch	"	"	"
AL61	2034-2071	"	"	"	pe	"	"	"
AL62	2072-2115	"	"	lc	ch	0.4	"	"
AL63	2116-2154	"	"	"	pe	"	"	"
AL64	2155-2192	"	"	pc	ch	"	"	"
AL65	2193-2231	"	"	"	pe	"	"	"
AL66	2232-2256	"	"	"	pe	"	79.5	26.0
AL67	2257-2286	"	"	"	ch	"	"	"
AL68	2287-2313	"	"	lc	ch	"	78.0	"
AL69	2314-2340	"	"	"	pe	"	"	"
AL70	2341-2373	"	"	"	ch	1.0	79.5	"
AL71	2432-2461	"	"	"	pe	"	"	"
AL72	2400-2431	"	"	pc	ch	"	"	"
AL73	2374-2399	"	"	"	pe	"	"	"
AL74	2462-2499	7300	"	-	-	dummy	"	30.5
AL75	2500-2530	5500	"	-	-	"	78	26.0
AL76	2531-2560	7300	"	-	-	"	"	"
AL77	2561-2592	5500	"	-	-	"	"	30.5
AL78	2593-2617	3500	"	pc	ch	1.0	79.5	"
AL79	2618-2637	"	"	"	"	"	"	26.0
AL80	2638-2662	"	"	"	pe	"	"	30.5

exp.	exp.	n	\bar{T}_O	caulk	feed	h	D _{gr}	R _O
code	nr.	[rpm]	[°C]	type (*)	type (**)	[mm]	[mm]	[mm]
AL81	2663-2688	3500	50	pc	pe	1.0	79.5	26.0
AL82	2689-2718	"	"	"	ch	0.4	"	30.5
AL83	2719-2753	"	"	"	"	"	"	26
AL84	2754-2778	"	"	"	pe	"	"	30.5
AL85	2779-2805	"	"	"	"	"	"	26
AL86	2806-2836	4500	"	"	"	"	83	30.5
AL87	2837-2854	"	"	"	"	"	79.5	26.0
AL88	2855-2886	"	"	"	ch	"	83	30.5
AL89	2887-2907	"	"	"	"	"	79.5	26.0
AL90	2908-2947	"	"	"	"	1.0	83	30.5
AL91	2948-2981	"	"	"	"	"	79.5	26.0
AL92	2982-3011	"	"	"	pe	"	83	30.5
AL93	3012-3037	"	"	"	"	"	79.5	26.0
AL94		2500	"	pc	pe	1.0	83	30.5
AL95		7300	"	lc	ch	0.4	79.5	26
AL99	3038-3073	"	"	pc	ch	0.4	83	30.5
AL100	3074-3101	"	"	"	"	"	79.5	26.0
AL101	3102-3133	"	"	"	pe	"	83	30.5
AL102	3134-3160	"	"	"	"	"	79.5	26.0
AL103	3161-3191	"	"	lc	"	1.0	83	30.5
AL104	3192-3223	"	"	"	"	"	79.5	26.0
AL105	3224-3257	"	"	"	ch	"	83	30.5
AL106	3258-3291	"	"	"	"	"	79.5	26.0
AL107	3292-3325	"	"	pc	"	"	83	30.5
AL108	3326-3351	"	"	"	"	"	79.5	26.0
AL109	3352-3376	"	"	"	pe	"	83	30.5
AL110	3377-3399	"	"	"	"	"	79.5	26.0
AL111	3400-3423	"	"	lc	"	0.4	83	30.5
AL112	3424-3460	"	"	"	"	"	79.5	26.0
AL113	3461-3494	"	"	"	ch	"	83	30.5
AL114	3495-3526	"	"	"	"	"	79.5	26.0

Notes: *) lc = long caulks
pc = point caulks
**) pe = peripheral
ch = channel

Dual measurements (caulk and channel position) were available for the experiments 1-184 and 213-514 and single measurements for the experiments 185-212 (channel position) and 1342-3526 (caulk position). Experimental data belonging to the interface experiments are reported by Hrubec [38].

Appendix E

HYDRAULIC CAPACITY EXPERIMENTAL CONDITIONS

exp. code	exp. nr.	h (mm)	feed type *)	R _o (mm)	T _o (°C)	caulk type **)	
HC 1	1	50	0.4	ch	26	50	1
HC 2	51- 80	0.4	pe	26	50	50	1
HC 3	81- 101	0.6	pe	26	50	50	1
HC 4	102- 121	0.6	ch	26	50	50	1
HC 5	122- 146	1.0	pe	26	50	50	1
HC 6	147- 170	1.0	ch	26	50	50	1
HC 7	171- 194	0.4	pe	26	50	50	p
HC 8	195- 220	0.4	ch	26	50	50	p
HC 9	221- 246	0.6	ch	26	50	50	p
HC10	247- 272	0.6	pe	26	50	50	p
HC11	273- 298	1.0	pe	26	50	50	p
HC12	299- 324	1.0	ch	26	50	50	p
HC13	325- 342	0.4	ch	30.5	20	20	1
HC14	343- 365	0.4	pe	30.5	20	20	1
HC15	366- 377	1.0	ch	30.5	20	20	1
HC16	378- 391	1.0	pe	30.5	20	20	1
HC17	392- 409	0.4	ch	30.5	25	25	1
HC18	410- 431	0.4	pe	30.5	25	25	1
HC19	432- 445	1.0	ch	30.5	25	25	1
HC20	446- 460	1.0	pe	30.5	25	25	1
HC21	461- 475	0.4	ch	30.5	32	32	1
HC22	476- 494	0.4	pe	30.5	32	32	1
HC23	495- 508	1.0	ch	30.5	32	32	1
HC24	509- 522	1.0	pe	30.5	50	50	1
HC25	523- 537	0.4	ch	30.5	50	50	1
HC26	538- 555	0.4	pe	30.5	50	50	1
HC27	556- 570	1.0	ch	30.5	50	50	1
HC28	571- 588	1.0	pe	30.5	50	50	1
HC29	589- 604	0.4	ch	30.5	50	50	p
HC30	605- 622	0.4	pe	30.5	50	50	p
HC31	623- 638	1.0	ch	30.5	50	50	p
HC32	639- 658	1.0	pe	30.5	50	50	p
HC33	659- 671	0.4	ch	30.5	90	90	1
HC34	672- 690	0.4	pe	30.5	90	90	1
HC35	691- 705	1.0	ch	30.5	90	90	1
HC36	706- 724	1.0	pe	30.5	90	90	1

Notes: *) ch = channel feed; pe = peripheral feed
 **) 1 = long caulks ; p = point caulks

Experimental data belonging to the hydraulic capacity experiments are reported by Hrubec [37].

Appendix F

SHORT CUT MODEL (CHANNEL FEED)

Assumptions:

1. No pressure drop within the distribution channel, hence uniform liquid loading of the disc spaces.
2. No weir effects involved at the entrance of the distribution channel;
 $R_{ch} = \text{constant}$.

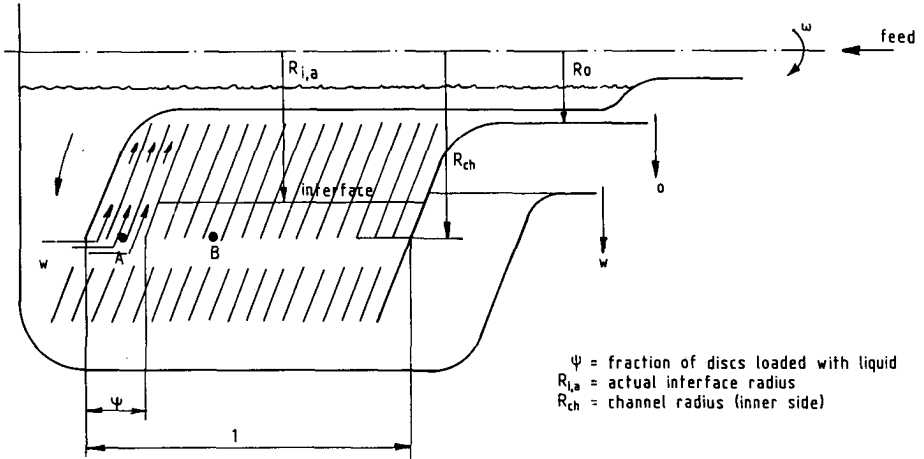


Fig.F1 Short cut.

In the situation drawn in figure F1 the hydrostatic pressure at locations A and B amounts to

$$P_A = \frac{1}{2} \rho_o \omega^2 (R_{ch}^2 - R_o^2) + \frac{1}{\psi} \Delta p_{disc,a} + \Delta p_{weir} + \Delta p_{grad} \quad (F1)$$

$$P_B = \frac{1}{2} \rho_w \omega^2 (R_{ch}^2 - R_{i,a}^2) + \frac{1}{2} \rho_o \omega^2 (R_{i,a}^2 - R_o^2) + \Delta p_{weir} + \Delta p_{grad} \quad (F2)$$

In a normal situation short cutting is absent while the interface position is outside the disc-stack. In the above-described situation, maintaining identical operation parameters (Q , ω , $D_{gr}...$) the hypothetic pressure $P_{B,h}$ is calculated, assuming the short cutting to be absent:

$$P_{B,h} = \frac{1}{2} \rho_w \omega^2 (R_{ch}^2 - R_{i,h}^2) + \Delta p_{disc,h} + \frac{1}{2} \rho_o \omega^2 (R_{i,h}^2 - R_o^2) + \Delta p_{weir} + \Delta p_{grad} \quad (F3)$$

Equating P_B and $P_{B,h}$ an equation can be derived which expresses the actual interface position as function of the hypothetic interface, of which the latter can be calculated with a model or extrapolated from measurements outside the disc-stack:

$$R_{i,a}^2 = R_{i,h}^2 - \frac{2 \Delta p_{disc,h}}{(\rho_w - \rho_o) \omega^2} \quad (F4)$$

Setting:

$$\frac{\Delta p_{disc,a}}{\Delta p_{disc,h}} = \alpha \quad (F5)$$

the fraction of discs being loaded with liquid ψ can be calculated equating (F1) and (F3) and inserting equation (F5):

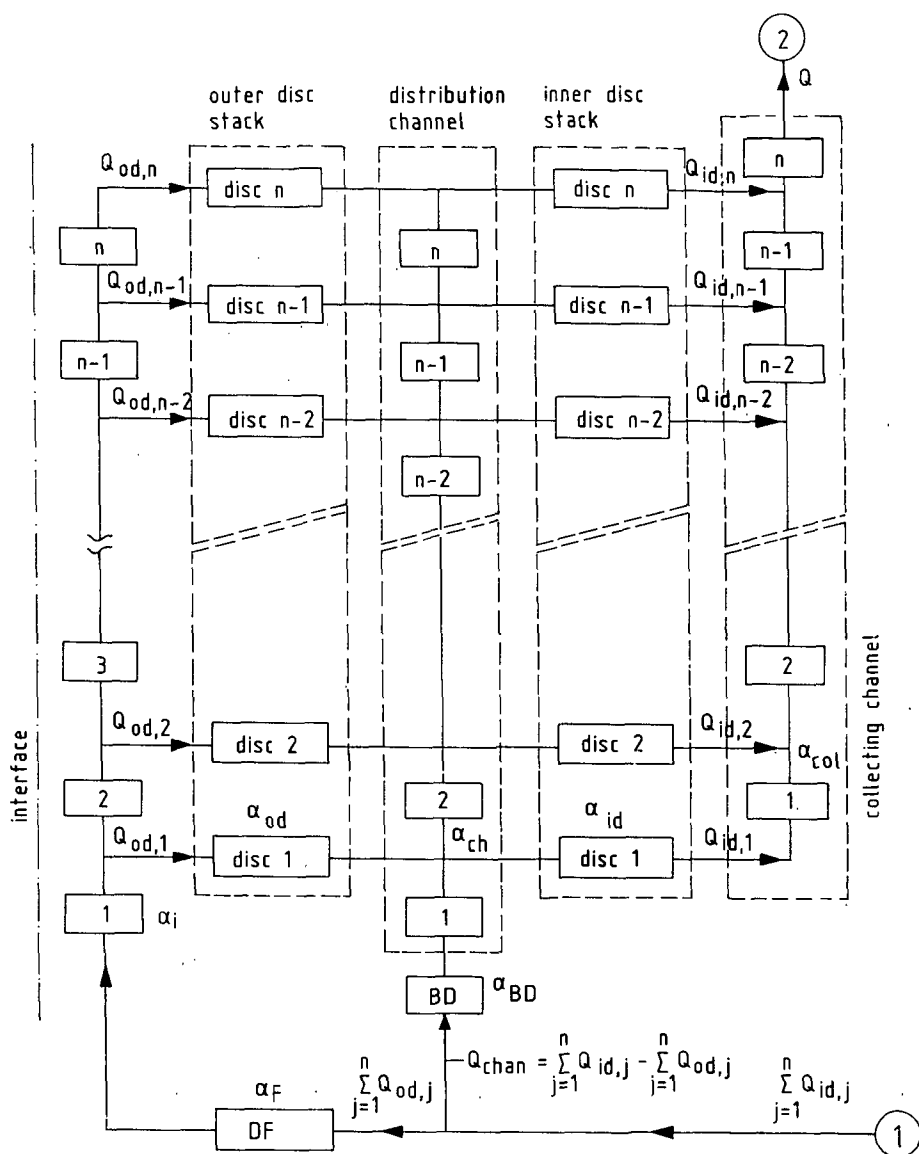
$$\psi = \frac{\alpha}{\frac{(\rho_w - \rho_o) \omega^2}{2 \Delta p_{disc,h}} (R_{ch}^2 - R_{i,h}^2) + 1} \quad (F6)$$

Table F1 Numerical results of the short cut model

exp nr	ω [rad/s]	$R_{i, h}^{*)}$ [mm]	$\Delta P_{disc, h}^{**})$ [Pa]	$R_{i, a}^{***})$ [mm]	$\psi^{****})$ [-]	$\psi \Sigma$ [m ²]	β [-]
13	764	63.5	2712	62.98	0.205	236	.672
14	524	64.7	1539	64.08	0.435	252	.742
15	367	66.1	878	65.39	0.866	266	.812

Notes: *) extrapolated from acoustic measurements outside disc-stack
 **) equation (3.21) and (3.23), $R_2 = R_{ch}$
 ***) $\Delta \rho = 140 \text{ kg/m}^3$
 ****) $\alpha = 1$, $R_{ch} = 65.5 \text{ mm}$

For the experiment trio 13/14/15 reported in paragraph 2.5.2 the quantitative results are presented in table F1. It can be observed that ψ sharply decreases on increasing rotation speed together with the corrected Ambler Σ -value for which the actual interface radius was substituted for R_2 . The latter result is consistent with the measured efficiency, β , which also decreases on increasing rotation speed.



BD = blind disc
DF = distributor foot

Fig.G1 Schematic representation of the disc stack.

Appendix G

DISTRIBUTION MODEL

Assumptions:

1. All pressure terms involved are linear to flow.
2. Interface positioned outside disc-stack.
3. One phase flow.

Figure G1 shows a schematic representation of the disc-stack consisting of n disc spaces, incorporated in a network of resistances. The choice of configuration was mainly determined by the need of flexibility. Various disc-stacks with different caulk thickness, number of spaces and caulk types had to be inserted without too many difficulties. Moreover, those resistances, being more or less independent of the choice of disc-stack, such as the channels, had to be modelled accordingly. The disc resistance factors are related to the inner and outer disc part being positioned respectively inwards and outwards of the channels.

By definition:

$$\alpha_{id} = \frac{\Delta p_{\text{inner disc},j}}{Q_{id,j}} \quad (G1)$$

$$\alpha_{od} = \frac{\Delta p_{\text{outer disc},j}}{Q_{od,j}} \quad (G2)$$

The distribution channels with length L are subdivided into n sections for which analogue expressions are written:

$$\alpha_{ch} = n \frac{\Delta p_{\text{distribution channel section } j}}{Q_{\text{distribution channel section } j}} \quad (G3)$$

$$\alpha_{col} = n \frac{\Delta p_{\text{collecting channel section } j}}{Q_{\text{collecting channel section } j}} \quad (G4)$$

$\frac{1}{4}\beta\alpha_{ch}$ $\frac{1}{4}\alpha_{col}\alpha_{id}$	$\frac{1}{4}\beta\alpha_{ch}$ $\frac{3}{4}\alpha_{col}$	$\frac{1}{4}\beta\alpha_{ch}$ $\frac{2}{4}\alpha_{col}$	$\frac{1}{4}\beta\alpha_{ch}$ $\frac{1}{4}\alpha_{col}$	$-\frac{1}{4}\beta\alpha_{ch}$	$-\frac{1}{4}\beta\alpha_{ch}$	$-\frac{1}{4}\beta\alpha_{ch}$	$-\frac{1}{4}\beta\alpha_{ch}$	$Q_{id,1}$	$p_1 - p_2$
$\frac{1}{4}\beta\alpha_{ch}$ $\frac{3}{4}\alpha_{col}\alpha_{id}$	$\frac{2}{4}\beta\alpha_{ch}$ $\frac{3}{4}\alpha_{col}$	$\frac{2}{4}\beta\alpha_{ch}$ $\frac{2}{4}\alpha_{col}$	$\frac{2}{4}\beta\alpha_{ch}$ $\frac{1}{4}\alpha_{col}$	$-\frac{2}{4}\beta\alpha_{ch}$	$-\frac{2}{4}\beta\alpha_{ch}$	$-\frac{2}{4}\beta\alpha_{ch}$	$-\frac{1}{4}\beta\alpha_{ch}$	$Q_{id,2}$	$p_1 - p_2$
$\frac{1}{4}\beta\alpha_{ch}$ $\frac{2}{4}\alpha_{col}\alpha_{id}$	$\frac{2}{4}\beta\alpha_{ch}$ $\frac{2}{4}\alpha_{col}$	$\frac{3}{4}\beta\alpha_{ch}$ $\frac{2}{4}\alpha_{col}$	$\frac{3}{4}\beta\alpha_{ch}$ $\frac{1}{4}\alpha_{col}$	$-\frac{3}{4}\beta\alpha_{ch}$	$-\frac{3}{4}\beta\alpha_{ch}$	$-\frac{2}{4}\beta\alpha_{ch}$	$-\frac{1}{4}\beta\alpha_{ch}$	$Q_{id,3}$	$p_1 - p_2$
$\frac{1}{4}\beta\alpha_{ch}$ $\frac{1}{4}\alpha_{col}\alpha_{id}$	$\frac{2}{4}\beta\alpha_{ch}$ $\frac{1}{4}\alpha_{col}$	$\frac{3}{4}\beta\alpha_{ch}$ $\frac{1}{4}\alpha_{col}$	$\frac{4}{4}\beta\alpha_{ch}$ $\frac{1}{4}\alpha_{col}\alpha_{id}$	$-\frac{4}{4}\beta\alpha_{ch}$	$-\frac{3}{4}\beta\alpha_{ch}$	$-\frac{2}{4}\beta\alpha_{ch}$	$-\frac{1}{4}\beta\alpha_{ch}$	$Q_{id,4}$	$p_1 - p_2$
$-\frac{1}{4}\beta\alpha_{ch}$	$-\frac{2}{4}\beta\alpha_{ch}$	$-\frac{2}{4}\beta\alpha_{ch}$	$-\frac{4}{4}\beta\alpha_{ch}$	$\frac{4}{4}\alpha_{i1}\alpha_F + \alpha_{od}$	$\frac{3}{4}\alpha_{i1}\alpha_F$	$\frac{2}{4}\alpha_{i1}\alpha_F$	$\frac{1}{4}\alpha_{i1}\alpha_F$	$Q_{od,4}$	0
$-\frac{1}{4}\beta\alpha_{ch}$	$-\frac{2}{4}\beta\alpha_{ch}$	$-\frac{3}{4}\beta\alpha_{ch}$	$-\frac{3}{4}\beta\alpha_{ch}$	$\frac{3}{4}\alpha_{i1}\alpha_F$	$\frac{3}{4}\alpha_{i1}\alpha_F + \alpha_{od}$	$\frac{2}{4}\alpha_{i1}\alpha_F$	$\frac{1}{4}\alpha_{i1}\alpha_F$	$Q_{od,3}$	0
$-\frac{1}{4}\beta\alpha_{ch}$	$-\frac{2}{4}\beta\alpha_{ch}$	$-\frac{2}{4}\beta\alpha_{ch}$	$-\frac{2}{4}\beta\alpha_{ch}$	$\frac{2}{4}\alpha_{i1}\alpha_F$	$\frac{2}{4}\alpha_{i1}\alpha_F$	$\frac{2}{4}\alpha_{i1}\alpha_F + \alpha_{od}$	$\frac{1}{4}\alpha_{i1}\alpha_F$	$Q_{od,2}$	0
$-\frac{1}{4}\beta\alpha_{ch}$	$-\frac{1}{4}\beta\alpha_{ch}$	$-\frac{1}{4}\beta\alpha_{ch}$	$-\frac{1}{4}\beta\alpha_{ch}$	$\frac{1}{4}\alpha_{i1}\alpha_F$	$\frac{1}{4}\alpha_{i1}\alpha_F$	$\frac{1}{4}\alpha_{i1}\alpha_F$	$\frac{1}{4}\alpha_{i1}\alpha_F + \alpha_{od}$	$Q_{od,1}$	0

Fig.G2. Equations for a four space disc-stack in matrix notation.

$$\alpha_F = \frac{\Delta p_{\text{distributor foot}}}{Q_{\text{distributor foot}}} \quad (G5)$$

$$\alpha_{BD} = \beta \cdot \alpha_{ch} \quad (G6)$$

$$\alpha_i = \frac{\Delta p_{\text{in between disc periphery and interface section } j}}{Q_{\text{in between disc periphery and interface section } j}} \quad (G7)$$

The distributor foot is the part in between the channel and the periphery where the liquid must pass 6 narrow slits in between the distributor's lower end and the blind disc. The feed type is modelled by introduction of a fictional resistance which is taken $\beta \cdot \alpha_{ch}$ with β an arbitrary high value (e.g. 10^4), hence forcing the channel flow zero. Solving the problem for a disc-stack with n spaces is preceded by forming 2n equations. As an example the 8 equations for four spaces are written in matrix notation (see figure

G2). As a result of the regularity of the matrix structure, generalization towards more disc spaces will be no problem at all.

This set of equations is symmetric positive definite and is solved with Cholesky's decomposition method.

Parameter estimation

For the disc factors the disc pressure equation is used. The limited Reynolds value within the distribution and collecting channels allow the application of Poiseuille's law with shape correction factors for the cross sections (distribution channels are ellipses with semiaxis $a = \frac{1}{2} D_{ch}$, $b = a \sin\theta$, see fig. 3.17, collecting channel is a rectangle, see fig. 3.16, width = 4×23.3 mm, height 6.5 mm). The distributor foot consists of 6 grooves with a width of 20 mm and a depth of approximately 3 mm extending from $r = 54$ mm to $r = 80.5$ mm (see figure 3.16, paragraph 3.4.1). Application of the symmetrical disc pressure equation, corrected for the width ($2\pi r/6w$), produces unrealistic values (~ 50 kPa), whereas local Reynolds numbers will undoubtedly exceed the critical value of 53 reported in paragraph 3.3.4.4. Lacking a justified description, Poiseuille's law with correction factor was chosen. For the pressure effect in between the periphery of the disc-stack and the interface, Poiseuille's law for broad parallel plates was taken, substituting twice the interface periphery distance for the plate spacing, hence assuming zero viscosity of the water phase as well as symmetry. Under the above-mentioned assumptions α_{col} and α_i are found to be identical, whenever the interface is positioned 2 millimetres outside the periphery.

With the below-presented estimations calculations have been made:

$$\alpha_{col} = .044 \cdot 10^9 \quad n \quad (G8)$$

$$\alpha_{ch} = .183 \cdot 10^9 \quad n \quad (G9)$$

$$\alpha_F = .088 \cdot 10^9 \quad n \quad (G10)$$

$$\alpha_i = \frac{.227 \eta}{(R_i - R_4)^3} \quad (G11)$$

CURRICULUM VITAE

Naam : Van der Linden

Voornamen : Johannes Petrus

Geboren : 14 juni 1958 te 's-Gravenhage

Nationaliteit : Nederlandse

Adres : Ds. van den Boschlaan 299
2286 PL Rijswijk

Opleiding : HAVO, 1976
VWO, 1977

Erkend Assurantie-agent (B)
Stichting examens assurantiebedrijf, 1981

Werktuigkundig ingenieur
Technische Hogeschool Delft, 1982

Werkkring : Student-assistent
Laboratorium Apparatenbouw voor de
Procesindustrie,
Technische Hogeschool Delft 1981-1982

Wetenschappelijk assistent op bovenvermeld
laboratorium 1982-1986

Research medewerker
Unilever Research Laboratorium, Vlaardingen
Nederlandse Unilever Bedrijven B.V. 1986-heden

foto omslag: Foto Vanderfeesten, Veldhoven
druk: ICG Printing B.V. Dordrecht